Motor neuron output in the crustacean cardiac ganglion is organized and maintained by homeostatic conductance relationships

---

A Dissertation

Presented to

The Faculty of the Graduate School

At the University of Missouri

In Partial Fulfillment

Of the Requirements for the Degree

Doctor of Philosophy

By

RANSDELL, JOSEPH L. (MU-STUDENT)

Dr. David J. Schulz, Dissertation Supervisor

July 2013

The undersigned, appointed by the dean of the Graduate School,

have examined the dissertation entitled

MOTOR NEURON OUTPUT IN THE CRUSTACEAN CARDIAC GANGLION IS ORGANIZED AND MAINTAINED BY HOMEOSTATIC CONDUCTANCE RELATIONSHIPS

Presented by Ransdell, Joseph L. (MU-Student)

A candidate for the degree of

Doctor of Philosophy

And hereby certify that, in their opinion, it is worthy of acceptance.

Dr. David J. Schulz

Dr. Andrew D. McClellan

Dr. Michael L. Garcia

Dr. Troy Zars

Dr. Satish S. Nair

ACKNOWLEDGEMENTS

My Ph.D., and the work herein, is a product of the David Schulz lab at University of Missouri- Columbia.

I would like to first thank my advisor David Schulz. Dr. Schulz had the foresight to understand the *Cancer borealis* cardiac ganglion is a terrific model system, and if investigated in the right way, can help answer important questions in neuroscience. As an advisor Dr. Schulz was excellent for several reasons: his teaching methods can condense many hours of studying and thinking into a few minutes of patiently listening, he is passionate about research in a way that motivates his students to pursue science for the right reasons and finally, Dr. Schulz knowingly or not, continuously discusses experiments and scientific questions in a way which drives his students thinking and understanding forward.

My advisory committee: David Schulz, Andrew McClellan, Michael Garcia, Troy Zars and Satish Nair have been supportive and very helpful throughout my Ph.D. In this committee the range of expertise spans the large field of neuroscience; this however did not keep each of my committee members from taking an active interest in the research I was doing and my project has benefited from their diverse points of view.

The Schulz lab has been a terrific place to spend my Ph.D. I have had the pleasure to work and interact with lab members Simone Temporal, Kawasi Lett, Brian Lane, Aihua Dai and Virginia Garcia on a daily basis. This group has always been knowledgeable and helpful during research endeavors, and, perhaps more importantly, they were fun and friendly to spend working and slacking time with; I am grateful to each of them.

In coming to Mizzou, I was able to also return to my home town, Columbia. This opened up tremendous support from my immediate family. My Mother (Beverly) and Father (John), have continuously and selflessly, helped me pretend to be an adult. My two brothers, Greg and Josh, and sister, Andrea, have always been available for advice and friendship.

Finally, before starting my Ph.D., I married my wife Chi. Since coming to Columbia we have extended our small family from just the two of us, to include our son Joseph, our crazy dog Dexter, and we will soon be welcoming a sibling to Joseph. None of this would have been possible without the support, dedication and hard work of my wife Chi.

TABLE OF CONTENTS

LIST OF FIGURES

ABSTRACT

Generating appropriate and functional neuronal output is a matter of fundamental importance to nervous systems across species and phyla. Potential perturbations to a neurons intrinsic excitability alone include hebbian style plasticity, ion channel turnover and neuromodulation. With these dynamic processes in place, it is remarkable that neurons are able to maintain stable and functional output throughout the life of an organism. Yet little is known about the cellular mechanisms in neurons and networks which act to stabilize functional output. Here we utilize large cell motor neurons of the *Cancer borealis* cardiac ganglion to investigate how these cell's important burst output is generated, maintained and synchronized across cells in a rhythmic motor network.

The *C. borealis* cardiac ganglion (CG) acts as a nine cell central pattern generator (CPG) which drives the rhythmic contraction of the C. borealis heart. The ganglion is made up of 4 pacemaker neurons (small cells) which drive 5 motor neurons (large cells) to elicit burst organized potentials responsible for the heart contraction. Recently the large cells have been the basis for both a biological (Tobin et al., 2009), as well as two conductance based computational modeling studies (Franklin et al., 2010). Results in these studies suggest Large Cell (LC) motor neurons in the CG may regulate and preserve their important electrophysiological output using variable intrinsic conductance organization. This supports an intriguing and relatively new hypotheses, that important neuronal outputs are maintained by conserving key intrinsic conductance relationships, rather than constraining the magnitude of individual ionic currents (Goldman et al., 2001a, Golowasch et al., 2002, Prinz et al., 2004a, Schulz et al., 2006, Schulz et al.,

2007a); these conserved conductance relationships act to balance properties of excitability resulting in an appropriate electrophysiological output. Studies across model systems have provided evidence for this hypothesis by demonstrating compensatory regulation between voltage and ligand gated ion channels (Guo et al., 2005, Nerbonne et al., 2008), as well as the currents they mediate (LeMasson et al., 1993, Turrigiano et al., 1994, Turrigiano et al., 1995, Golowasch et al., 1999), which then cause properties of electrophysiological output to be maintained; this type of regulation has become known as homeostatic plasticity.

The *C. borealis* CG studies mentioned above utilize either conductance based computational modeling, or molecular biology to study how LCs organized their electrophysiological output. Here we investigate the electrical properties of the *C. borealis* LCs, as well as profile additional channel gene mRNA expression in LCs relate to the conductances mediated by those channel genes. We find that large cell motor neurons utilize multiple intrinsic currents to mediate burst potentials, and these currents are in part localized to the LC somata, distal from action potential generating currents. Next we examine the functional organization of these intrinsic currents and show that LC motor neurons, which have synchronous burst activity during normal network behavior, have differential intrinsic tuning even across LCs even in a single network.

The LC burst waveform is maintained across network LCs in part by a rapid compensatory relationship between the two potassium currents, I_A and I_{HTK}. This relationship results in in a negative correlation between the two currents across LCs. We show that this relationship is maintained via a fast compensatory response, which is in part dependent on levels of intracellular calcium. Using single cell quantitative PCR we find channel genes which mediate these two currents also have a conserved relationship across cells, although the correlation is positive rather than negative. We hypothesize that this difference is due to an existing pool of channel mRNA or protein which allows a rapid compensatory interaction between the two currents.

While this differential tuning is likely the result of conserved conductance relationships, we demonstrate that conserved relationships which act in maintaining output also bridge intrinsic properties of the cell with network level properties; namely we show a conserved relationship between the transient potassium current I_{HTK} and strength of LC to LC electrical coupling. Using dynamic clamp to manipulate electrical coupling, and pharmacological blockers to manipulate I_{HTK}, we demonstrate that this relationship is important in maintaining synchronized bursts between network LCs.

Together these data demonstrate that burst output of the LC motor neuron, while driven via SC input, is heavily influenced by several ionic conductances and network

level properties. These properties are tuned in a differential manner, though with conserved relationships, to maintain appropriate LC excitability and burst output.

INTRODUCTION

In considering the electrophysiological output of neurons we often think of action potential waveforms, these brief events consist of a rapid upswing and downswing in membrane potential, mediated primarily by fast inactivating sodium current and delayed rectifier potassium current. This idea of neuronal output neglects cells which, instead of firing single action potentials, fire in bursts of action potentials. Bursting output relies on a slow wave depolarization which places the neuronal membrane potential above action potential threshold for an extended period of time; this involves several additional ionic currents and can result in several action potentials grouped together (Rutecki, 1992, Overton and Clark, 1997). Several studies have found functionality behind this mode of output, which spans sensory and motor neurons, in both vertebrate and invertebrate species (Cattaneo et al., 1981, Bair et al., 1994, Tseng and Nadim, 2010). Neuronal bursts have been shown to increase both the reliability and efficiency of synaptic transmission as well as provide greater information content than single spikes (Lisman, 1997, Koulakov et al., 2002). However coming up with a detailed understanding of how a neuron intrinsically instigates this slow wave burst potential presents a problem for most model organisms. Measuring all or even several properties which coordinate the biophysical basis of a neuronal burst is a challenge, and measuring this in several neurons with a conserved electrophysiological signature is often impossible.

In this regard LC motor neurons of the *C. borealis* cardiac ganglion make an ideal system to investigate underlying properties responsible for burst output. The *C. borealis* CG is able to maintain rhythmic output even after it is removed from the heart musculature of the animal, meaning, if the CG is left intact, it can continue rhythmic motor output in the absence of external stimuli and musculature feed-back; we classify these types of motor networks as central pattern generators (Marder and Bucher, 2001). Central pattern generators (CPG) are neural networks responsible for rhythmic motor output often vital to the survival of the animal. Some of the behaviors these networks are responsible for include breathing, walking, chewing and swallowing (Marder et al., 2005). Simple CPG networks in invertebrate animals have become invaluable models for studying not only principles behind CPG function, but also general principles in regards to how neurons and networks are able to maintain and regulate appropriate excitability and output. Properties which make these invertebrate CPG networks particularly useful to researchers include the large size of the neurons, simple network architecture and the ability to unambiguously identify the same neuron from animal to animal (Selverston, 2010). In the following experiments we investigate how the LC motor neurons in the *C. borealis* CG generate and maintain synchronous burst potentials which allow the single chambered *C. borealis* heart to rhythmically contract.

The C. *borealis* cardiac ganglion is a central pattern generator made up of nine neurons which cause rhythmic contractions of the crab heart (Cooke, 2002b, Cruz-Bermudez and Marder, 2007b). Two neuronal types are involved: four pacemaker

neurons known as Small Cells (SC) and five motor neurons known as Large Cells (LC). The SCs endogenously burst providing excitatory input to the LC motor neurons causing a large cell burst potential; this LC burst of action potentials causes the motor output of the network, which is a single contraction of the crab heart (Hartline, 1967; Tazaki and Cooke, 1979, 1983c, a; Berlind, 1989). The anterior LC motor neurons offer several advantages for investigating properties responsible for burst output. Conductances which work in eliciting the intrinsic slow wave burst potential are present in anterior LC somata, whereas the action potential generating conductances of the anterior LCs, are localized to the distal neurite. This network architecture is present in other crustacean species CG (Tazaki and Cooke, 1986) as well as in C. *borealis* CG (for *C. borealis* network architecture see Figure 1.1). The C. *borealis* anterior LCs also have conserved LC somata spacing, allowing the use of thread ligatures to isolate and study the burst generating properties in a single identified LCs (Figure 1.1A). Finally, the somata of each LC is large enough to be individually harvested for single cell quantitative PCR.

In the following studies we characterize the native intrinsic organization underlying LC motor neuron burst potentials, along with mechanisms by which these underlying properties are regulated and maintained. To study how burst output is intrinsically mediated we eliminate external stimuli from an individual cell, and subsequently characterize / study the complement of intrinsic biophysical properties which integrate stimuli and elicit the resulting burst output. These biophysical properties can be broken into two main categories: the suite of intrinsic ionic conductances which

sum to elicit a unique change in membrane potential and the network level properties which influence the activation of voltage gated intrinsic conductances. In this group of experiments we use the three anterior LCs as a reduced preparation to investigate how the LC ionic conductances are organized, maintained and finally, interact with network level properties to generate appropriate LC burst output.

We begin by characterizing the depolarizing conductances present in anterior LC somata (chapter 1). In chapter two we characterize three outward potassium currents, and go on to study a negative compensatory relationship between two of those currents. In chapter three we show that LCs within a network have disparate intrinsic organization, which are tuned to respond to network driven depolarizing stimuli in very similar ways. Finally, in chapter 4 we show that synchronization across LCs is in part maintained by a relationship between an intrinsic potassium current and LC t0 LC electrical coupling strength.

CHAPTER 1

Characterization of inward currents and channels underlying burst activity in motor neurons of the crab cardiac ganglion

Large cell motor neurons in the *Cancer borealis* cardiac ganglion generate rhythmic bursts of action potentials responsible for cardiac contractions. While it is well known these burst potentials are dependent on coordinated interactions among depolarizing and hyperpolarizing conductances, the depolarizing currents present in these cells, and their biophysical characteristics, have not been thoroughly described. In this study we used a combined molecular biology and electrophysiology approach to look at channel identity, expression, localization, and biophysical properties for two distinct high-voltage activated calcium currents present in these cells: a slow calcium current (I_{CaS}) and a transient calcium current (I_{CaT}). Our data indicate that CbCaV1 is a putative voltage-gated calcium channel subunit in part responsible for an L-type current, while CbCaV2 (formerly *cacophony*) is a subunit in part responsible for a P/Q-type current. These channels appear to be localized primarily to the somata of the motor neurons. A third calcium channel gene (CbCaV3) was identified that encodes a putative T-type calcium channel subunit and is expressed in these cells, but electrophysiological studies

failed to detect this current in motor neuron somata. In addition, we identify and characterize for the first time in these cells a calcium-activated nonselective cationic current (I_{CAN}), as well as a largely non-inactivating TTX sensitive current reminiscent of a persistent sodium current. The identification and further characterization of these currents allows both biological and modeling studies to move forward with more attention to the complexity of interactions among these distinct components underlying generation of bursting output in motor neurons.

Bursts of action potentials are vital to appropriate motor output in central pattern generator networks. The organization of burst potentials often relies on calcium- and sodium-mediated depolarizing currents which have an influence on neuronal function beyond eliciting a direct change in membrane potential. For example, calcium influx via voltage-gated calcium currents are known to affect second messenger systems involved in transcriptional regulation (Clapham, 2007), activate other ionic currents (Wisgirda and Dryer, 1994, Yamoah et al., 1994, Sah, 1995) as well as trigger neurotransmitter release at the synapse (Mulkey and Zucker, 1993). Sodium has been shown to activate sodium-dependent potassium currents and influence neuronal excitability (Rose, 2002, Hage and Salkoff, 2012). These higher order cation effects are also known to act as the mechanism behind different forms of plasticity in the ongoing output of a cell and/or network (Cummings et al., 1996, Turrigiano, 2008, George et al., 2012)**.** However before we can fully understand the role of inward currents and resulting cation influx during a burst potential, we must have a thorough understanding of what depolarizing components exist in a given cell type.

The Large Cell (LC) motor neuron of the *Cancer borealis* cardiac ganglion has been a successful model for studying how underlying conductances interact to mediate burst potentials (Tobin et al., 2009, Ball et al., 2010a, Franklin et al., 2010) and new evidence shows there is rapid calcium-dependent homeostatic compensation among potassium currents which impacts both LC intrinsic excitability as well as appropriate network bursting (Ransdell et al., 2012). However there is little characterization of what depolarizing properties are active in the *C. borealis* LC burst, hindering a more complete understanding of how the LC bursts are generated and maintained. The goal of this study is to characterize the depolarizing components intrinsic to the LC motor neuron in the *C. borealis* cardiac ganglion.

Despite the extensive use of crustacean motor systems as models for understanding neuronal network function and modulation (Marder and Bucher, 2007), the inward currents have been less thoroughly studied than their outward counterparts. In neurons of the stomatogastric ganglion (STG), total voltage-activated calcium current has been successfully measured using sensitivity to cadmium chloride as an effective blocker (Golowasch and Marder, 1992). Further pharmacological dissection of STG calcium currents suggest there are two distinct high threshold calcium currents present: an L-type (CaV1) and a P/Q type (CaV2) (Hurley and Graubard, 1998, Johnson et al., 2003). Molecular cloning studies support the presence of these two calcium channel types in neurons of the STG (French et al., 2002). Because the calcium dependence of synaptic transmission in STG neurons has a more hyperpolarized threshold (-60 mV) than these

two high threshold currents, there is thought to be an additional low threshold or T-type (CaV3) current involved in neurotransmitter release (Graubard et al., 1983, Harris-Warrick et al., 1992). In the cardiac ganglion, some analysis of calcium currents has taken place in the LCs (Tazaki and Cooke, 1979, 1986), particularly in the lobster *Homarus americanus* (Tazaki and Cooke, 1990). However, a more thorough analysis of these currents is necessary to understand their role in generating burst output in LC motor neurons.

Beyond calcium currents, evidence for persistent sodium currents (TTX sensitive) has also been reported in both the STG (Turrigiano et al., 1995, Elson and Selverston, 1997) as well as the cardiac ganglion LCs of the lobster *H. americanus* (Berlind, 1993). The somata of these crustacean motor neurons do not contain spike-mediating sodium currents(Golowasch and Marder, 1992). However, a characterization of persistent sodium currents has yet to be performed in these crustacean systems. In addition, plateau potentials in the dorsal gastric neurons of the STG depend on activation of a calcium-dependent voltage-independent cationic current, or "CAN current" (Zhang and Harris-Warrick, 1995, Zhang et al., 1995), but this current has yet to be identified or characterized in LC motor neurons.

With the *C. borealis* LC motor neuron being the focus of several recent studies exploring how intrinsic conductances and channels are organized and conserved during burst generation (Tobin et al., 2009, Ball et al., 2010a, Franklin et al., 2010, Ransdell et al., 2012) a more thorough characterization of the inward currents in this species and cell

type are both important and valuable to moving research in this area forward. Here we utilize multiple techniques, including two-electrode voltage clamp, immunohistochemistry and single cell PCR analysis of channel gene expression to explore these depolarizing components in the LCs of the crab, *Cancer borealis*.

Materials and Methods

C. borealis crabs were purchased and shipped overnight from The Fresh Lobster Company (Gloucester, MA, USA). Crabs were kept between 24 hours and two weeks in artificial sea water at 12 °C before use. Crabs were anesthetized in ice for 15 minutes prior to the dissection. The dissection took place in chilled physiological saline comprised of 440 mM NaCl, 26 mM $MgCl_2$ 13 mM $CaCl_2$, 11 mM KCl, and 10 mM HEPES (pH = 7.4). Details of the cardiac ganglion dissection can be found in Cruz-Bermúdez et al. (2007)(Cruz-Bermudez and Marder, 2007a). All experiments were conducted on the three anterior LCs (see Figure 1, black arrows; Figure 1C). To isolate large cell somata from action potentials and network activity individual strands of bulking nylon (made by Gütermann Creative) were used to ligate the nerve at the anterior branch point of the CG (Figure 1). To impale large cells each cell was desheathed using a desheathing pin. LC3 / LC4 were isolated from the rest of the network in a pair.

Electrophysiology

All experiments were done in physiological saline cooled to 12°C. Two-electrode voltage clamp (TEVC) and two-electrode current clamp (TECC) protocols were carried out by impaling a large cell with two glass electrodes filled with 3M KCl (8-17 MΩ resistance) using an Axoclamp 2A amplifier (Axon Instruments, Union City CA). In TEVC experiments when all potassium currents needed to be blocked, the current injecting electrode was filled with 1 M tetraethylammonium (TEA) + 1M cesium chloride (CsCl) (17-18 MΩ resistance). All recordings were made from large cell somata; action potential conductances were blocked (unless noted otherwise) by tightening a thread ligature past the anterior branch point on the nerve the LC was located in (Fig. 1A). TEVC and TECC protocols were created, driven and recorded with Clampex 9.2 software (Molecular Devices). Current and voltage recordings were analyzed with Clampfit 9.2 software (Molecular Devices). Current and voltage traces were filtered with a digital lowpass boxcar filter using 7 smoothing points at a sample frequency of 5 kHz.

Pharmacology. Pharmacological blockers were dissolved in physiological saline and perfused onto the cardiac ganglion using a Rabbit peristaltic pump (Rainin Instrument Company) at a rate of 1.5 mL / min. or added from a concentrated stock solution via pipette. Prior to TEVC or TECC protocols perfusion was stopped for at least five minutes to let the preparation temperature stabilize.

Voltage Clamp Protocols

To voltage clamp inward currents, potassium currents were blocked by perfusing 50mM TEA, 1mM 4-aminopyridine (4AP) and injecting 1M TEA + 1M CsCl using

iontophoresis (300 msec 1.2 nA pulses at 2 Hz) for a minimum of one hour. To isolate calcium currents, 10^{-6}M tetrodotoxin (TTX) also was added for a minimum of 45 minutes. When necessary, calcium currents were blocked using 250μM cadmium chloride ($CdCl_2$) perfusion for a minimum of 45 minutes. Because of difficulty in fully blocking outward currents we often carried out trace subtractions before and after $CdCl_2$ (45 min.) and before and after TTX (45 min.) to isolate Cd-sensitive currents and TTX-sensitive currents respectively.

To separate inactivating and non-inactivating high-voltage activated calcium currents, two TEVC protocols were carried out: one from a holding potential of -40 mV and 680 ms depolarization steps from -50 mV to +15 mV in 5 mV increments (V_h = -40 mV) and a second identical protocol except from a holding potential of -80 mV (V_h = -80 mV). Trace subtractions were used to isolate the additional inward current clamped with the -80mV holding potential, this current is labeled throughout the paper as "I_{CaT}" while the inward calcium current clamped from a -40 mV holding potential is labeled "I_{CaS}" (Liu et al., 1998, Prinz et al., 2003). I_{CaT} inactivation was measured in TEVC using a 800 ms prestep (-80 mV to -40 mV, 5 mV increments) prior to a 500 ms, -20 mV depolarizing step. To remove I_{CaS} the current generated with the -40 mV pre-step was subtracted from each sweep. I_{CaS} inactivation was measured in TEVC using 2 s pre-steps (-50 mV to + 5mV, 5 mV increments) followed by a 500 ms 0 mV depolarizing step.

Inward tail current was isolated with the same pharmacological agents as voltage-gated calcium currents and its magnitude was measured at -80mV holding potential after

680 ms depolarizing pre-steps between -50 and +15mV. To isolate I_{CaS} contribution to tail current, a-40mV holding potential was used prior to the depolarizing voltage step; in this protocol the tail current was still measured at -80 mV (Fig. 5B). Reversal of I_{CAN} was measured after a 1s +20 mV depolarizing voltage step. Magnitude of I_{CAN} was always measured at peak tail current after depolarizing voltage step.

TTX-sensitive current was isolated with the same pharmacological agents used to isolate calcium currents, with the addition of 250 μM $CdCl_2$. Depolarizing step TEVC protocols (steps = 680 ms,-50 mV to +15 mV; V_h = -40 mV) and voltage ramp TEVC protocols (4 s ramp, -80 mV to +20 mV) were carried out before and after 30 min. exposure to 10^{-6} M TTX and trace subtractions were used to isolate the TTX sensitive current.

Sequencing of Calcium Channels

We obtain *de novo* partial ORF sequence corresponding to three calcium channel alpha subunit cDNAs to aid in characterizing the channels potentially underlying calcium currents in LC motor neurons. The methods for this degenerate PCR approach are as described in detail previously (Schulz et al., 2006, Schulz et al., 2007a). Briefly, channel transcripts were amplified from a cDNA template derived from total RNA extracted from mixed nervous system tissue from *C. borealis*. We first designed and employed degenerate primer pairs based on conserved amino acid sequence compared across multiple invertebrate and vertebrate species, including *Lymnaea stagnalis, Drosophila*

melanogaster, *Apis mellifera*, *Daphnia pulex*, *Mus musculus*, and *Homo sapiens*. We used these primers in RT-PCR reactions (GoTaq Green, Promega) to obtain PCR products of predicted length, which were subsequently ligated into pGEM-T easy plasmid vector (Promega) and sequenced using dye terminator cycle sequencing (DTCS Quick Start Kit, Beckman Coulter). Sequences obtained were compared to orthologous sequences using BlastX (NCBI). Initial sequence obtained was extended by a process of additional RT-PCR reactions, each using one gene-specific primer within the newly elucidated sequence and one degenerate primer outside the known sequence that would allow us to extend the sequence. Once we obtained enough sequence information to feel that we definitively could identify a calcium channel ortholog, a final PCR (Platinum Taq DNA polymerase, Invitrogen) was performed with gene-specific primers that spanned the entire assembled sequence to ensure a contiguous cDNA existed in our template pool. Accession numbers for these new sequences are as follows: (Cb = *Cancer borealis*) CbCaV1: JN809809, CbCaV2: JN809808, CbCaV3: JN809810. Primer sequences that will result in PCR products that contain the entirety of the assembled sequence thus far are as follows: CbCaV1-Forward 5'- CAATGCATTACGATGGAGGGG – 3' ; CbCaV1-Reverse 5' – AAACCTCCTGAAGTAGTCTTG – 3'; CbCaV2-Forward 5' – TGGAACATTATGGACTTCGTTG – 3' ; CbCav2-Reverse 5' - CCAGCCCCACCAAGCCTCCTG – 3' ; CbCav3-Forward 5' – CAAGGATGGCTGGGTCAACAT – 3' ; CbCav3-Reverse 5' – GGCTCTAATGCCCTTGGCCAT – 3'.

Single-cell PCR

Details regarding the harvesting of individual LC motor neurons for single-cell molecular analysis are provided in a previous publication (Tobin et al., 2009). Briefly, ganglia were desheathed around the area where large cells (LCs) were visually identified, and to facilitate removal of the neurons, the ganglia were exposed to protease (Sigma) for several minutes. The protease was replaced with a cold (~0˚ C) solution of 70% ethylene glycol and 30% saline, and the ganglia were put in a -20˚ C freezer for up to 1 hour. The cells were then manually removed with fine forceps and each cell was placed in a cryogenic tube with 350 ml lysis buffer (buffer RLT, Qiagen) and 1% ß-mercaptoethanol. The tubes were immediately placed on ice, then stored at -80˚C until RNA extraction.

Quantitative RT PCR was performed as in Schulz et al. 2006, and modified as in Tobin et al. 2009. Primers specific for real–time PCR detection of CbCaV1, CbCaV2, and CbCaV3 using SYBR Green were developed and designed using Primer3 software as follows: CbCaV1–Forward 5'– GATGGAGGGAGACGACAAGA –3'; CbCaV1–Reverse 5' – GGTTGTTGAGCCTCGTCATT – 3'; CbCaV2–F 5'–GTATCCGGCGGACAGTAAAG –3'; CbCaV2–R 5'–AAACTTGGTGAGAAATGGCG –3'; CbCaV3–F 5'– CCAGTTGGATGTGTTCATCG –3'; CbCaV3–R 5'– ATGATGGTTGGGTTGATTGG –3'. PCR amplicon sizes were 90bp (CbCaV1), 120bp (CbCaV2), and 93bp (CbCaV3). Primer sets were validated for PCR efficiency, linear dynamic range, and limit of detection using both a plasmid template that contained the gene of interest, as well as cDNA generated from total RNA

extracted from crab neural tissue. All qPCR reactions were carried out with a final primer concentration of 0.25 μM for each primer, using RT² SYBR Green qPCR Mastermix (SABiosciences). RNA from single neurons was extracted using RNeasy micro kit (Qiagen), and reverse transcription using SuperScript III (Invitrogen). See Schulz et. al 2006, Schulz et. al. 2007 for more details. Assay quality and variability was monitored via 18S rRNA quantitation (Schulz et al., 2006, Schulz et al., 2007a, Tobin et al., 2009, Ransdell et al., 2010). Data in this study are presented as raw copy number per cell (see Tobin et al. 2009).

Cell fills and Immunohistochemistry

To visualize stereotypical localization of LC somata and projections in the cardiac ganglion, we iontophoresed a fluorescent tracer (AlexaFluor 568, Invitrogen) using backfilled microelectrodes by overriding the electrode capacitance compensation for 5 minutes. Dye was allowed to diffuse throughout the ganglia for 24 hours in physiological saline at 4˚ C, and then preparations were directly imaged using a Leica M205F Stereomicroscope with a Leica DFC 345 FX camera.

For immunohistochemistry, cardiac ganglia with desheathed LCs were pinned to Sylgard and fixed in 0.1 M phosphate buffered saline (PBS; 440 mM NaCl, 11 mM KCl, 10 mM Na_2HPO_4, 2 mM KH_2PO_4, pH 7.4) containing 2% paraformaldehyde for 40-90 minutes and then washed 2 x 10 minutes in PBS containing 0.1% Triton-X (PBT). Rabbit pan polyclonal primary antibody to CaVα1 subunit (Anti-CaVpan α1; Alomone Labs)

was applied overnight at a concentration of 1:100 in PBT at 4 ˚C. Ganglia were rinsed 4 x 10 min. in PBT. CaVα1-like immunoreactivity was investigated with 1:250 dilution goat anti-rabbit IgG conjugated to Alexa Fluor® 568 dye in PBT (Molecular Probes/Invitrogen) for 12-20 hours. Ganglia were rinsed again in PBS at least 5 x 15 min., and mounted in ProLong Gold which contained DAPI (Invitrogen). Images were acquired with an Olympus IX81 epifluorescent microscope with MicroSuite software.

Statistics

Analyses were done using SigmaPlot 11.0. R-values reported are results of Pearson correlation (Fig. 3I). After passing Shapiro-Wilk tests for normality, changes in current magnitude before and after pharmacological treatments were analyzed with paired *t*-tests.

Results

Calcium channel expression in LCs

To determine which calcium current subtypes may be present in LC motor neurons, we decided first to adopt a molecular approach and look for expression of voltage-gated calcium channels at the mRNA level. The most thorough combined molecular and electrophysiological characterization of voltage-gated calcium channels in invertebrates has been performed for the snail, *Lymnaea stagnalis* (Spafford et al., 2003,

Spafford et al., 2006, Senatore and Spafford, 2010). Thus we will use direct comparisons of our channels and currents to these well characterized invertebrate examples as basis for interpretation of our molecular calcium channel genes. We obtained *de novo* sequence, or extended partial sequences, for three channel genes that appear to be orthologous to single representatives for each of three calcium channel gene families CaV1 (L-type), CaV2 (P/Q-type), and CaV3 (T-type) found in most invertebrates (Jeziorski et al., 2000, Spafford and Zamponi, 2003). We will refer to each crab gene as CbCaV1, CbCaV2, and CbCaV3, Cb to denote *C. borealis* and 1, 2, or 3 for the gene family to which the sequence is most orthologous. We assigned gene identities to our channel transcripts by comparing our three putative calcium channel genes to the orthologous *L. stagnalis* calcium channel sequences (Figure 2A). Obtaining partial sequence of the calcium channel genes allowed us to develop primers to analyze single large cell mRNA expression of each channel gene (Fig. 2B). LC motor neurons expressed detectable amounts of all 3 putative calcium channel subunits, with CbCaV1 having the lowest mRNA copy number, while higher levels of both CbCaV2 and CbCaV3 were detected (Fig. 2B).

Across the respective stretches of these channel sequences between *Cancer borealis* and *Lymnaea stagnalis*, CbCaV1 sequence shares 581 out of 801 identical amino acids with *Lymnaea stagnalis* (LCaV1; 73%), CbCaV2 (initially referred to as *cacophony*; see Tobin et al. 2009) shares 970 out of 1483 identical amino acids (65%) to LCaV2, and CbCaV3 shares 325 out of 428 identical amino acids (76%) to LCaV3. The location of these regions of overlap between *C. borealis* and *L. stagnalis* are shown in Figure 2C

with respect to putative transmembrane domains and IQ-like binding motifs of these channels (Van Petegem et al., 2005). These binding domains and their amino acid similarity to mammalian orthologs are shown in Figure 2D. In addition, to confirm their identity as calcium channels we identified and aligned the EEEE and EEDD loci of the pore forming loops with consensus mammalian sequences. These EEEE/EEDD loci are known to confer divalent cation selectivity to these channels (Tang et al., 1993, Yang et al., 1993, Cens et al., 2007), and are a hallmark for the identification of voltage-gated calcium channels.

Calcium currents

To isolate voltage-gated calcium currents we minimized competing sodium and potassium currents with pharmacological blockers (see methods). Total inward current under these conditions was measured (Figure 3A). This revealed what appeared to be a faster transient inward current (I_{CaT}; Figure 3A), a slower more persistent inward current (I_{CaS}; Figure 3A), a late outward current, and an inward tail current (Figure 3A). Addition of $CdCl_2$ (see Figure 4F) completely eliminates the inward currents and reduces or eliminates the tail current, leaving behind only a small residual outward current that is presumably due to an incomplete block of I_A and/or $I_{Kd.}$ Taken together, these data plus the gene expression results suggest the presence of multiple distinct calcium and calcium-dependent inward currents in the LC motor neurons.

We then attempted to characterize these distinct currents by a combination of pharmacology and voltage-clamp protocol manipulation. Low-threshold, T-type calcium currents in *L. stagnalis* (LCaV3) activate at hyperpolarized voltages around -60 mV, are transient, and sensitive to block with nickel (Senatore and Spafford, 2010). We were unable to elicit inward current in LC motor neuron somata for any voltages lower than -30 mV (see Figure 3D), and application of $NiCl_2$ (75-250 μM, N = 4) resulted in no change in inward current magnitude or kinetics (data not shown). Therefore, although we detected relatively abundant transcripts for CbCaV3 in LC motor neurons (Figure 2B), we were unable to detect any active T-type current from somatic voltage-clamp experiments in these cells.

P/Q-type calcium currents (e.g. LCav2) are more rapidly transient than L-type calcium currents (e.g. LCav1) and inactivate at more hyperpolarized holding potentials (Tsien et al., 1988, Hille, 2001). Therefore, we set out to separate these potentially distinct native high-threshold calcium currents by subtracting inward current clamped with a -40 mV holding potential from inward current with a -80 mV holding potential in LC motor neurons. The more persistent calcium current (I_{CaS}; Figure 3B) activates at -30 mV and reaches its peak near 0 mV (Figure 3D). The transient current (I_{CaT}; Figure 3C) activates at similar voltage as I_{CaS} (i.e. -30 mV), but reaches its peak at more hyperpolarized voltages near -20 mV (Figure 3D). Native current levels for I_{CaS} and I_{CaT} in individual LC motor neurons was variable from cell to cell, and ranged from approximately 3 to 6 nA for both currents (Figure 3E). However, the most noticeable distinction between I_{CaS} and I_{CaT} in these cells is the voltage dependence of inactivation.

I_{CaT} shows an approximately 30 mV more hyperpolarized half-inactivation voltage than I_{CaS} (Figure 3F). In addition, ICaS and ICaT are distinguished by differences in time constant of inactivation (Figure 3G), and time to peak (Figure 3H), as a function of voltage. There is a consistent relationship between time to peak current for I_{CaS} and I_{CaT} that would suggest these currents are able to maintain distinct impacts on cell voltage across a range of activation voltages (Figure 3I). These characteristics are consistent with differences reported between high-voltage activated calcium currents LCaV1 and LCaV2 in *L. stagnalis* (Spafford et al., 2006) and similar to differences among L- and P/Q-type calcium currents in mammals (Tsien et al., 1988, Hille, 2001). Based on these results, we propose that I_{CaS} current in crab LC motor neurons is homologous to CaV1 current as described in *L. stagnalis* (Spafford et al., 2006), and reminiscent of mammalian L-type calcium currents (Tsien et al., 1988, Hille, 2001), while I_{CaT} is homologous to LCaV2 as described in *L. stagnalis* (Spafford et al., 2003, Spafford et al., 2006) and reminiscent of mammalian P/Q-type currents (Tsien et al., 1988, Jeziorski et al., 2000, Hille, 2001).
To further confirm the characteristics of these calcium currents, as well as investigate any calcium-dependent aspects of their kinetics, we performed our voltage clamp experiments with $BaCl_2$ substituted for $CaCl_2$ in the saline, as well as with addition of $CdCl_2$ to the saline. Both I_{CaS} and I_{CaT} are carried by Ba^{2+}, and show similar activation characteristics to the native calcium currents (Figures 4A and 4C). Furthermore, both I_{CaS} and I_{CaT} are eliminated by $CdCl_2$ administration (Figure 4F). This further supports the hypothesis that these inward currents are indeed calcium mediated. We also noted that the slow inactivation of I_{CaS} is eliminated or significantly reduced ($P < 0.01$; N=5) in the corresponding I_{Ba} (Figure 4B, black arrows; Figure 4E), suggesting that the inactivation

of this current is not purely voltage-dependent, but rather a calcium-dependent inactivation (CDI). This is also a characteristic consistent with mammalian and other invertebrate L-type calcium currents (Hille, 2001). We were able to identify in our CbCaV1 sequence an IQ-binding motif that has been shown to strongly influence CDI in mammalian L-type channels (Zuhlke et al., 2000). Site directed mutagenesis shows that the IQ amino acid residues of this motif, as well as an FRK motif within the domain are significant mediators of CDI, with the mutagenesis of K to A having the least impact in the motif (Zühlke et al. 2000). Our putative IQ-domain shows this same pattern of amino acid residues (Figure 2D), differing only in the K-residue, which is consistent with the observation of CDI in our I_{CaS} characterization. Additionally, we sometimes detected a decrease in the magnitude of I_{CaT} following barium substitution (Figure 4D), which could be indicative of a calcium-dependent facilitation of the native transient calcium current in these cells (Tazaki and Cooke, 1990). While these collective data are consistent with CDI of I_{CaS} as suggested by barium substitution, it is possible that barium influences other currents that may be incompletely blocked by our experimental protocol, altering the apparent inactivation kinetics of I_{CaS}.

Barium did not cause a change in inactivation kinetics of I_{CaT} (Figure 4D; 4E), suggesting that this current does not show CDI. There is less known about the molecular basis of CDI and the IQ-domain in P/Q-type currents. However, CDI in these channels has been linked to an interaction with an IQ-like binding domain (including IM amino acid residues; see Figure 2D) with a calmodulin binding domain within CaV2 channels in mammals (Lee et al., 2003). While this interaction is not yet well characterized, it is

noteworthy that our CbCaV2 IQ-like domain lacks the IM motif implicated in CDI, consistent with our lack of evidence for CDI for I_{CaT}.

CAN (calcium-activated nonselective cationic) current

We observed a native inward tail current (Figure 3A) that is eliminated following $CdCl_2$ administration (Fig. 4F) and significantly decreased after $BaCl_2$ substitution (pre-Ba^{2+} mean = -5.7 ± 0.5 nA; post-Ba^{2+} mean = -2.7 ± 1.0 nA; N = 3; P = 0.03) (Fig. 4B, 4C; gray arrows), suggesting the presence of a calcium-activated depolarizing conductance in these cells. The observed characteristics of this current are very similar to a calcium-activated nonselective cationic current (I_{CAN}) found in STG neurons of lobster, and described in detail by Zhang et. al. (1995). We performed subsequent voltage-clamp and pharmacological manipulations to determine whether the current we observe in LC motor neurons shares the same kinetics and properties of I_{CAN} as described in lobster(Zhang et al., 1995).

To analyze I_{CAN} in LC motor neurons, we bath applied TTX, TEA, 4-AP and iontophoresed Cs^+ intracellularly as described in the Methods. We then elicited inward currents with increasing depolarizing voltage steps, followed by clamping tail currents at -80 mV. As seen in Figure 3A, as well as Figure 5A (inset), these protocols resulted in initial inward current activation, usually a late outward current, and then an inward tail current measured at -80 mV (see Figure 5A inset, arrow). The tail current activated at

voltages above -30 mV (concomitant with I_{Ca}, see Figure 3D), reaching a peak around +15 mV (Figure 5A).

We next investigated if the pre-pulse voltage and thus activation of distinct voltage-dependent calcium currents (I_{CaS} and I_{CaT}) is correlated to tail current activation by clamping the LC to depolarized potentials which activate both currents (holding potential = -80 mV). We found that while using a holding potential of -80 mV (eliciting both I_{CaS} and I_{CaT}) results in a larger overall tail current (Figure 5B), holding at -40 mV (activating only I_{CaS}) still is sufficient to activate the tail current (Figure 5B) but reduced in magnitude approximately 35%. These results suggest that the tail current is activated by calcium influx via both I_{CaS} and I_{CaT}.

To measure the reversal potential of the tail current, inward current was activated with a depolarizing step from a holding potential of -40 mV up to +20 mV, and then the tail current clamped across a range of voltages from -85 mV to -20 mV (Figure 5C). Through these experiments we obtained an I-V curve based on measurements of the peak tail current, from which we extrapolated the reversal potential of the tail current to be approximately -30 mV (Figure 5D).

Finally, we investigated whether the tail current is sensitive to increases in intracellular calcium release. Figure 5E demonstrates that caffeine exposure (bath applied for 10 minutes at 10 mM), known to stimulate intracellular calcium release (Friel and Tsien, 1992b, a, Zhang and Harris-Warrick, 1995, Yoshimura, 2005) as well as an

increased level of calcium induced calcium release (Mironov and Usachev, 1991, Levi et al., 2003), causes an increase in the inward tail current (N = 4, P = 0.047). These results suggest that the tail current is indeed calcium-activated and not solely dependent on extracellular calcium influx via voltage-gated calcium currents. Taken together these results are very similar to the characteristics of the CAN current in lobster, including sensitivity to caffeine exposure(Zhang and Harris-Warrick, 1995), indicating the same current is indeed present in LC motor neurons of the crab.

TTX application reveals a largely non-inactivating TTX-sensitive current in LC motor neurons

During our experiments, we observed that in the presence of TEA and 4-AP, $CdCl_2$ alone does not consistently prevent all voltage-activated inward current (Figure 6A), but rather $CdCl_2$ and TTX combined are required to eliminate inward current (Figure 6A). These observations suggest that there is a TTX-sensitive current, distinct from spike-mediated sodium currents, involved in bursting in these cells. We attempted to voltage-clamp this current by subtracting the TTX sensitive inward current in both step and ramp voltage clamp protocols, with inconsistent results. Because of the small magnitude of the TTX-sensitive current (on the order of 2 nA or smaller, clamped from the soma), voltage-clamp protocols using step depolarizations often were not adequate to clearly characterize this current above background noise, though they did suggest the current is largely non-inactivating (Figure 6B). Voltage ramp protocols used before and after TTX (10^{-6} M, 30 min.) to isolate the TTX sensitive current during a -80 to +20 mV

ramp demonstrated TTX-sensitive current activation began at -37.5 mV ± 4.7 mV and peak activation occurred at 6 mV ± 3.2 mV (Figure 6B, N=3).

Because we had mixed success voltage-clamping the TTX-sensitive current, and because of its often smaller magnitude, we set out to determine whether this current plays an active role in the burst dynamics of LC motor neurons. To investigate this, we induced exaggerated burst potentials in isolated LCs by adding 50 mM TEA to the saline and generating large burst potentials with depolarizing current pulses (Figure 6C). These potentials are intrinsically driven because the depolarizing potential lasts longer than the brief current injection. After burst potentials were successfully generated, 10^{-6} M TTX was added, thus eliminating the TTX-sensitive inward current. In 6 out of 6 experiments, TTX administration completely eliminated these burst potentials (Figure 6C), supporting the presence of this current and suggesting an active role for this current in burst output. However, the exact impact of this TTX-sensitive current on burst dynamics in these cells is beyond the scope of this study. Nevertheless, it does appear that despite its small magnitude, this current is present and plays a role in the output of these cells.

Hyperpolarization-activated mixed cationic current (I_H)

We also employed hyperpolarized voltage steps in voltage-clamp, as well as negative current inject in current clamp, to investigate the presence of hyperpolarization-activated mixed cationic current (I_H) in the somata of these cells. Although relatively abundant mRNAs for the HCN channel have been detected in these cells (Tobin et al.

2009), we did not see any evidence for the H current in the somata of these cells (data not shown) for voltages as low as -120 mV from a holding potential of -40 mV.

Immunohistochemical localization of voltage-gated calcium channels in LC motor neurons

The crustacean CG LC burst potential is mediated by intrinsic conductances at least in part isolated to the LC somata. In many crustacean species this intrinsic burst, termed a driver potential, can be regularly elicited in an isolated LC somata with a short depolarizing current injection (Tazaki and Cooke, 1983a, Cooke, 2002b). However, in *C. borealis* CG the isolated LC soma will rarely fire an intrinsic burst without the application of potassium current blockers such as TEA. While outward currents are clearly present (Ransdell et al. 2012), our voltage-clamp showed relatively low calcium current levels in the LC somata. This could be due to the fact that the calcium channels are localized more distant to the soma, or reflect a low overall calcium current in the soma itself. Therefore, we sought to find if and to what degree calcium channels are localized to the LC somata. We used a pan-species primary antibody selective for high-voltage-activated calcium channels (i.e. L-type and P/Q-type) combined with fluorescence microscopy to investigate the distribution of CbCaV1/CbCaV2 channels in the cardiac ganglion. The 19-amino acid residue epitope against which the primary antibody was raised is a 100% amino acid identity match to CbCaV1 and matches 17 of 19 amino acids in CbCaV2 (Figure 7; see also Figure 1C). No similarity of the epitope to CbCaV3 or full length LCaV3 was detected via BLASTP comparison.

LC somata and their projections are stereotypically distributed and clearly identifiable in this preparation (see Figure 1C), making rudimentary subcellular localization fairly straightforward. We found clear punctate staining localized to the LC somata and to a lesser degree staining in the neurites extending from the LC somata (Figure 7). In all, 9 whole mount cardiac ganglion preparations were stained, and in each preparation we were able to detect punctate staining localized to the LC somata. Additionally, we often detected staining in the processes of the anterior branch point of the ganglion (Figure 7C), where synaptic connectivity seems to be most prevalent amongst the cells of the *C. borealis* cardiac ganglion. We performed additional DAPI staining within these preparations to determine whether the punctate immunoreactivity on the somata may be the result of glia or other support cells positively staining. Immunofluorescence + DAPI overlays showed no evidence of overlapping fluorescence to indicate this was the case (e.g. see Figure 7D2). We also performed secondary antibody-only incubations that showed no significant fluorescence indicative of non-specific signal attributable to the secondary antibody. Finally, pre-absorption of the primary antibody with the antigen peptide eliminated immunolabeling as well.

Discussion

The crustacean LC is a valuable model for studying motor neuron burst organization. The robust nature of the LC somata in electrophysiology experiments and segregation from action potential conductances as well as other network components

make these cells ideal in experiments (Hartline, 1967b, Cooke, 2002b). However, a detailed understanding of the ionic conductances and their underlying ion channels, particularly depolarizing conductances, is lacking in these cells. Here we report the results of sequence from three voltage-gated calcium channel alpha-subunit genes in the crab, *Cancer borealis*, and then characterize their expression as well as the depolarizing currents present in LC motor neurons of the cardiac ganglion. While we detect mRNA for three different channel types in individual LCs, we measured and can distinguish only two distinct voltage-activated calcium currents in LC somata. We additionally identified a calcium-activated nonspecific cationic current (CAN) as well as a TTX sensitive persistent inward current in these cells. Finally, we performed immunostaining that demonstrates the high voltage-activated calcium channels described are at least partially localized to the LC somata.

Sequence analysis reveals that the three calcium channel alpha subunits in this study, namely CbCaV1, CbCaV2, and CbCaV3, correspond very closely to identified calcium channel subunits of the snail, *L. stagnalis* (LCaV1, LCav2, and LCaV3) respectively. Thorough sequence and expression analyses of these snail channels have been performed, and the resulting current properties and kinetics of each channel reported (Spafford et al., 2003, Spafford et al., 2006, Senatore and Spafford, 2010). Based on the extensive similarities between these expressed snail currents and the native crab currents characterized in our study, we are confident that we can use this analysis to infer the identity of these channels and currents. The characteristics of crab LC I_{CaS}, a slowly inactivating high-voltage activated calcium current, are very similar to the current carried

by the LCaV1 channel(Spafford et al., 2006), which has been classified as an invertebrate L-type calcium channel and current. Therefore, based on the similarities in sequence between CbCaV1 and LCaV1, and the similarities between crab I_{CaS} and current carried by LCaV1, we suggest that CbCaV1 encodes an L-type calcium current with the properties described here as the slow calcium current, I_{CaS}. Similarly, the characteristics of crab I_{CaT}, a transient inactivating high-voltage activated calcium current, are very similar to the current carried by the LCaV2 channel(Spafford et al., 2003), which has been classified as an invertebrate calcium channel with biophysical characteristics found in mammalian P/Q and N-type channels. Based on the similarities in sequence between CbCaV2 and LCaV2, and the similarities between crab I_{CaT} and current carried by LCaV2, we suggest that CbCaV2 encodes a P/Q-type calcium current with the properties described here as the transient calcium current I_{CaT}.

The two voltage gated calcium currents (I_{CaS} and I_{CaT}) both were present in experiments where the LC soma was isolated, indicating that these channels are present in the LC somata. This result is supported by immunohistochemistry experiments where high voltage activated calcium channel antibody was used to stain entire CG, resulting in immunostaining largely localized to the LC soma, although some staining also could be seen on neuronal processes in different regions of the ganglia. These results are also consistent with previous immunolocalization of calcium channel subunits in the lobster stomatogastric ganglion; Ca1A (P/Q-type) and Ca1D (L-type) immunoreactivity both were localized to STG somata, as well as primary neurites (French et al. 2002).

Calcium currents previously have been studied in crustacean motor neurons, particularly in the STG. Total calcium current has been characterized in STG neurons of two species of lobster (Turrigiano et al. 1995; Zhang and H-W 1995; Johnson et al. 2003), as well as crab (Golowasch and Marder 1992; Hurley and Graubard 1998). However, across these studies there are species and cell-specific differences in the calcium current types reported. For example, Hurley and Graubard (1998) specifically searched for, but failed to find, two distinct calcium currents with differing kinetics in the somata of STG neurons of the crab, *Cancer productus*. However, Turrigiano et al. (1995) measured calcium currents in isolated STG neurons of the lobster *Panulirus interruptus* in culture and noted both transient and persistent components to these currents, ultimately deciding to model calcium current in these cells as two separate components. Much of these discrepancies also may be explained by the fact that these inward currents have been, and continue to be, difficult to characterize in voltage clamp (Golowasch and Marder 1992; Turrigiano et al. 1995). Here, with the additional insight of molecular biology and a scaffolding of comparison provided by work in *L. stagnalis*, we believe we have made substantial progress toward a better understanding of these complex native currents in crustacean motor neurons.

Beyond the voltage-activated calcium currents, LCs also possess a calcium-activated inward current represented by the CAN current. The calcium activated non-specific cationic current is found in a variety of excitable cell types (Partridge and Swandulla, 1988) but is often implicated in neuronal bursting (Swandulla and Lux, 1985, Wilson et al., 1998, Rubin et al., 2009). This current in invertebrates has been best

characterized in crab STG (dorsal gastric) neurons. In these cells, the current is important in coordinating bistability of output; voltage-gated calcium currents allow calcium influx which activates I_{CAN}, inducing plateau potentials indicative of the output of these cells (Zhang and Harris-Warrick, 1995, Zhang et al., 1995). LC motor neurons of the cardiac ganglion do not undergo plateau potentials during normal network output, so this is unlikely the role of this current in the cardiac output. While we do not yet know the role of I_{CAN} in the cardiac motor neurons, a model for similar rhythm generation in mammalian pre-Bötzinger complex invokes CAN current as vital in triggering network-wide bursts after recurrent synaptic excitation - a role which may have parallels to CAN current in LCs (Del Negro and Hayes, 2008).

Finally, we also report for the first time in crab LCs a largely non-inactivating TTX sensitive current, that is necessary for driver potential generation in these cells, which could indicate the presence of a persistent sodium current (I_{NaP}). I_{NaP} currents are often implicated in burst potential generation. In mammalian pre-Bötzinger neurons, I_{NaP} presence is known to be important in burst generation and its relationship with leak conductances is thought to dictate whether the neuron spontaneously bursts or requires excitatory input (Del Negro et al., 2002a, Del Negro et al., 2002b). There is evidence that DG neurons of the STG contain I_{NaP} important to plateau potential generation (Elson and Selverston, 1997) and a TTX sensitive persistent current has been voltage clamped in cultured STG cells (Turrigiano et al., 1995). While there is no channel gene known to directly mediate this current, indeed there is only one voltage gated sodium channel known in invertebrates (Loughney et al., 1989, Olson et al., 2008), there is the possibility

that the I_{NaP} current is mediated by the same channel population as the fast inactivating sodium current as seen in rat tuberomammillary neurons (Taddese and Bean, 2002). However, because there are no spike-mediating sodium currents in these crustacean motor neuron somata (Golowasch et al. 1992), it seems unlikely that these persistent sodium currents represent a window in fast-spiking sodium currents. Rather, it seems more likely that a distinct channel isoform could mediate these currents, perhaps as a result of a splice variant (Lin et al., 2009) or RNA editing event (Liu et al., 2004) of the previously identified CbNaV channel (Dai et al., 2010).

The specific roles of the inward currents in these cells, especially those which are calcium-mediated, are still to be experimentally determined. The crustacean cardiac motor neurons share extensive similarities with other excitatory central pattern generator circuits. For example, over 90% of rat pre-Bötzinger complex neurons elicit burst potentials only when driven by excitation; and like LC motor neurons these neurons also express I_{CAN}, I_{NaP}, and intrinsic calcium currents (Del Negro et al., 2002b, Pena et al., 2004, Morgado-Valle et al., 2008). Whether the CG network LC burst potential is a result of summed EPSPs or requires some or all of these intrinsic inward components to generate its intrinsic burst potential is currently under investigation (Ball et al., 2010a, Franklin et al., 2010).

The depolarizing components found in the LC bursting neurons are prevalent across animal phyla especially in those neurons which are also bursters. The experimental advantages of the crustacean CG and the simplicity of the network make it an ideal

system to study how these components interact with each other and other network characteristics to shape and maintain output. In characterizing the inward components of *C. borealis* LC motor neuron, we obtain critical information to now move forward in investigating how the LC intrinsic components function within the rest of the cardiac network, and how this model can be applied broadly to understand neural network function in general.

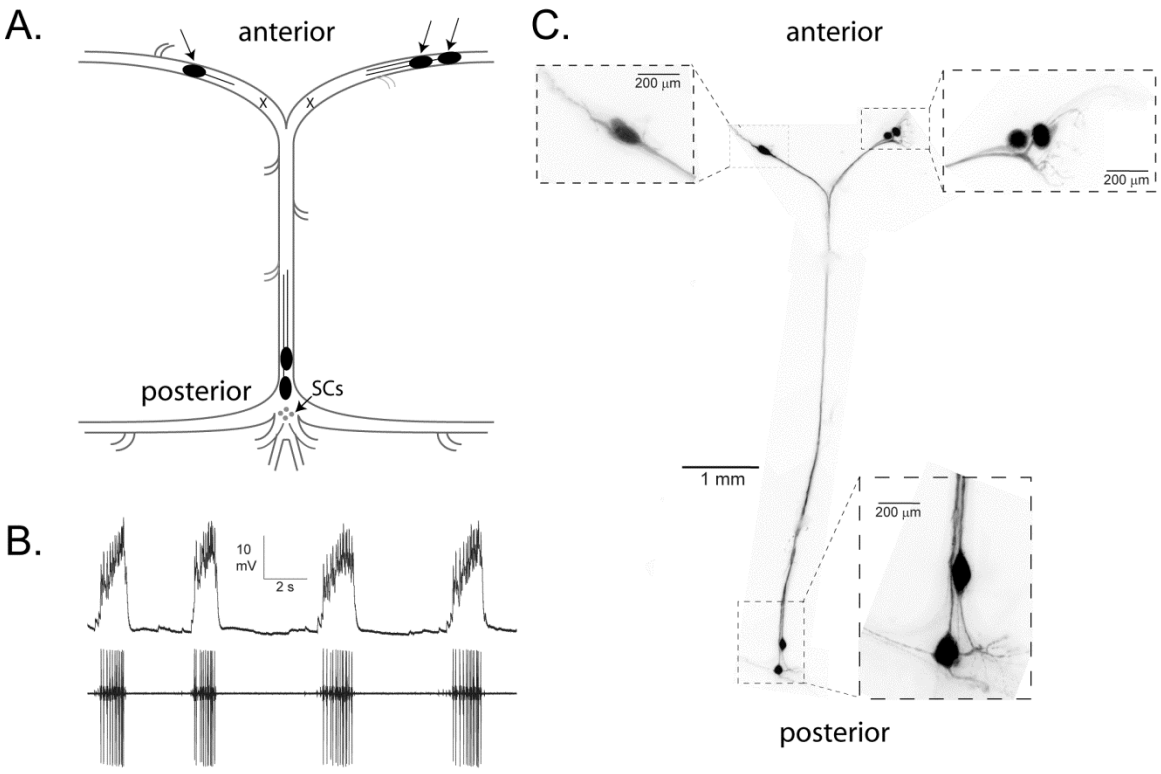

FIGURE 1.1 The crustacean cardiac ganglion as a model system. A. Schematic showing the location of the 5 LC motor neurons (black ovals), with the anterior cells used in this study marked with black arrows. The somata of these anterior large cells were isolated from the remainder of the ganglion via thread ligatures placed at the branch points labeled by "X". Small cell (SC) pacemakers are indicated as well. **B.** Electrophysiological recording showing the endogenous network activity, with a simultaneous intracellular recording of a LC3 motor neuron (top trace) with an extracellular recording of the entire network output (bottom trace). **C.** Dye fills (AlexaFluor 568) of the 5 LC motor neurons of an intact cardiac ganglion, showing the relative locations as well as clarity with which LC somata can be identified visually.

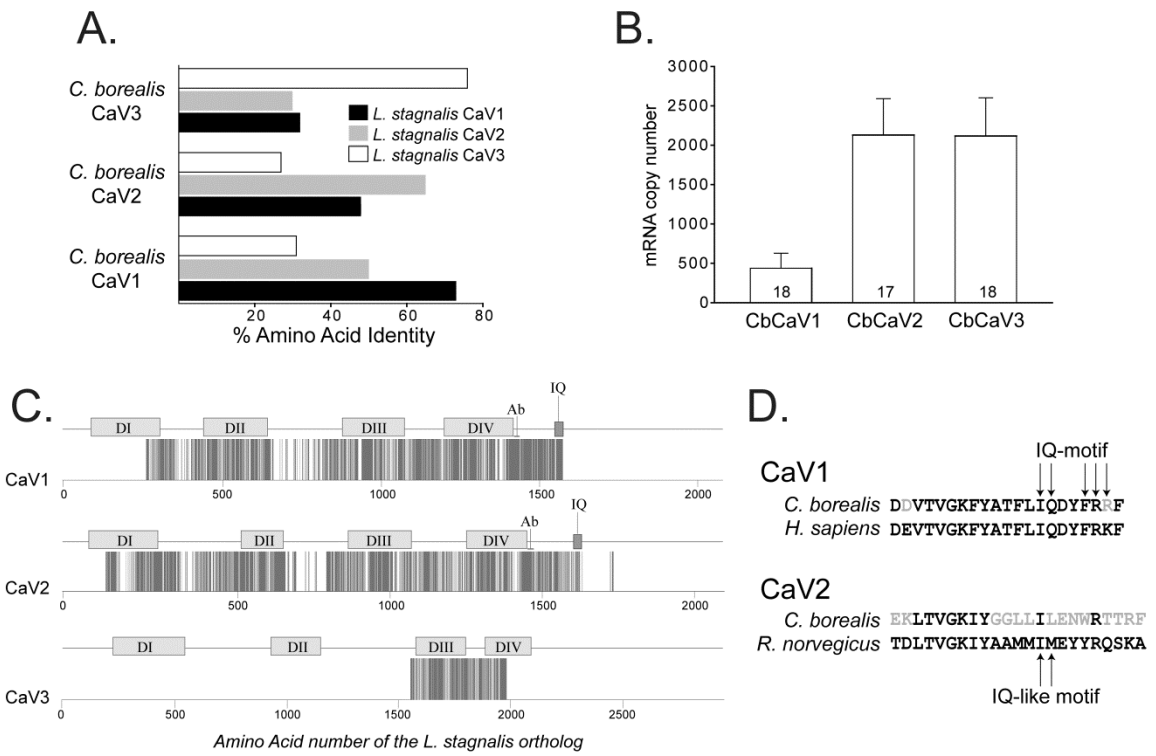

E.

	DOMAIN I	DOMAIN II	DOMAIN III	DOMAIN IV
Consensus Cav2.1	QCITMEGWTDVLY	VFQILTGEDWNEVMY	LFTVSTGEGWPQVL	LFRSATGEAWQEIML
C. borealis Cav2	QCITQEGWTAILY	VFQILTGEDWNEVMY	LFAVQTGEGWPQVL	LFRCATGEAWQSIML
Consensus Cav1.2	QCITMEGWTDVLY	VFQILTGEDWNEVMY	LFTVSTGEGWPQVL	LFRSATGEAWQEIML
C. borealis CaV1	QCITMEGWTDMMY	VFQILTGEDWNVVMY	LFTVSTFEGWPGVL	LFRSATGEAWQEIML

	DOMAIN III
Consensus Cav3.2	LFVLSSKDGWVNIMY
C. borealis Cav3	LFVLSSKDGWVNIMY

FIGURE 1.2 Sequencing of voltage-gated calcium channel alpha subunits from *Cancer borealis*. **A.** Percent amino acid identity for sequence obtained of putative CbCaV channel genes and their orthologs in the snail, *Lymnaea stagnalis*. **B.** Mean (± SD) single LC copy number for CbCaV1, CbCaV2, and CbCaV3 mRNAs. Samples sizes as shown in each bar. **C.** Graphical amino acid alignment between full-length *L. stagnalis* protein sequence for each voltage-gated calcium channel subtype (amino acid position represented by the x-axes) and the corresponding portion identified in *C. borealis*. Identical amino acids, as quantified in Fig 2A, are denoted with a vertical bar at each amino acid position along the x-axis. Putative transmembrane domains (DI – DIV), the IQ-binding domain (IQ), and the epitope to which the primary antibody was made (Ab) are denoted above each channel sequence. **D.** Amino acid alignments of the IQ- and IQ-like binding domains of CbCaV1 and CbCav2 with human (Accession: 2BE6_D) and rat (Accession: NP_037050.2) orthologs respectively. Gray residues indicate differences in the crab sequence relative to mammal sequence. Arrows denote key residues identified in modulating properties of these channels with respect to calcium-dependent inactivation in mammalian systems (described in text). **E.** Sequence alignments of the pore-forming loops of consensus mammalian sequence from alpha subunits for Cav2.1, Cav1.2, and Cav3.2 with the corresponding *C. borealis* ortholog. Gray boxes highlight the position of EEEE (HVA channels) or EEDD loci (LVA channels) in each domain of the channel subunit that confer divalent cation selectivity. Sequence from CbCaV3 (inset box) was sufficient only for comparison of Domain III.

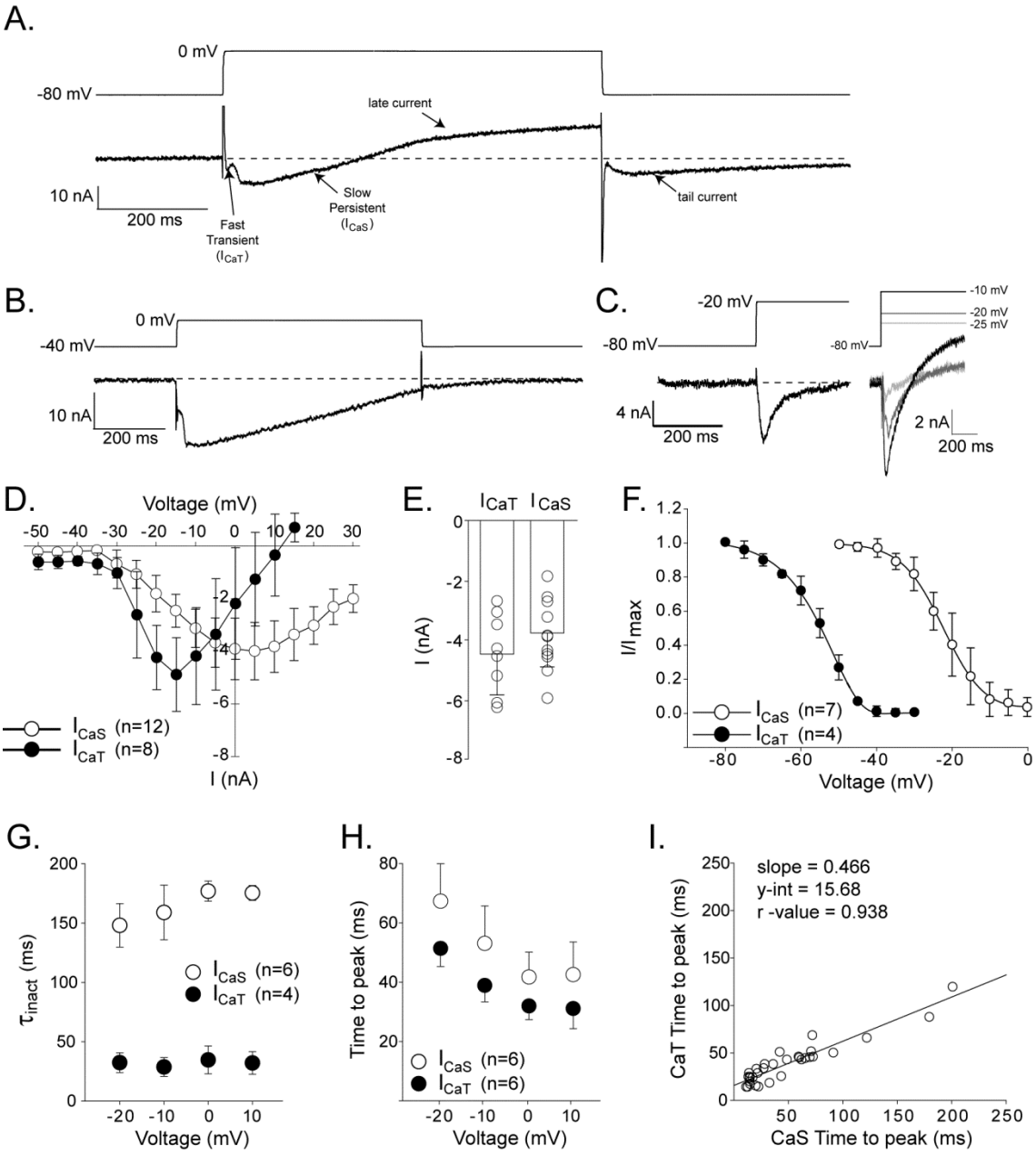
A.
0 mV
-80 mV
late current
10 nA
200 ms
Fast Transient (I_{CaT})
Slow Persistent (I_{CaS})
tail current
B.
0 mV
-40 mV
10 nA
200 ms
C.
-20 mV
-80 mV
-10 mV
-20 mV
-25 mV
-80 mV
4 nA
200 ms
2 nA
200 ms
D.
Voltage (mV)
-50 -40 -30 -20 -10 0 10 20 30
I_{CaS} (n=12)
I_{CaT} (n=8)
I (nA)
E.
I_{CaT} I_{CaS}
I (nA)
F.
I/I max
I_{CaS} (n=7)
I_{CaT} (n=4)
Voltage (mV)
G.
τ_{inact} (ms)
I_{CaS} (n=6)
I_{CaT} (n=4)
Voltage (mV)
H.
Time to peak (ms)
I_{CaS} (n=6)
I_{CaT} (n=6)
Voltage (mV)
I.
slope = 0.466
y-int = 15.68
r -value = 0.938
CaT Time to peak (ms)
CaS Time to peak (ms)

FIGURE 1.3 Properties of voltage-gated calcium currents in LC motor neurons. A. Raw trace of total current elicited at 0 mV from a holding potential of -80 mV in saline containing TEA, 4-AP, and TTX. Four distinct aspects of the total current are labeled, including a "transient" inward (I_{CaT}), "slow"-inactivating inward (I_{CaS}), late outward (late current), and an inward tail current (tail current). The voltage trace used to elicit the current trace is shown above the current recording. **B.** Typical recording of I_{CaS} at 0 mV from a holding potential of -40 mV in saline containing TEA, 4-AP, TTX and Cs^+ loaded to reduce K^+ currents to the minimum possible. The voltage trace used to elicit the current is shown above the current recording. **C.** Representative recording of I_{CaT} at -20 mV from a holding potential of -80 mV in saline containing TEA, 4-AP, TTX and Cs^+ loaded to reduce K^+ currents to the minimum possible. The voltage trace used to elicit the current is shown above the current recording. -20 mV allowed us the best recordings of I_{CaT} with a minimal contamination of I_{CaS}, as the current shown is the result of a subtraction of current elicited from holding potential of -40 mV (i.e. I_{CaS}) from the current elicited from a holding potential of -80 mV ($I_{CaS} + I_{CaT}$). We also provide representative traces of voltage-dependent activation of this current at -25 mV, -20 mV, and -10 mV. **D.** The mean (± SD) I-V relationship for I_{CaS} and I_{CaT} indicating the voltage dependence of activation. **E.** Mean (± SD) current levels for I_{CaS} and I_{CaT} across LC motor neurons. Individual points represent one cell. These data are from the same cells used to generate the I-V curves in Fig. 3D (N's as described). I_{CaS} measurements were taken at 0 mV, while I_{CaT} at -20 mV. **F.** Mean (±SD) I-V relationships for voltage dependence of inactivation of I_{CaS} and I_{CaT} as shown by normalized currents measured at 0 mV and -20 mV respectively, from a varying holding potential plotted on the X-axis. **G.** Mean (±SD) time constant of inactivation of I_{CaS} and I_{CaT} as a function of voltage. **H.** Mean (±SD) time to peak current of I_{CaS} and I_{CaT} as a function of voltage. **I.** Correlation of time to peak current of I_{CaS} and I_{CaT} across voltages from -20 to +10 mV (data are from cells used in Figure 2H). R-value is the result of a Pearson correlation test.

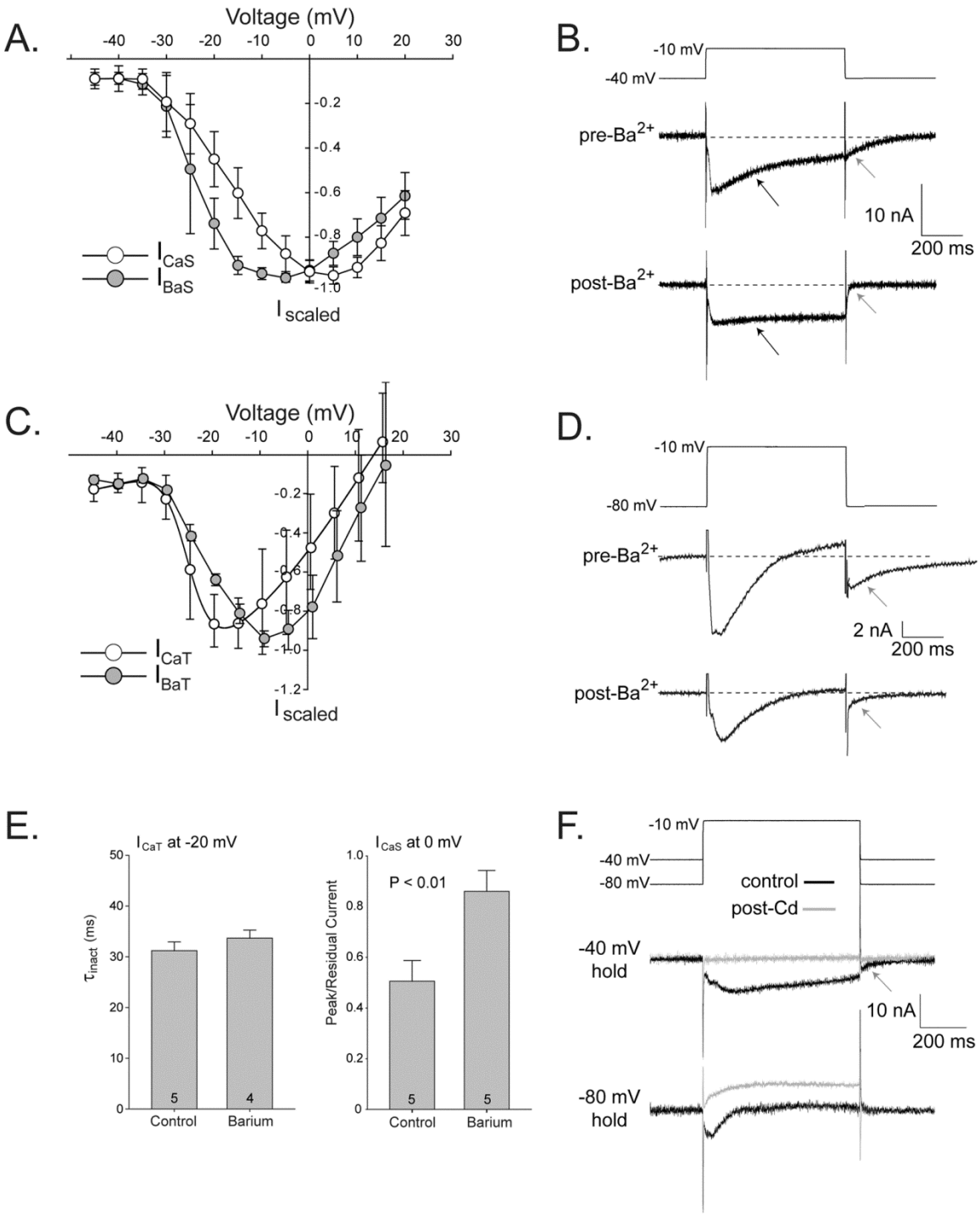
A.
Voltage (mV)
-40 -30 -20 -10 0 10 20 30
-0.2
-0.4
-0.6
-0.8
-1.0
I CaS
I BaS
I scaled
B.
-10 mV
-40 mV
pre-Ba2+
10 nA
200 ms
post-Ba2+
C.
Voltage (mV)
-40 -30 -20 -10 0 10 20 30
-0.2
-0.4
-0.6
-0.8
-1.0
-1.2
I CaT
I BaT
I scaled
D.
-10 mV
-80 mV
pre-Ba2+
2 nA
200 ms
post-Ba2+
E.
I CaT at -20 mV
τ inact (ms)
50
40
30
20
10
0
5
4
Control
Barium
I CaS at 0 mV
P < 0.01
Peak/Residual Current
1.0
0.8
0.6
0.4
0.2
0
5
5
Control
Barium
F.
-10 mV
-40 mV
-80 mV
control
post-Cd
-40 mV
hold
10 nA
200 ms
-80 mV
hold

FIGURE 1.4 Barium currents in LC motor neurons. A. The mean (± SD) I_{scaled} -V relationship for I_{CaS} (N = 8) and the corresponding current in barium substituted saline (N = 4). Because post-Ba2+ currents often varied much greater in magnitude relative to native Ca2+ currents, we plotted normalized currents to allow direct comparison of activation characteristics. Scaled currents are normalized relative to the peak current in each cell by dividing I_{Ca} or I_{Ba} at a given voltage by the absolute value of I_{peak} for each cell. **B.** Typical recordings of I_{CaS} at -10 mV from a holding potential of -40 mV before (pre-Ba^{2+}; top trace) and after (post-Ba^{2+}; bottom trace) barium substitution. *Black* arrows show the apparent loss or decrease of inactivation in this current after barium substitution, *gray* arrows show the loss of tail current after barium substitution. **C.** The mean (± SD) I_{scaled} -V relationship for I_{CaT} and the corresponding current in barium substituted saline (N = 5 for both). Currents were scaled as in panel A. **D.** Typical recordings of I_{CaT} at -10 mV from a holding potential of -80 mV before (pre-Ba^{2+}; top trace) and after (post-Ba^{2+}; bottom trace) barium substitution. *Gray* arrows again show the loss of tail current after barium substitution. **E.** Quantification (mean ± SD) of changes in inactivation time constant for I_{CaT} (*left*) and the ratio of peak to residual I_{CaS} (*right*) following barium substitution. Sample sizes as indicated in each bar. Significant differences are reported for the results of a paired t-test. **F.** Effects of cadmium chloride on I_{CaS} and I_{CaT}. All four traces taken from the same cell before and after cadmium exposure. -40 mV hold traces are unsubtracted. -80 mV traces represent the difference current before and after cadmium, as obtained by subtracting the current from the -40 mV hold from the -80 mV hold to get the difference current. One representative cell is shown, but this experiment was performed N = 4 times. *Gray* arrow shows the loss of tail current after cadmium substitution.

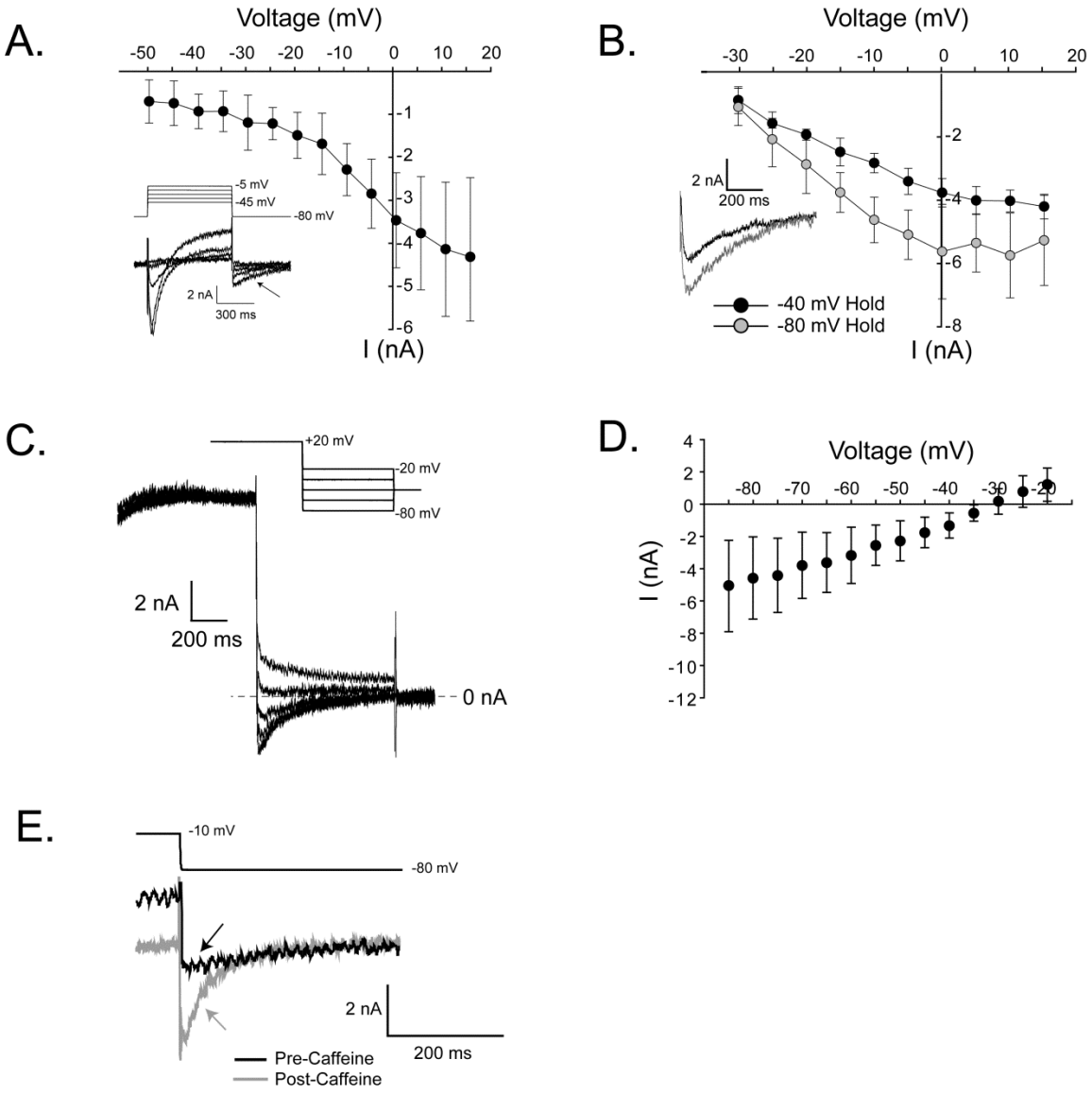
A.
Voltage (mV)
-50 -40 -30 -20 -10 0 10 20
-1
-2
-3
-4
-5
-6
-5 mV
-45 mV
-80 mV
2 nA
300 ms
I (nA)
B.
Voltage (mV)
-30 -20 -10 0 10 20
-2
-4
-6
-8
2 nA
200 ms
-40 mV Hold
-80 mV Hold
I (nA)
C.
+20 mV
-20 mV
-80 mV
2 nA
200 ms
0 nA
D.
Voltage (mV)
-80 -70 -60 -50 -40 -30 -20
I (nA)
4
2
0
-2
-4
-6
-8
-10
-12
E.
-10 mV
-80 mV
2 nA
200 ms
Pre-Caffeine
Post-Caffeine

FIGURE 1.5 Properties of calcium activated nonselective cationic current (CAN) in LC motor neurons. Recordings were made in saline containing TEA, 4-AP, TTX, and cells loaded with Cs^+. **A.** Mean (±SD) I-V relationships for activation of I_{CAN} measured at -80 mV from a varying depolarizing pulse potential (x-axis) to elicit calcium currents (holding potential of -80 mV, N = 5). *Inset:* Typical recordings of the total current, including tail current (black arrow) elicited from these voltage protocols. **B.** Mean (±SD) I-V relationships for activation of I_{CAN} from holding potentials of -40 mV (black circles) activating predominantly I_{CaS} or -80 mV (gray circles) which activates both I_{CaS} and I_{CaT} (N = 3) *Inset:* representative tail currents in the same cell elicited from a holding potential of -40 mV (black trace) or -80 mV (gray trace). **C.** Typical recordings used to measure the reversal potential of tail current. Current traces were obtained by depolarizing the LC neuron from a holding potential of -50 mV to +20 mV and then measuring tail currents at varying tail holding potentials from -80 mV to -20 mV (as shown in the voltage traces). **D.** Mean (±SD) I-V relationships used to interpolate the reversal potential (dotted line) of these tail currents (N = 8). **E.** Caffeine-evoked increase in tail current amplitude in LCs. Recording of tail currents from a holding potential of -80 mV before (black trace/arrow) and after (gray trace/arrow) bath application of 10 mM caffeine (this experiment was performed N = 4 times).

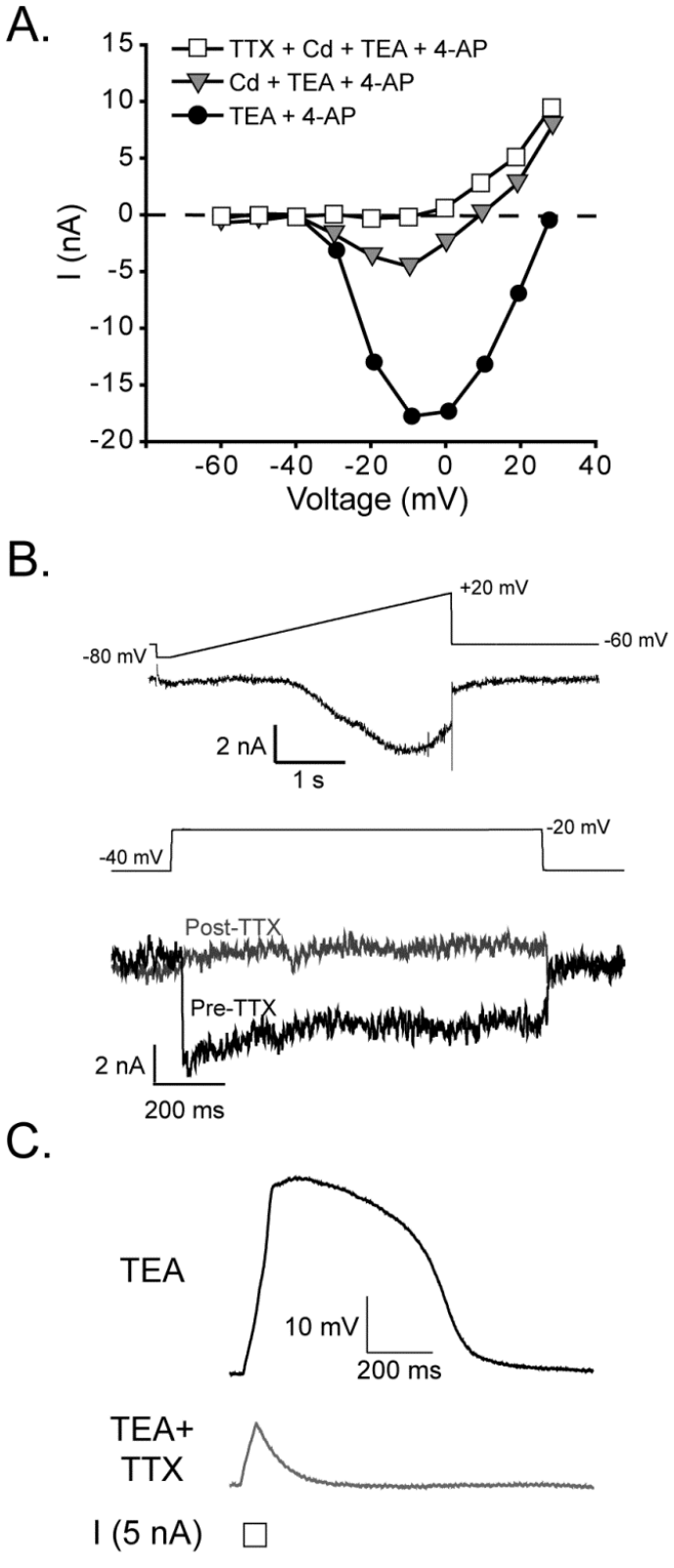
A.
TTX + Cd + TEA + 4-AP
Cd + TEA + 4-AP
TEA + 4-AP
I (nA)
Voltage (mV)
B.
+20 mV
-80 mV
-60 mV
2 nA
1 s
-20 mV
-40 mV
Post-TTX
Pre-TTX
2 nA
200 ms
C.
TEA
10 mV
200 ms
TEA+
TTX
I (5 nA)

FIGURE 1.6 TTX-sensitive persistent current in LC motor neurons. A. I-V relationship in a LC motor neuron indicating the presence of a TTX-sensitive current. Inward currents were measured from a holding potential of -40 mV at depolarizing voltage steps under subsequent blocker conditions. Currents first were elicited in TEA + 4-AP (black circles), then Cd^{2+} was added to block calcium currents (gray triangles), revealing a residual inward current that was subsequently blocked with TTX (white squares). **B.** Representative recording of TTX-sensitive current elicited in saline containing TEA, 4-AP, and Cd^{2+} with a -80 mV to +20 mV voltage ramp, and then subtracted from this current was the same voltage ramp with the addition of TTX (top trace) N = 3. Step depolarizations also reveal a persistent TTX sensitive inward current. *Gray trace*- inward current in the presence of $CdCl_2$; *black trace*- current after the addition of 10^{-6}M TTX (bottom trace) N =4. **C.** TTX-sensitive current is necessary for burst potential generation in LC motor neurons. Exaggerated driver potentials are elicited in 50 mM TEA and a short depolarizing current injection (5 nA, 50 ms; top trace). These driver potentials are eliminated in the presence of TTX, even though calcium currents remain intact (bottom trace) N = 6.

Anti-Ca(v) Pan-α1	DNFDYLTRDWSILGPHHLD
CbCaV1	DNFDYLTRDWSILGPHHLD
CbCaV2	DNFDYLTRDSSILGAHHLD

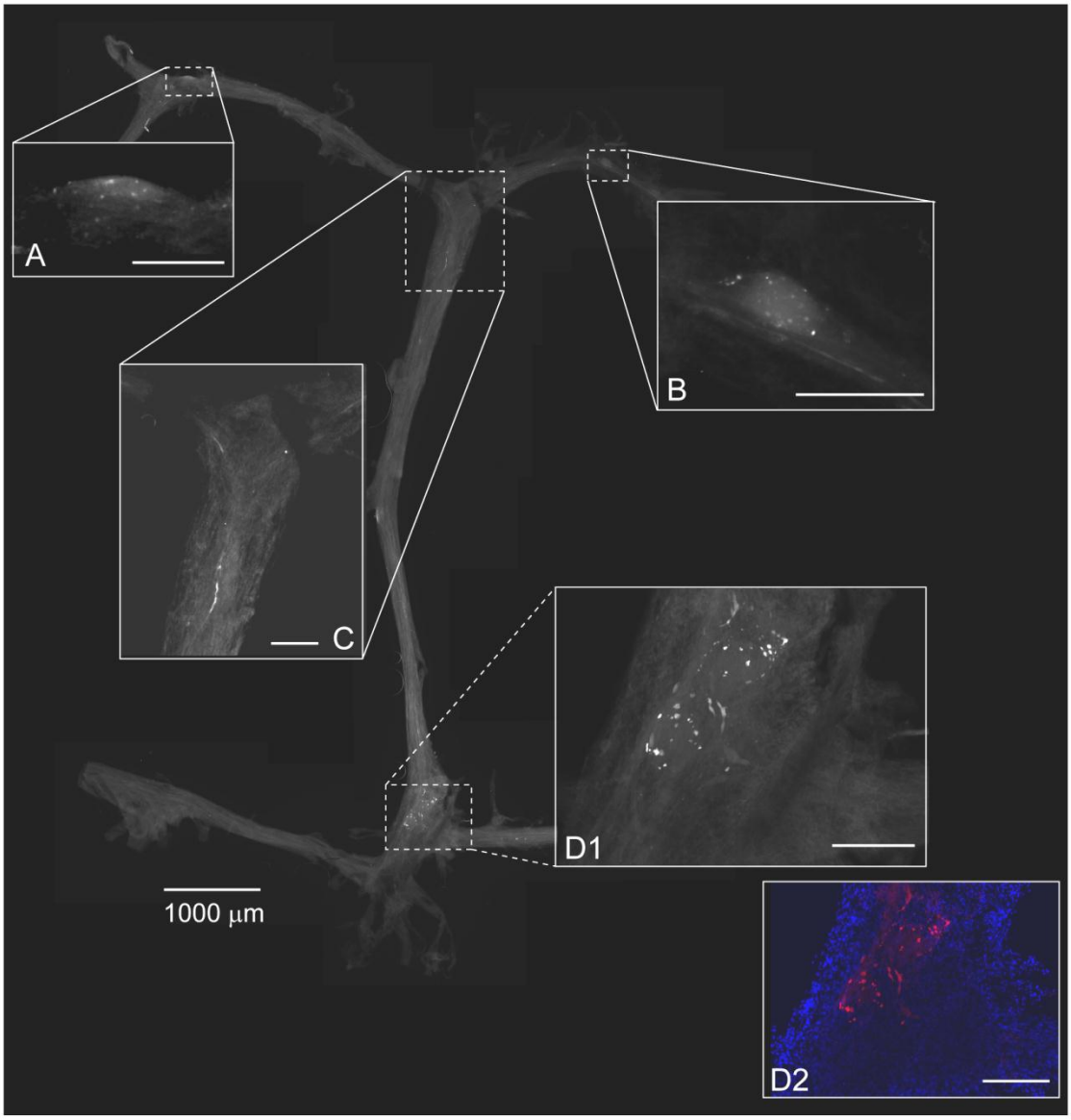

FIGURE 1.7 High-voltage activated calcium channels (HVACC) are localized to the somata of LC motor neurons. We used an Anti-CaV Pan-α1 primary antibody to detect putative HVACC immunoreactivity in the cardiac ganglion. The alignment of the antibody epitope with the corresponding amino acid sequence in CbCaV1 and CbCaV2 is shown at the top of the figure. The entire cardiac ganglion is shown based on assembled tiled images taken at 4x magnification. Insets are magnified images of the corresponding portion of the ganglion marked with dashed boxes. We detected immunoreactivity for HVA calcium channels in the somata of all five LC motor neurons. A and B. HVACC immunoreactivity in anterior LCs appears to be localized to the somata, consistent with the ability to measure these currents in isolated LC somata. C. Immunoreactivity was also detected in processes of neurons in the cardiac ganglion, particularly in the anterior branch point. D1. The paired posterior LC neurons also showed immunoreactivity apparently localized to the somata, which (D2) is not the result of glial or support cell staining as revealed by co-localization of immunoreactivity (RED) and DAPI counter stain (BLUE). Scale bars in insets all represent 200 μm.

CHAPTER TWO

Rapid homeostatic plasticity of intrinsic excitability in a central pattern generator network stabilizes functional neural network output

Neurons and networks undergo a process of homeostatic plasticity that stabilizes output by integrating activity levels with network and cellular properties to counter longer-term perturbations. Here we describe a rapid compensatory interaction among a pair of potassium currents, I_A and I_{KCa}, that stabilizes both intrinsic excitability and network function in the cardiac ganglion of the crab, *Cancer borealis*. We determined that mRNA levels in single identified neurons for the channels which encode I_A and I_{KCa} are positively correlated, yet the ionic currents themselves are negatively correlated, across a population of motor neurons. We then determined that these currents are functionally coupled; decreasing levels of either current within a neuron causes a rapid increase in the other. This functional interdependence results in homeostatic stabilization of both the individual neuronal and the network output. Furthermore, these compensatory increases are mechanistically independent, suggesting robustness in the maintenance of neural network output that is critical for survival. Taken together, we

generate a complete model for homeostatic plasticity from mRNA to network output where rapid post-translational compensatory mechanisms acting on a reservoir of channels proteins regulated at the level of gene expression provide homeostatic stabilization of both cellular and network activity.

The balance of plasticity and stability in generating appropriate output is a matter of fundamental importance in the nervous system across all functional levels. These processes occur even at the most fundamental level, the excitability of individual neurons, and yet little is known about mechanisms governing these processes (Marder, 2011b, Turrigiano, 2011b). Early work identified such processes of "homeostatic plasticity" of intrinsic excitability (LeMasson et al., 1993, Turrigiano et al., 1994, Turrigiano et al., 1995, Golowasch et al., 1999), but subsequent focus more intensely shifted to determining how stabilization of synapses is accomplished through synaptic scaling (Turrigiano, 2012). Recently, a resurgence of interest in plasticity of intrinsic excitability has accompanied work on synaptic scaling (Debanne and Poo, 2010, Misonou, 2010, Turrigiano, 2011b).

Fewer studies on homeostatic plasticity have considered functional compensation in the context of endogenous network activity. The most dramatic example may be complete recovery of motor network output following loss of central inputs as a result of changes in conductances in the crustacean stomatogastric ganglion (STG) (Thoby-Brisson and Simmers, 1998, 2002). Knockouts of K^+ channels in mice have been shown to have modest effects on phenotype and cellular output as a result of compensation by

other K^+ channels (Guo et al., 2005, Nerbonne et al., 2008). Additionally, overexpression of A-type K^+ channels in STG neurons results in little change in neuronal output as a result of compensatory increases in H-current (MacLean et al., 2003, MacLean et al., 2005). However, these examples feature mechanisms that act over longer time scales of days to weeks. While initial reports of plasticity in intrinsic excitability were found over shorter time scales (Desai et al., 1999, Golowasch et al., 1999), surprisingly little is known of the role these mechanisms may play in short-term ongoing activity of biologically intact networks, specifically where an expectation for rapid conservation of output could be argued, such as in central pattern generators (CPGs).

Compensation in CPG circuits may be inferred from the fact that normal populations of unmanipulated motor neurons of two invertebrate CPGs, the cardiac and stomatogastric ganglia, show correlations in expression levels of mRNAs for ion channels (Schulz et al., 2007a, Tobin et al., 2009) and membrane conductances (Khorkova and Golowasch, 2007, Temporal et al., 2012). One relationship detected in previous work (Tobin et al., 2009) is a positive correlation between *BKKCa* and *shaker* mRNA levels in neurons of the cardiac ganglion. These channels encode calcium-activated and A-type K^+ currents, respectively. However, it is unclear how a neuron would use two similar hyperpolarizing conductances additively to generate or maintain its output. In this study we focused on elucidating the functional relationship between these two conductances in motor neurons of the crab cardiac ganglion. We discovered a striking discrepancy in the relationship of these channels across functional levels: mRNAs for these channels were *positively* correlated, while their conductances were

negatively correlated. Therefore, we propose a comprehensive hypothesis for plasticity of excitability from mRNA to network output whereby rapid compensation provides stabilization of cellular and network activity.

MATERIALS AND METHODS

Animals

Cancer borealis crabs of either sex were purchased and shipped overnight from The Fresh Lobster Company (Gloucester, MA). Crabs were kept between 24 hours and two weeks in artificial sea water at 12 °C before use. Crabs were anesthetized in ice for 15 minutes prior to the dissection. The dissection took place in chilled physiological saline comprised of 440 mM NaCl, 26 mM $MgCl_2$ 13 mM $CaCl_2$, 11.2 mM Trizma base, 11 mM KCl, and 5 mM Maleic acid (pH = 7.4). When we wanted to isolate individual large cells, individual strands of bulking nylon were used to ligate the nerve on both sides of a large cell soma. To impale large cells, each cell was individually desheathed using a tungsten needle (Fine Science Tools, Foster City CA).

Quantitative single-cell RT-PCR

Quantitative RT-PCR was performed as previously described (Schulz et al., 2006a; Tobin et al., 2009). Primers specific for real–time PCR detection of *shal*, *BKKCa*, *shab*, and *shaker* using Sybr Green were developed and designed using Primer3 software

and are the same as previously reported (Schulz et al., 2006a; Tobin et al., 2009). Briefly, total RNA was isolated using RNeasy micro column based RNA extraction kit (Qiagen, Valencia, CA), reverse transcribed using SuperScript III reverse transcriptase (Invitrogen), and used as a template in real-time RT-PCR with Sybr Green (SABiosciences, Frederick, MA) in a RotorGene 3000 real-time PCR machine (Corbett Research, Australia). Previous studies have determined that in LC motor neurons, correlations can be equally well detected among channel mRNA levels with and without normalization of real-time results to 18S rRNA (Tobin et al., 2009). Values reported here are total copy numbers from a single neuron, and are not normalized with respect to 18S levels.

Pharmacology

Pharmacological blockers were dissolved in physiological saline and perfused onto the cardiac ganglion using a Rabbit peristaltic pump (Rainin Instruments Company, Oakland, CA) at a rate of 1.5 mL / min or added to the preparation from a stock solution via pipette. The following pharmacological agents were used: tetraethylammonium dissolved in saline at 25mM, 4-aminopyridine dissolved in saline at 1mM, cadmium chloride dissolved in saline at 250μM (Acros Organics, Geel, Belgium), tetrodotoxin dissolved in saline at 1μM (Alomone Labs, Jerusalem, Israel), BAPTA-AM dissolved DMSO and applied at 30μM in saline, ryanodine dissolved DMSO and applied at 100μM in saline, staurosporine dissolved in DMSO and applied at 5μM in saline, okadaic acid dissolved inDMSO and applied at 500nM in saline (Ascent Scientific; Cambridge, MA),

cyclosporine A dissolved in DMSO and applied at 2μM in saline (Tocris Biosciences, Minneapolis, MN). All DMSO applications resulted in a final concentration of DMSO that was <1% (range: 0.000025% to 0.5%).

Pharmacological agents used to investigate intracellular mechanisms involved in the compensatory response (BAPTA-AM, ryanodine, okadaic acid, cyclosporine A, staurosporine) were applied to the cardiac ganglion 1 hour prior (2 hours prior with ryanodine) to the application of the blocker which caused the compensation (TEA or 4AP). A cell or preparation was exposed only to one channel blocker type (TEA or 4AP) for a given experiment.

Current Measurements

All experiments were carried out in physiological saline cooled to 12°C. To measure current magnitudes and activation properties, two-electrode voltage clamp (TEVC) experiments were carried out by impaling a large cell with two glass electrodes filled with 3M KCl (8-17 MΩ resistance) and an Axoclamp 2A amplifier (Axon Instruments, Union City CA). All recordings were made from anterior large cell somata; action potential conductances were blocked (unless noted otherwise) by tightening thread ligatures on both sides of the large cell soma, preserving space clamp. TEVC protocols were created, driven and recorded with clampex 9.2 software (Axon Instruments, Union City CA). Current recordings were analyzed with Clampfit 9.2 software (Axon Instruments, Union City CA). Current and voltage traces were sometimes filtered with a

lowpass boxcar filter using 7 smoothing points. Most voltage clamps were modified from those used previously in STG preparations (Golowasch and Marder, 1992, Khorkova and Golowasch, 2007, Temporal et al., 2012). High threshold potassium current (I_{HTK}) magnitude was measured using a leak subtracted TEVC protocol with a holding potential of -40mV and 16 voltage steps from -55mV to +20mV (5mV intervals). A-type potassium current (I_A) magnitude was measured by subtracting the I_{HTK} current traces from a TEVC protocol that is identical except for a holding potential of -80mV. Calcium-activated potassium current (I_{KCa}) was isolated by subtracting post-cadmium (250μM $CdCl_2$, 1 hour) I_{HTK} current traces from pre-cadmium I_{HTK} current traces (isolating the cadmium sensitive outward current). Delayed rectifier potassium current (I_{Kd}) was isolated using the I_{HTK} TEVC protocol after cadmium exposure (250μM $CdCl_2$, 1 hour). All current magnitude measurements were taken at 0mV on an I-V plot made from the current traces.

Large Cell Excitability and Network Output

Cardiac network output was monitored with a single intracellular recording (using same equipment as TEVC protocols) taken from one of the three anterior large cells and an extracellular differential recording made with a model 1700 A-M Systems AC amplifier (Sequim, WA) and two stainless steel wires; one placed inside and one outside a vaseline well located around the central nerve of the CG (see Figure 1). Pharmacological blockers (TEA or 4AP) were perfused on the entirety of the CG with the exception of the four small cell and two posterior large cell somata. These cells were

isolated from the perfusion by a vaseline well placed around these cells and the posterior branch point containing regular physiological saline (see Figure 1). Using this experimental configuration we monitored the effect of the LC compensatory response (isolated to the best of our ability from small cells) in the context of the functioning network. Network activity was recorded in 10 minute intervals before and during blocker perfusion. These recordings were analyzed using Spike2 v6.00 software (Cambridge Electronic Design Limited, Cambridge, UK).

LC intrinsic excitability was examined under similar conditions except 10^{-6}M TTX saline was placed in the vaseline well around the four small cell and two posterior LC somata. This eliminated spontaneous network activity and small cell excitatory input into the anterior LCs. Excitability in the anterior LCs was then monitored using two-electrode current clamp (TECC) protocols run prior to and every five minutes after TEA or 4AP perfusion. TECC protocol was a six step depolarizing current injection (from 1-6nA) lasting six seconds per step and six seconds between steps.

Statistics

All statistical tests were performed with SigmaPlot v11.0 (Systat, Aspire Software International, Ashburn, VA). All data were confirmed to be of normal distribution as required by statistical analyses employed. Relationships between channel mRNAs and ionic currents were analyzed using Pearson's correlation test, and coefficients of

determination were calculated from the resulting correlation coefficients. In the case of Figures 2C and 2D, a potential outlier was identified that could be anchoring a false positive for the Pearson's test (see arrows). Analyses on these data sets were carried out both with and without the data point in question and both results reported. Bonferroni corrections were employed for multiple comparisons in the correlation analyses, and the p-value adjusted to 0.017 for statistical significance (three comparisons each for mRNA and ionic currents). Changes in current magnitude before and after pharmacological block were analyzed in one of two ways. Raw currents were analyzed before and after blockade via paired *t*-tests, and these are reported in Figure 3. In Figure 5, significant changes in a current relative to baseline were expressed as a percent change from zero, and analyzed via one-sample *t*-test with the hypothesized population mean set to 0. Overall changes in burst duration, spikes per burst, and spike frequency within the burst reported in Figure 4 were analyzed as with repeated measures ANOVA.

RESULTS

The crustacean cardiac ganglion as a model for central pattern generator network activity

The rhythmic pumping of the heart in decapod crustaceans such as the crab, *Cancer borealis* (our model organism), is neurogenic in nature, and under the control of a simple central pattern generator network called the cardiac ganglion (Alexandrowicz,

1932) (see Fig. 1). The ganglion consists of only nine neurons: four ‘small cell’ interneurons (SCs) that generate the pacemaker activity and five ‘large cell’ motor neurons (LCs) that innervate the heart musculature (Hartline, 1967; Tazaki and Cooke, 1983c). The SCs of the cardiac ganglion are endogenous oscillators, i.e., they undergo spontaneous and rhythmic generation of a depolarizing wave of membrane potential that leads to a bursting phenotype of multiple spikes per burst (Tazaki and Cooke, 1983a, Cooke, 2002b). The LCs of the CG produce bursts of action potentials as a result of synaptic pacemaker input from the SCs, ultimately leading to muscle contraction (Hartline, 1967; Tazaki and Cooke, 1979, 1983c, a; Berlind, 1989). The behavioral output of the ganglion represents a direct correlation of the influence of LCs on heart muscle (Sakurai and Wilkens, 2003, Garcia-Crescioni et al., 2010), and thus a direct measure of heart activity. Yet the entire network can be dissected out intact, and maintained in physiological saline for extended periods of recording while continuing to produce its endogenous rhythmic output. The motor neurons are all individually identifiable, and due to their distributed nature within the ganglion (Fig. 1), we can perform pharmacological manipulations on one or multiple motor neurons, either in isolation or in the intact, functional network. (Tazaki and Cooke, 1983a; Cooke, 2002). The underlying burst potentials of the LCs represent functional output at the motor neuron level, and our preliminary modeling studies show how the simplicity of this model system can be used to study functional implications of the relationships between mRNAs and ionic conductances on cellular output (Ball et al., 2010; Franklin et al., 2010).

Relationship between I_A and I_{KCa} in a population of large cell motor neurons

Potassium currents were measured using protocols developed for the STG cells of the same species (Golowasch and Marder, 1992). The total outward current of LC motor neurons consists primarily of three K^+ currents (Fig. 2B; Golowasch and Marder 1992): A-type transient K^+ current (I_A), calcium-activated K^+ current (I_{KCa}), and delayed rectifier K^+ current (I_{Kd}). I_{KCa} and I_{Kd} can be found in one combined current trace elicited from holding potentials at -40 mV or higher, and is termed here as the high-threshold K^+ current (I_{HTK}), while the A-type current can be measured by subtracting I_{HTK} from the total outward current elicited from a holding potential of -80 mV.

We first examined the relationships among mRNA levels in single identified LC motor neurons for three channel genes that correspond to these three K^+ currents (Atkinson et al., 1991, Tsunoda and Salkoff, 1995, Kim et al., 1998): *BKKCa* (I_{KCa}), *shaker* (I_A), and *shab* (I_{Kd}). We detected a significant correlation between *BKKCa* and *shaker* mRNA levels across a population of 20 LC motor neurons (Fig. 2A; *left*), but no correlations among any other channel mRNAs (Fig. 2A; *middle* and *right*). A fourth channel mRNA encoding an A-type K^+ current, *shal*, also was significantly positively correlated to *BKKCa* mRNA levels ($P < 0.005$; $R^2 = 0.58$), as well as to *shaker* ($P < 0.002$; $R^2 = 0.42$) but not to *shab*, suggesting an overall relationship between I_{KCa} and I_A, but not with I_{Kd}, in these cells.

We next examined the relationships among the ionic currents encoded by these channel genes across a population of LC motor neurons. I_A, I_{KCa}, and I_{Kd} were all measured in each cell across a population of LC motor neurons. A similar pattern of correlated current levels was seen as with the mRNA with one striking distinction: only I_A and I_{KCa} showed a significant correlation (Fig. 2A), but the correlation was strongly *negative* as opposed to positive as seen in the mRNA measurements. No significant correlations were found between I_A and I_{Kd}, or I_{KCa} and I_{Kd} (Fig. 2A). Because of the striking difference between the mRNA correlation (positive), and the current correlation (negative), we were most interested in pursuing the relationship between I_A and I_{KCa}, but had concerns about the effects of pharmacological blockers used to measure I_{KCa} (see Fig 3F); we use Cd^{2+} to block calcium currents that evoke I_{KCa} in order to measure this current via subtraction from I_{HTK}, as we have not identified any blockers specific to I_{KCa} in our preparation despite many attempts. Therefore, we decided to use the peak I_{HTK} as an indicator of I_{KCa} abundance in these experiments.

I_{HTK} (High Threshold K^+) is known from previous work (Golowasch and Marder, 1992, Haedo and Golowasch, 2006, Khorkova and Golowasch, 2007) to, in large part, consist of I_{KCa}, particularly the transient portion, as I_{Kd} shows no transient peak that could account for the peak in I_{HTK} (see Figure 2B). We also determined that measurements of the peak I_{HTK} were likely sufficient to reveal the relationship between I_{KCa} and $I_{A,}$ as the only transient peak seen in the currents that underlie I_{HTK} belongs to I_{KCa} (see Fig. 2B, *right*). Peak I_{HTK} also shows the same negative relationship with I_A as does I_{KCa} (Fig. 2C *left*), and peak I_{KCa} itself very strongly correlates with peak I_{HTK} (Fig. 2C *middle*), but not

I_{Kd} (Fig 2C *right*). *Accordingly, for the remainder of the study, we used I_{HTK} peak current from baseline as a measure of I_{KCa} abundance,* to allow for measurement of all K^+ currents under the least manipulative pharmacological blocker regime, i.e., without the need to block voltage-gated calcium currents.

I_{KCa} and I_A are rapidly up-regulated within the same LC motor neuron

Because the focus of the study was on the negative relationship between I_A and I_{KCa}, we decided to repeat the initial measurements in a new population of LC motor neurons to confirm the original finding before examining the functional impact of this relationship. In a distinct population of 20 LC motor neurons, we once again found a strong negative relationship between I_A and I_{KCa} (as revealed by I_{HTK} measurements; Fig. 3A), confirming our original finding. This strongly suggested a causal relationship between I_A and I_{KCa}. Specifically, we hypothesized that if these two currents are functionally interrelated, then a decreased level of I_A should result in an increased level of I_{KCa} and vice versa. We tested this hypothesis by blocking one current in this pair and determining whether there was an effect on the magnitude of the other. We measured baseline levels of I_A in a given cell, then used tetraethylammonium (TEA) to block the HTK-current for 60 minutes, and then measured I_A again post-TEA. 60 minutes of exposure to TEA significantly increased peak ($P < 0.001$; paired *t*-test) A-current (Fig 3B; 3C). The converse experiment was performed using 4-aminopyridine (4AP) for 60 minutes to block I_A. The peak ($P < 0.003$) of I_{HTK} was significantly increased following 60 minutes of 4-AP blockade (Fig 3B; 3C). Additionally, these results appear to be due

to an overall increase in conductance, since no change was seen in the voltages of activation of I_A and I_{HTK} concomitant with the changes in total current as a result of the block experiments (Fig 3D). No consistent or significant effects of TEA and 4-AP on neuronal input resistance were observed in these cells (ΔR_{IN} TEA: -1.87 ± 2.5 MΩ, ΔR_{IN} 4-AP: -0.52 ± 1.7 MΩ).

Our initial data strongly implicate I_{KCa} and I_A as the key pair of currents involved in this response. Since I_{HTK} is a mixed current comprised predominantly of I_{KCa} and I_{Kd}, and both of these currents are blocked by TEA, we determined whether the changes seen in I_{HTK} as a result of 4AP blockade were attributable to just one or to both of these currents. Most convincingly, while 4AP block significantly increases I_{HTK} (Fig 3C), one hour of exposure to 4AP had no significant effect on I_{Kd} magnitude itself (Fig 3E *left*). Unfortunately, we have not identified a blocker specific to I_{KCa} in our preparation to directly test the effects of blocking this current on changes in I_A. However, we can indirectly block I_{KCa} by using $CdCl_2$ to block voltage-gated Ca^{2+} channels that trigger I_{KCa}. Blocking with Cd^{2+} completely eliminates I_{KCa} in these cells, and causes a significant increase in I_A after one hour of exposure that is very similar to that seen with TEA (Fig. 3E *right*). Taken together, these data strongly suggest that the relationship between I_A and I_{HTK} identified in the experiments (Fig. 3) are the result of a causal relationship between the levels of I_A and I_{KCa} in a given motor neuron.

I_A and I_{KCa} act in a compensatory fashion to stabilize cellular excitability and network output

The negative correlation we measured between I_A and I_{KCa} in the normal population, together with the rapid change in currents seen within a cell after TEA and 4AP block, led us to hypothesize that levels of I_A and I_{KCa} may be acting in a compensatory fashion to stabilize both cellular and network output. To determine if such a functional compensation exists, we followed over time the activity of both isolated LCs, as well as LCs in an intact network, with either 4AP or TEA blockade, and then determined whether the output of the cells and of the network changed over the course of the blockade and the potential compensation.

As seen in Figures 4A and 4B, TEA blockade caused a substantial increase in the excitability of the LC motor neuron in the initial 10-20 minutes. However, over the time course of the measured increase in I_A seen in previous experiments (see Figure 2C) there was a compensatory change in the output of the cell and of the network towards the baseline level of activity. In isolated LCs (Figure 4A), both TEA and 4AP application shifted the cells from a less excitable state to a state characterized by large sustained burst potentials. However, over the time course of compensation, the excitability of isolated cells returned to control levels, losing the large burst potentials and showing firing patterns similar to those before the application of the blocker (Figure 4A).

In the intact network, TEA often caused a complex multi-phase bursting output in treated LCs (see Figure 4B; 10 min recording). Given this somewhat complex pattern of bursting, we determined that measurements of burst duration across a population of these

cells represented the clearest means to quantify changes in output over time. Over the course of 60-90 minutes, TEA blockade resulted in a significant change in burst duration ($P < 0.01$; ANOVA; Figure 4C *left*), initially increasing to nearly twice as long as control before re-establishing a stable burst duration indistinguishable from that at the control level (Figure 4B).

In the companion experiment with 4AP blockade in the intact network, we see a similar effect of compensation as in the LC motor neuron output (seen in Figures 4B and 4C). 4AP block does not cause the same change in burst duration as with TEA. Rather, 4AP blockade initially causes a significant increase in spike frequency and the number of spikes fired per burst ($P < 0.01$; ANOVA). Over the time course of the blockade, this spike frequency and number of spikes per burst returns to control levels (Figure 4D). These data indicate that the changes seen in the level of I_A and I_{KCa} as a result of TEA and 4AP block, respectively, are a functional compensatory response that stabilizes the output of the cells and of the network as a whole. However, the roles of I_A and I_{KCa} are not simply functionally redundant; blocking either current causes an initial change in the output of the cell that is not the same. These results implicate distinct roles for these two currents in addition to their ability to partially compensate for one another. However, we do not rule out the possibility that there could be other currents or mechanisms involved in the compensatory effect.

Compensatory changes in I_A and I_{KCa} follow distinct regulatory pathways

We then set out to determine the underlying mechanisms implementing the compensation in these currents. We first investigated whether the change in I_{KCa} elicited by 4AP blockade was dependent on intracellular calcium. To check this, we co-applied the calcium chelator BAPTA with the blocker. When BAPTA was co-applied with 4AP, there was no change in I_{HTK}, in contrast to the characteristically significant increase in I_{HTK} with 4AP blockade (Figure 5A). We also confirmed that this effect was not simply due to an effect of BAPTA on the calcium-dependence of I_{KCa}; BAPTA alone did not result in a significant reduction of I_{HTK} (data not shown; see also Turrigiano et al. 1994). More specifically, the calcium-dependence of the increase in I_{HTK} was attributable to the release from intracellular calcium stores since co-application of 4AP and the intracellular calcium release blocker ryanodine also prevented the compensatory increase in I_{HTK} normally seen with 4AP blockade (Figure 5A). These results suggest that the compensatory increase in I_{KCa} is dependent on intracellular calcium signaling mechanisms that depend on the release of intracellular calcium stores.

Because relatively rapid changes in current magnitude can often be attributed to changes in phosphorylation states of ion channels and associated regulatory proteins, we examined the effects of phosphatase and kinase inhibitors on the ability of the blockers to elicit the compensatory changes in these currents. Okadaic acid is a broad spectrum inhibitor of serine/threonine protein phosphatases (Cohen et al., 1990). While application of okadaic acid alone did not affect baseline levels of I_{HTK} (data not shown), co-application of okadaic acid with 4AP also abolished the compensatory increase in I_{HTK} (Figure 5A), suggesting the action of a serine/threonine protein phosphatase in this

compensatory effect. Because calcineurin is a well-known Ca^{2+}-dependent protein serine/threonine phosphatase (Klee et al., 1998), we used cyclosporine A to inhibit calcineurin activity in our system. Cyclosporine alone did not affect baseline levels of I_{HTK} (data not shown), but combined application of 4AP with cyclosporine eliminated the compensatory increase in I_{HTK} (Figure 5A), indicating that the increase in I_{HTK} is dependent, at least in part, on the activity of calcineurin.

In complete contrast, the compensatory influence of TEA on I_A appears to be implemented via mechanistically distinct pathways compared to those we found for the 4AP block on I_{HTK}. The increase of I_A in response to TEA blockade is neither calcium-dependent (Figure 5B) nor dependent on the activity of serine/threonine phosphatases (Figure 5B). Parallel experiments showed that BAPTA, ryanodine, okadaic acid and cyclosporine, when co-applied with TEA, failed to prevent a significant increase in I_A (Figure 5B). The only exception was that the application of ryanodine in conjunction with TEA appeared to reduce the magnitude of increase in I_A, although this effect was not statistically significant with respect to TEA alone ($P = 0.103$; *t*-test), or TEA plus BAPTA ($P= 0.08$).

We also examined the effects of inhibiting kinase activity on the compensatory effects of 4AP and TEA blockade. Staurosporine is a potent, cell permeable protein kinase C inhibitor which also partially inhibits other kinases such as PKA, PKG, and CAMKII (Ruegg and Burgess, 1989). Co-application of staurosporine with 4AP appears to cause a significant *decrease* in I_{HTK} (Figure 5A). However, this is a more complex

result than that for the other pharmacological blockers. Unlike any of the other pharmacological blockers used in this study, staurosporine was the only one to cause a change in baseline levels of I_{HTK} when applied alone (Figure 5C). Therefore, combined application of 4AP and staurosporine results in a relative decrease in I_{HTK} compared to that with staurosporine alone, but the net effect of 4AP + staurosporine is a restoration of I_{HTK} to baseline levels (Figure 5D).

Once again, the effects of staurosporine on I_A in the context of TEA blockade contrast with those for 4AP and I_{HTK}. There is no effect of staurosporine on baseline levels of I_A (Figure 5C), and while staurosporine co-applied with TEA results in an apparent decrease in the magnitude of the effect on I_A, there is still a significant increase in I_A with staurosporine present (Figure 5B), which is not statistically significant from the effect of TEA alone (P = 0.08; *t*-test).

DISCUSSION

Rapid compensation between I_A and I_{KCa} preserves both cellular and network outputs

We have identified a naturally occurring co-regulatory relationship between potassium currents (I_A and I_{KCa}) in an intact CPG network that results in homeostatic

compensation of neuronal excitability as well as network function. Furthermore, we have determined that these compensatory changes in K^+ current magnitudes are independently regulated by distinct mechanisms. Compensatory increases in I_{KCa} are calcium dependent and due, at least in part, to the activity of calcineurin-based phosphatase activity. Conversely, compensatory increases in I_A are independent of all of the regulatory pathways implicated in the I_{KCa} response. These effects are also fairly rapid, acting over the course of 60-90 minutes to stabilize the activity of a critical CPG network responsible for cardiac muscle contraction and heart beat generation in the animal. While such homeostatic responses and their role in stabilizing synaptic function have been well studied (Bergquist et al., 2010, Turrigiano, 2011b), we know much less about the mechanisms underlying homeostatic plasticity of intrinsic excitability and the role this form of plasticity plays in the stabilization of neuronal and motor network output (Turrigiano, 2011b).

Even neurons and networks with extremely robust output display highly variable underlying physiological parameters responsible for neuronal output, particularly membrane conductances (Schulz et al., 2006a; Khorkova and Golowasch, 2007; Schulz et al., 2007; Goaillard et al., 2009; Temporal et al., 2012). Our work reveals that embedded within this variability are co-regulatory relationships that act to stabilize the excitability of the cell, in part by balancing the sum total of major transient outward currents, I_A and I_{KCa}. A similar relationship between I_A and I_{KCa} was reported in the STG. Artificial depolarization of inferior cardiac neurons results in increased I_A and decreased I_{HTK},

which is abolished by Cd^{2+} blockade of calcium channels (Golowasch et al., 1999). These experiments did not reveal a naturally existing correlation between these currents (Golowasch et al., 1999), suggesting that excitability in the STG may be a more complex interaction among multiple conductances, or perhaps between conductances and their constitutive neuromodulation (Harris-Warrick, 2011). Although it is not known what effect this has on network output in the STG, our complementary results suggest that such homeostatic mechanisms may be common among motor neurons in different CPGs.

Distinct intracellular pathways mediate compensation

The mechanisms involved in the regulation of the compensatory response mediated by I_{KCa} after 4AP block in the CG network are consistent with work supporting changes in K^+ current density in a homeostatic fashion (Desai et al., 1999; Schulz et al., 2006b;(Debanne and Poo, 2010); Misonou, 2010). In particular, the mechanisms we see for the compensatory increase in I_{KCa} are similar to those found in regulation of excitability in cultured hippocampal neurons (Misonou et al., 2004; Misonou and Trimmer, 2004; Misonou et al., 2005). Increased excitability in these cultured neurons results in calcineurin-dependent dephosphorylation of Kv2.1 channels, leading to a functional potentiation of these channels via a shift in activation voltage, and to restoration of excitability (Misonou et al., 2004). While our data strongly suggest that I_{KCa} is primarily responsible for the observed change in I_{HTK}, we cannot conclusively rule

out a role for I_{Kd} (similar to Kv2.1). However, cyclosporine has been shown to alter I_{KCa} channels directly (Hay, 1998), and calcineurin is known to have widespread effects on neuronal plasticity and excitability beyond its effects on Kv2.1 activity (Groth et al., 2003). The effects seen in our experiments likely can be attributed to an overall increase in the maximal conductance of I_{KCa}, as we see no changes in either activation curves or any consistent or significant changes in input resistances of these cells (O'Leary et al., 2010).

The mechanisms underlying compensatory increases in I_A are less clear, but distinct from the pathways involved in the upregulation of I_{KCa}. Unlike for I_{KCa}, the increase in I_A is neither calcium-dependent, nor influenced by the activity of calcineurin or any other phosphatases that would be affected by treatment with okadaic acid (Cohen et al., 1990). Indeed, blocking neither phosphatase nor kinase activity by two broad spectrum blockers was able to prevent an increase in I_A as a result of TEA blockade, possibly precluding the contribution of phosphorylation state to this half of the compensation story. However, we were able to dampen the effect by blocking release of intracellular calcium with ryanodine, as well as by inhibiting kinase activity, suggesting a more complex path of regulation in this response. Given the potential non-specific effects of pharmacological treatment, we cannot rule out at least some role for a kinase in this pathway. For example, Kv1.2 potassium channels are known to be affected by cyclic AMP/protein kinase A pathways which enhance their conductance, in part by altering trafficking of these channels (Connors et al., 2008). Our staurosporine treatment

may result in only partial inhibition of PKA (Ruegg and Burgess, 1989), which could explain the intermediate effects seen on the A-type current compensation. Regardless, the fact that I_A and I_{KCa} are regulated by distinct pathways demonstrates an inherent robustness to this homeostatic response, which may be characteristic of networks responsible for critical functions, such as CPGs.

Reservoirs of channel proteins might implement rapid compensation

Our data also begin to shed light on a striking disparity between levels of regulation in this system. Namely, we see an entirely different relationship at the level of mRNA for the channel genes *BKKCA* and *shaker* (positive correlation), than we do for the currents I_{KCa} and I_A that these channels most directly encode (negative correlation). Indeed, to date every correlation we have found between channel mRNAs at the single cell level has been a positive correlation (Schulz et al., 2007; Tobin et al., 2009; Temporal et al., 2012). These data include measurements of at least nine different channel genes in seven different motor neuron types in the crustacean stomatogastric and cardiac ganglia (some data unpublished, S. Temporal and D.J. Schulz), for a total of no fewer than 60 correlations in channel expression detected among channel transcript levels, and every one has thus far been positive. In addition, our data impact the present, although admittedly limited, understanding of the relationship between channel mRNA and ionic current in a given neuron. Namely, that mRNA for a given K^+ channel

correlates positively with its corresponding ionic conductance (Schulz et al. 2006). Although both of these measurements were not made in the same cells in this study, logic dictates that there cannot simply be a positive relationship between mRNA and conductance for both K^+ currents in this study. Clearly, and not particularly surprisingly, our data demonstrate that more complexity lies within the relationship of mRNA and ionic conductance than a one-for-one tracking between these disparate levels of function in all cell types. However, our data continue to support the concept that correlation among mRNA levels (Schulz et al. 2007; Tobin et al. 2009) underlie a functional relationship at the conductance level.

So then why do we see only positively correlated mRNA levels for channel genes in these motor networks? The linkage to cellular and network output in our study enables us to propose a new hypothesis in this regard. We hypothesize that rapid compensation of intrinsic excitability, such as that reported in this study, is implemented via an already existing pool of protein. That is, protein pools for the two opposing channels must already be available in relatively equivalent numbers, even if they are not functionally equally represented. This requires that mechanisms must occur at the level of gene regulation to ensure a sufficient "reservoir" of protein capable of compensating for the loss of a given channel. Thus, regardless of whether channels act in concert to set neuronal output (Ball et al., 2010; Franklin et al., 2010), or act in a compensatory fashion, the overall gene regulation between the two must be relatively balanced. Such a reservoir perspective is reminiscent of mechanisms seen for synaptic vesicle protein dynamics

(Fernandez-Alfonso et al., 2006), or extra-synaptic AMPA receptors that serve as a reservoir during synaptic plasticity (Hayashi et al., 2000; Zhu et al., 2000). Interestingly, insertion of AMPA receptor during synaptic plasticity is also under the control of phosphorylation-dependent processes (Lin et al., 2009). Therefore, this hypothesis provides a compelling framework for future investigation of the relationship between mRNA levels and ionic conductance, as well as the interplay between gene expression and post-transcriptional mechanisms involved in homeostatic plasticity of intrinsic excitability over different time scales.

Putting it all together

Our findings represent one of the first comprehensive demonstrations of rapid homeostatic plasticity of intrinsic excitability that results in a stabilization of output in a mature, intact network of a CPG. These rapid compensatory increases are mechanistically independent, suggesting robustness in the maintenance of neural network output that is critical for survival. Furthermore, this study reveals a distinct mechanism for compensation that leads us to at least one working model of homeostatic plasticity in this system (see Figure 6). We hypothesize that one pathway to functional compensation in this system relies on intracellular calcium concentration as a measure of cell excitability (Kennedy, 1989; Ross, 1989; LeMasson et al., 1993). A block of A-type K^+ channels leads to an increase in the excitability of the cell, causing release of intracellular calcium

stores. This calcium influx alters calcineurin activity, resulting in dephosphorylation of targets, perhaps the KCa-channels themselves, that increases I_{KCa}. This ultimately restores the outward current balance that was lost during decreased I_A and thus restores excitability. The corresponding mechanism responsible for compensatory increases in I_A (Figure 6) is presently unknown, but is likely to involve distinct mechanisms for monitoring excitability (Dirnagl et al., 2003), as well as other candidate mechanisms that alter A-type conductances (Connors et al., 2008). Finally, we hypothesize that positive co-regulation of mRNA numbers for channel genes may ultimately provide a reservoir of channel protein (Figure 6) for implementing compensation over rapid time scales during which de novo synthesis may be insufficient to implement full compensation.

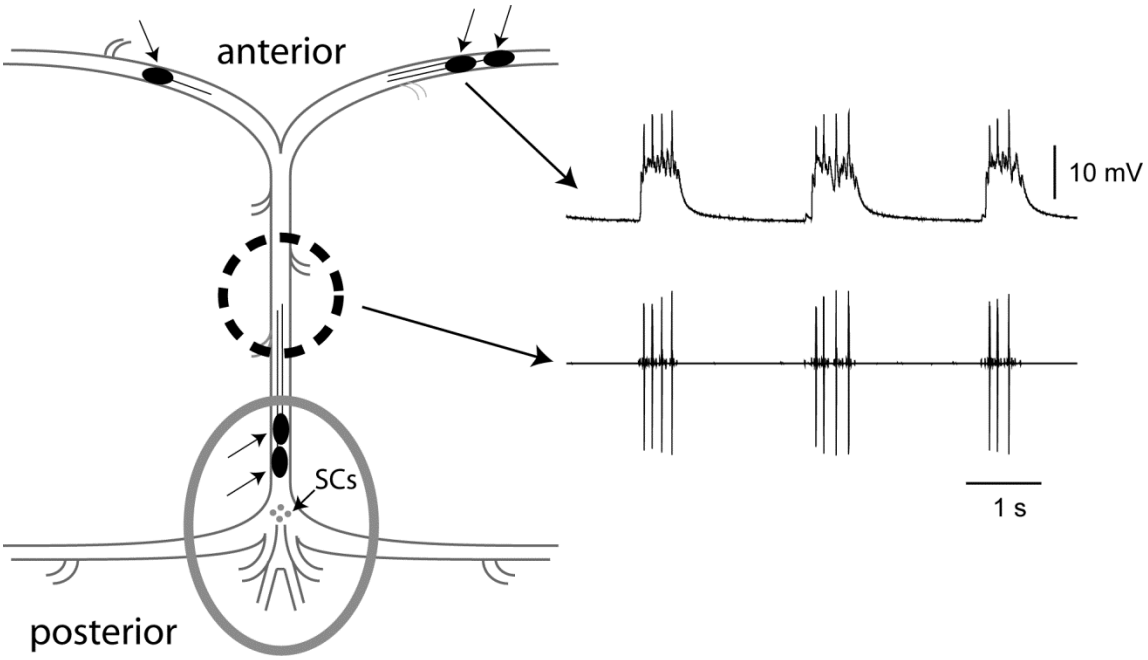

Figure 2.1 The crustacean cardiac ganglion. When dissected from the animal, the cardiac ganglion can be pinned flat and simultaneous recordings of network activity and intracellular recordings can be obtained. Five large cell somata (dark ovals marked with arrowheads) are distributed throughout the ganglion. Individual or pairs of large cells can be isolated for voltage clamp with thread ligature, or for pharmacological treatment with a vaseline well. The recording shows a simultaneous extra- and intracellular recording of network activity. The bursting of the network is seen at the site indicated by the dotted circle and corresponds to the extracellular (*bottom*) trace. Burst output of a single LC motor neuron is seen in the *top* trace, taken from an intracellular recording of a LC soma. This rhythmic motor activity corresponds directly to the contraction of the single-chambered crab heart muscle, showing an in vitro maintenance of biological network activity. The gray oval represents a vaseline well used in pharmacological blocker experiments. During measurements of individual LC excitability (Figure 4A), this well was used to apply TTX to the small cell pacemaker neurons (SCs, small gray circles) to silence the network activity but preserve output capability in anterior LCs. During measurements of compensation during ongoing network activity, this cell was used to protect SCs from blocker application in the bath (Figure 4B).

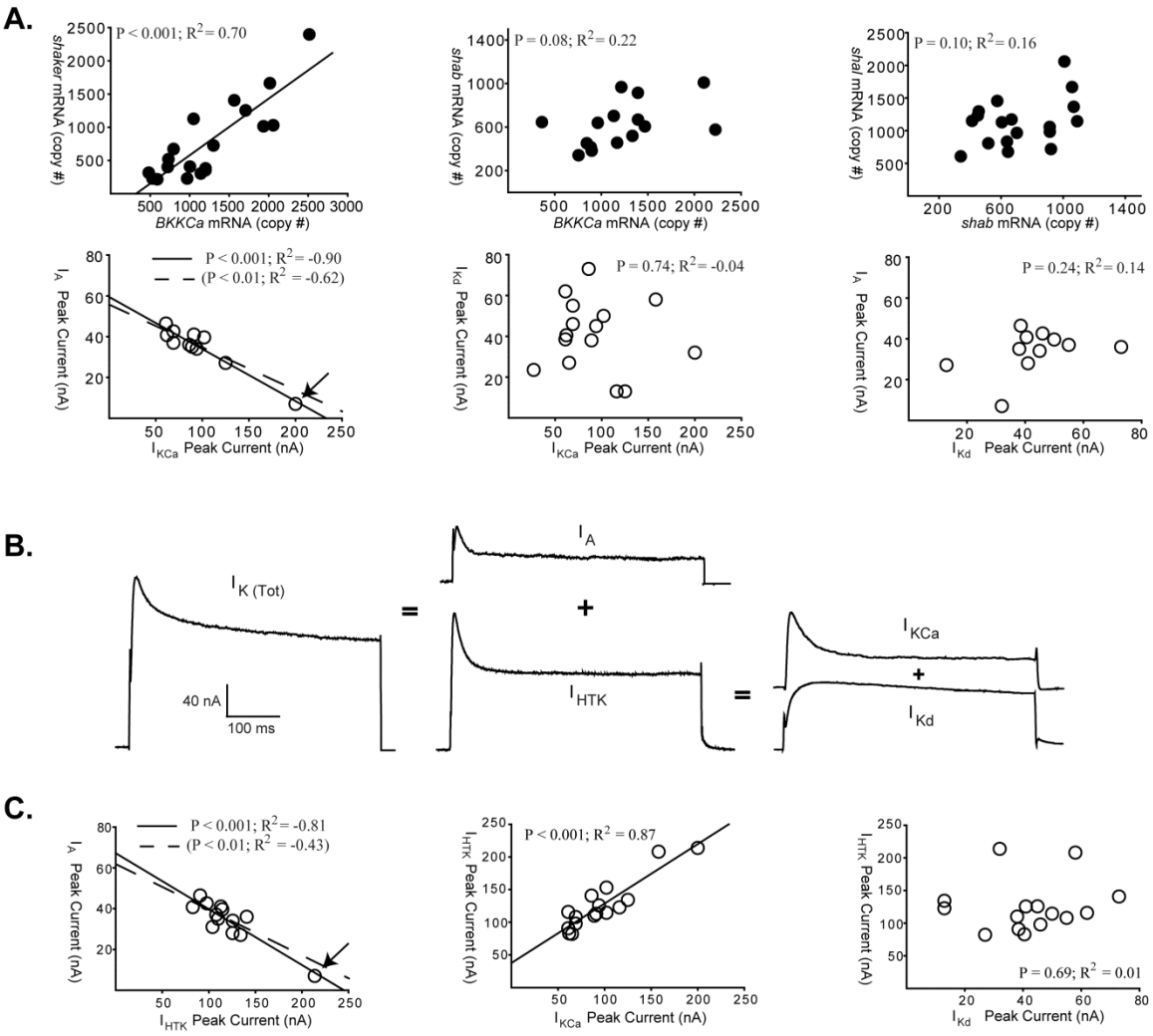
A.
P < 0.001; R2 = 0.70
shaker mRNA (copy #)
BKKCa mRNA (copy #)
P = 0.08; R2 = 0.22
shab mRNA (copy #)
BKKCa mRNA (copy #)
P = 0.10; R2 = 0.16
shal mRNA (copy #)
shab mRNA (copy #)
P < 0.001; R2 = -0.90
(P < 0.01; R2 = -0.62)
IA Peak Current (nA)
IKCa Peak Current (nA)
P = 0.74; R2 = -0.04
IKd Peak Current (nA)
IKCa Peak Current (nA)
P = 0.24; R2 = 0.14
IA Peak Current (nA)
IKd Peak Current (nA)
B.
IK (Tot)
40 nA
100 ms
=
IA
+
IHTK
=
IKCa
+
IKd
C.
P < 0.001; R2 = -0.81
(P < 0.01; R2 = -0.43)
IA Peak Current (nA)
IHTK Peak Current (nA)
P < 0.001; R2 = 0.87
IHTK Peak Current (nA)
IKCa Peak Current (nA)
P = 0.69; R2 = 0.01
IHTK Peak Current (nA)
IKd Peak Current (nA)

Figure 2.2 Relationships among channel gene mRNA levels and among ionic currents in a normal population of large cell motor neurons. A. Correlations between mRNA levels from single identified LC motor neurons for *BKKCa*, *shaker*, and *shab* channel genes (top row) and the corresponding K^+ current correlations from single identified LC motor neurons for I_{Kca}, I_A, and I_{Kd} (bottom row). Each point represents values from a single neuron. Regression lines shown only for significant correlations as revealed by Pearson's test, for which the P-value and R^2 values are reported in each plot. When two regression lines are present, the solid line and top set of statistics refers to the entire data set, while the dotted line and the bottom set of statistics represents the correlation with the single point indicated by the arrow removed. Despite having this outlier removed, the correlation is still significant and largely unchanged. **B.** The total K^+ current ($I_{K[Tot]}$) in LC motor neurons consists primarily of three distinct K^+ currents: A-type K^+ (I_A), and the high-threshold K^+ current (I_{HTK}) that can be subdivided into calcium-activated K^+ (I_{KCa}) and delayed rectifier K^+ (I_{Kd}). **C.** Correlations between currents reveal that I_{HTK} peak is highly representative of I_{KCa} levels, but not of I_{Kd}. With these results, we use I_{HTK} peak levels as an indicator of I_{KCa} for any given cell for the remainder of the study. Statistics as in panel A.

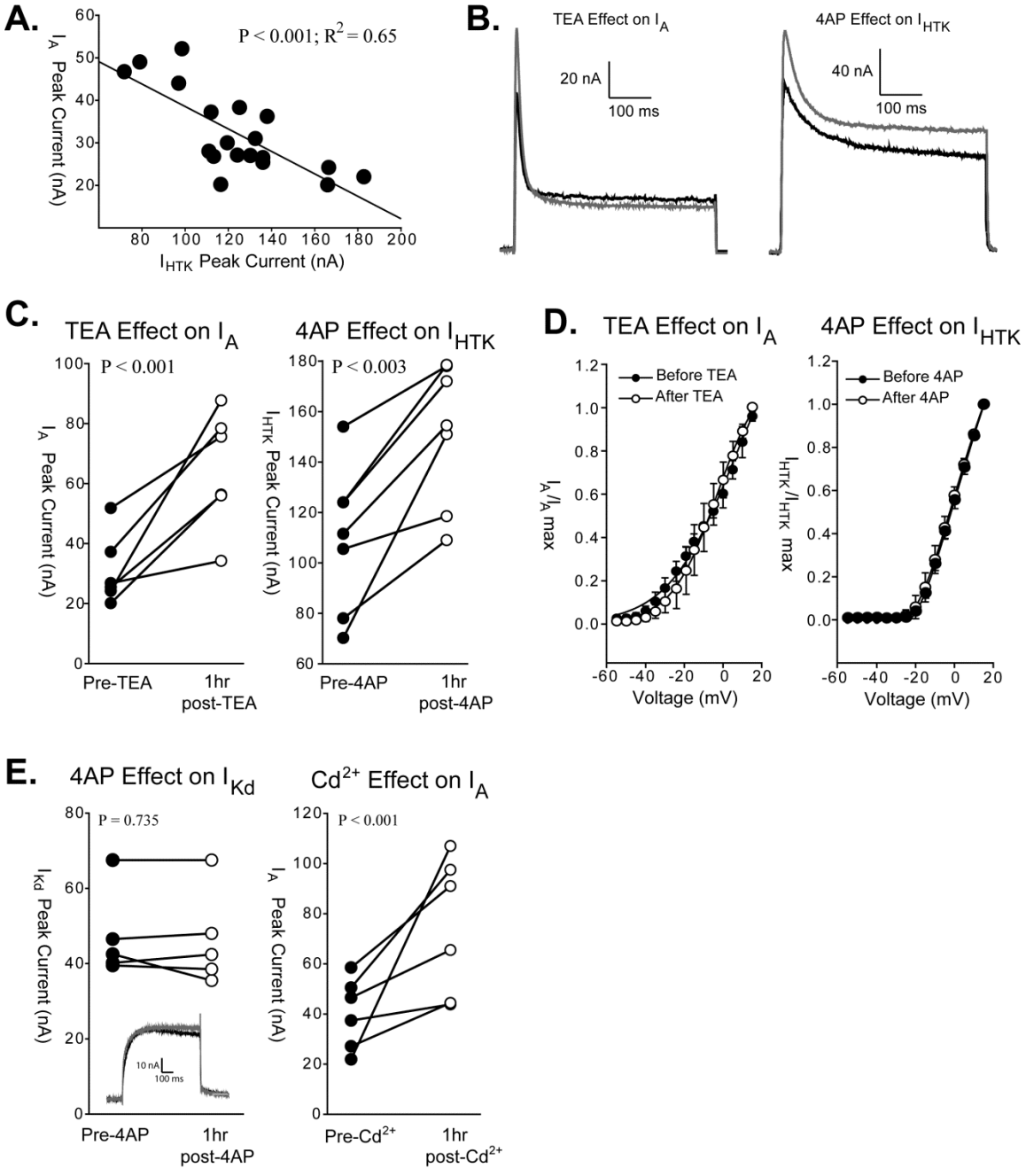
A.
P < 0.001; R2 = 0.65
IA Peak Current (nA)
IHTK Peak Current (nA)
B.
TEA Effect on IA
20 nA
100 ms
4AP Effect on IHTK
40 nA
100 ms
C.
TEA Effect on IA
P < 0.001
IA Peak Current (nA)
Pre-TEA
1hr post-TEA
4AP Effect on IHTK
P < 0.003
IHTK Peak Current (nA)
Pre-4AP
1hr post-4AP
D.
TEA Effect on IA
Before TEA
After TEA
IA/IA max
Voltage (mV)
4AP Effect on IHTK
Before 4AP
After 4AP
IHTK/IHTK max
Voltage (mV)
E.
4AP Effect on IKd
P = 0.735
IKd Peak Current (nA)
10 nA
100 ms
Pre-4AP
1hr post-4AP
Cd2+ Effect on IA
P < 0.001
IA Peak Current (nA)
Pre-Cd2+
1hr post-Cd2+

Figure 2.3 Reciprocal interaction of I_A and I_{HTK} levels in LC motor neurons. A. Correlation between peak I_A and I_{HTK} across a second population of LC motor neurons distinct from those in Figure 2. Statistics represent results of a Pearson's test (n=20). **B.** Representative recordings of the increase in I_A after TEA exposure (*left*) and the increase in I_{HTK} after 4AP exposure (*right*). Black trace is the control, gray trace is the same cell after 60 min exposure to blocker. **C.** Quantified effects of TEA (*left*) and 4AP (*right*) on the peak I_A and I_{HTK} respectively in N = 6 cells. The same cell before (black) and after (white) is connected with a solid line. Statistics represent paired *t*-test on mean current before and after blocker. **D.** Activation characteristics, expressed as I/I_{max} for an N = 5 cells, of I_A (*left*) and I_{HTK} (*right*) before and after block with TEA and 4AP respectively. Each point represents mean ± SD. **E.** Effects of 4AP on I_{Kd} (*left*; N = 5) and Cd^{2+} on I_A (*right*; N = 6). Insert in the left panel shows representative traces of I_{Kd} before (black) and after (*gray*) exposure to 4AP. Legends and statistics as in panel C.

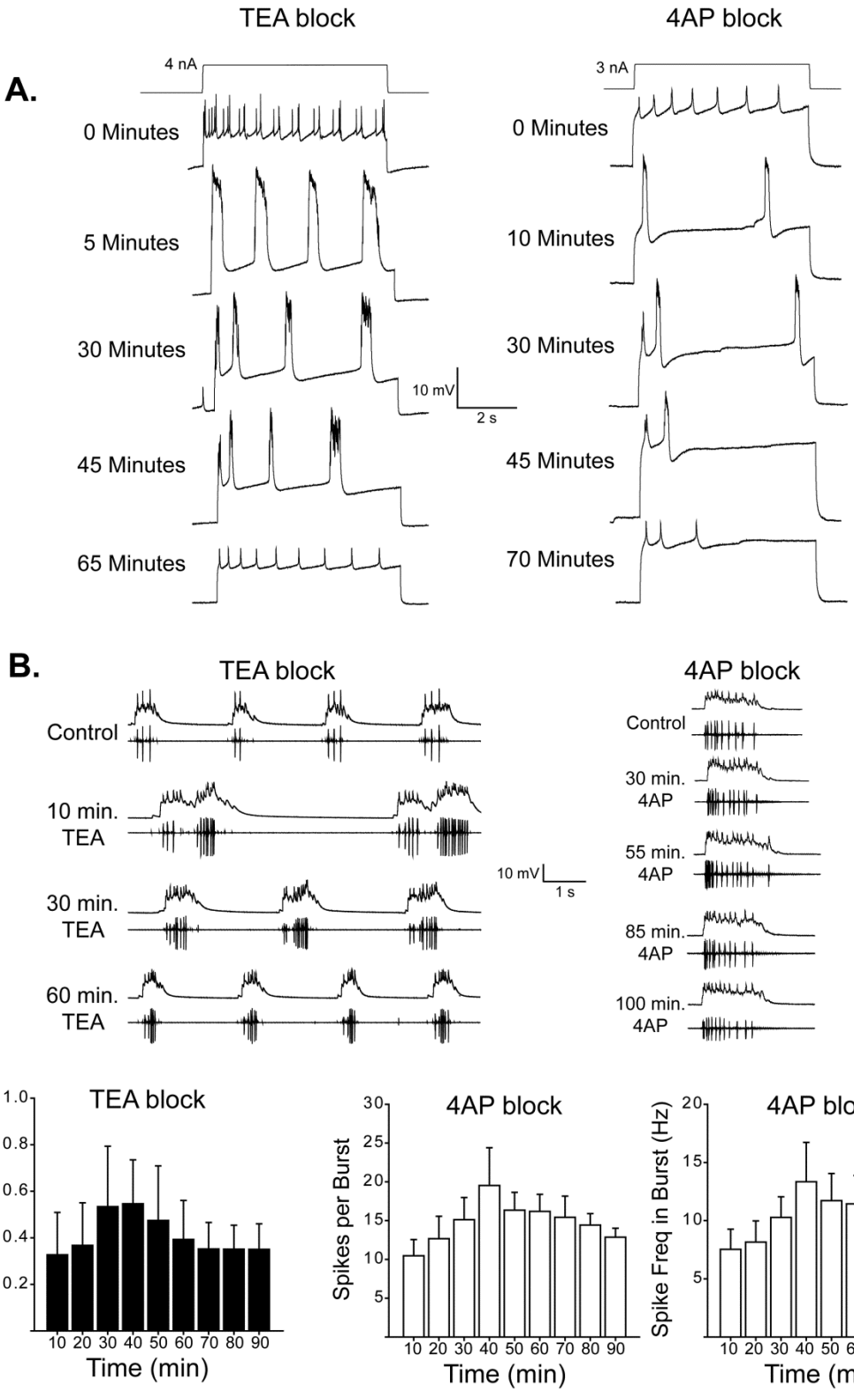
A.
TEA block
4AP block
4 nA
3 nA
0 Minutes
5 Minutes
30 Minutes
45 Minutes
65 Minutes
0 Minutes
10 Minutes
30 Minutes
45 Minutes
70 Minutes
10 mV
2 s
B.
TEA block
4AP block
Control
10 min. TEA
30 min. TEA
60 min. TEA
Control
30 min. 4AP
55 min. 4AP
85 min. 4AP
100 min. 4AP
10 mV
1 s
C.
TEA block
Burst Duration (s)
Time (min)
4AP block
Spikes per Burst
Time (min)
4AP block
Spike Freq in Burst (Hz)
Time (min)

Figure 2.4 I_A and I_{KCa} engage in a compensatory relationship that stabilizes neuronal excitability and network output. A. Representative recordings of the effects on the excitability of individual LC motor neurons isolated from network activity after exposure to TEA (*left*) and 4AP (*right*). Because the pacemaker neurons of the network were silenced with TTX in this experiment, DC current injections were used to elicit activity in LC motor neurons (current traces shown at top). **B.** Representative recordings of the effects of TEA (*left*) and 4AP (*right*) exposure on network output over time. Pacemaker cells were shielded from exposure to the blocker (see Figure 1), while the 3 upper motor neurons were exposed to blocker. Paired intracellular (*top* traces) and extracellular recordings were made over the time course of the experiment. **C.** Quantified effects of TEA and 4AP effects on burst characteristics of LC motor neurons in the intact network. Bars represent mean ± SD of N = 5 preparations at 10 minute intervals. The first 10 minute interval is baseline without blocker, and subsequent bins represent cumulative time after blocker exposure.

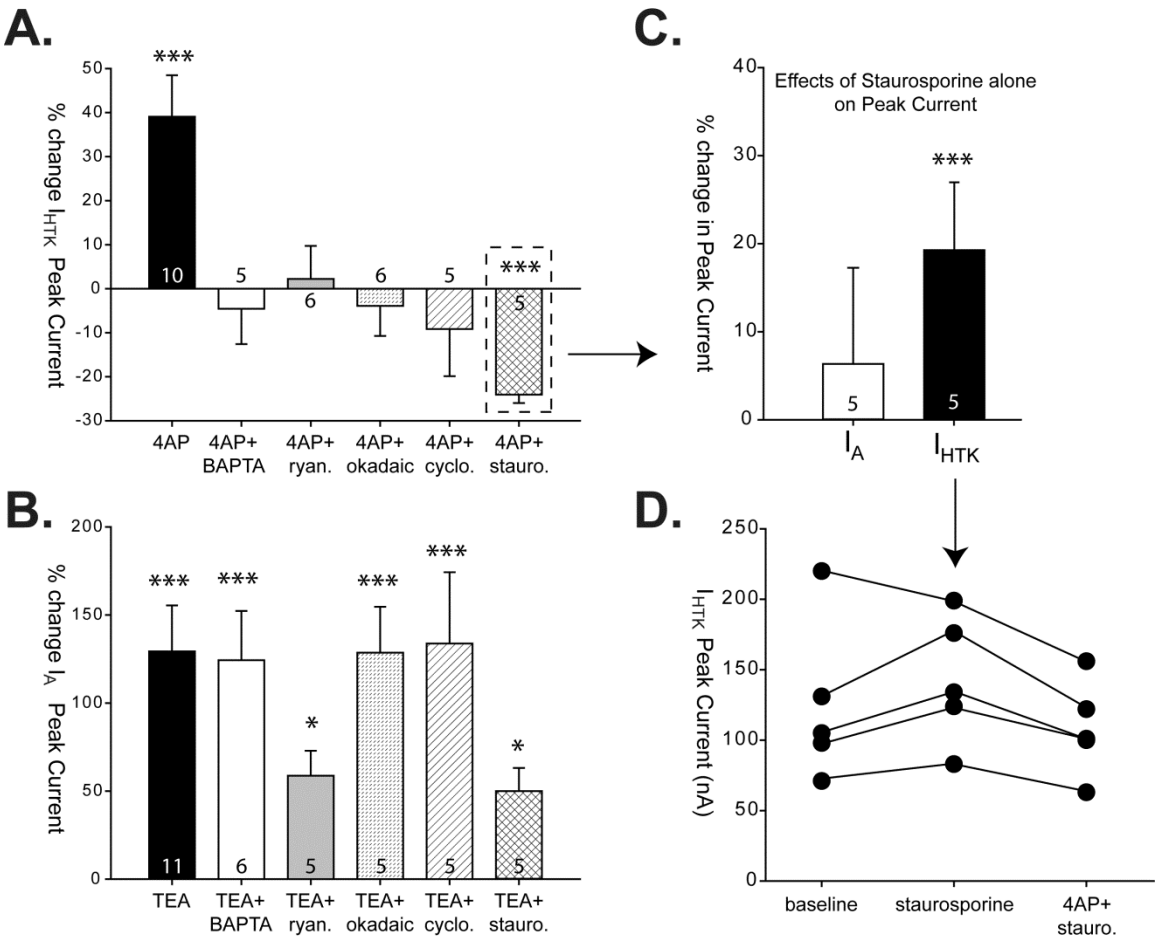
A.
% change I_{HTK} Peak Current
50
40
30
20
10
0
-10
-20
-30
***
10
5
6
6
5
***
5
4AP
4AP+ BAPTA
4AP+ ryan.
4AP+ okadaic
4AP+ cyclo.
4AP+ stauro.
B.
% change I_A Peak Current
200
150
100
50
0
***
***
***
***
*
*
11
6
5
5
5
5
TEA
TEA+ BAPTA
TEA+ ryan.
TEA+ okadaic
TEA+ cyclo.
TEA+ stauro.
C.
Effects of Staurosporine alone on Peak Current
% change in Peak Current
40
30
20
10
0
***
5
5
I_A
I_{HTK}
D.
I_{HTK} Peak Current (nA)
250
200
150
100
50
0
baseline
staurosporine
4AP+ stauro.

Figure 2.5 Use of pharmacological inhibitors to probe mechanisms of changes in I_A and I_{KCa}. **A.** Effects of BAPTA, ryanodine, okadaic acid, cyclosporine, and staurosporine (referred to as the *treatment*) on the induction of increased I_{HTK} with 4AP exposure. All bars are mean ± SD, sample sizes as shown in bars. All results are % change in peak I_{HTK} with 4AP + treatment relative to *treatment alone* (see methods). None of the treatments caused a change in baseline levels of I_{HTK} with the exception of staurosporine (dotted box; see panel C). *** represents a significant ($P < 0.001$) difference from 0 via one-sample *t*-test. **B.** Effects of BAPTA, ryanodine, okadaic acid, cyclosporine, and staurosporine on the induction of increased I_A with TEA exposure. All results are % change in peak I_A with TEA + treatment relative to *treatment alone* (see methods). None of the treatments caused a change in baseline levels of I_A. *** ($P < 0.001$) and * ($P < 0.01$) represent a significant difference from 0 via one-sample *t*-test. **C.** Effects of staurosporine alone on baseline levels of I_A and I_{HTK}. *** represents a significant ($P < 0.001$) difference from 0 via one-sample *t*-test. **D.** Overall effects of staurosporine alone and then 4AP + staurosporine on I_{HTK}. Each individual cell is connected with a solid line across the treatments.

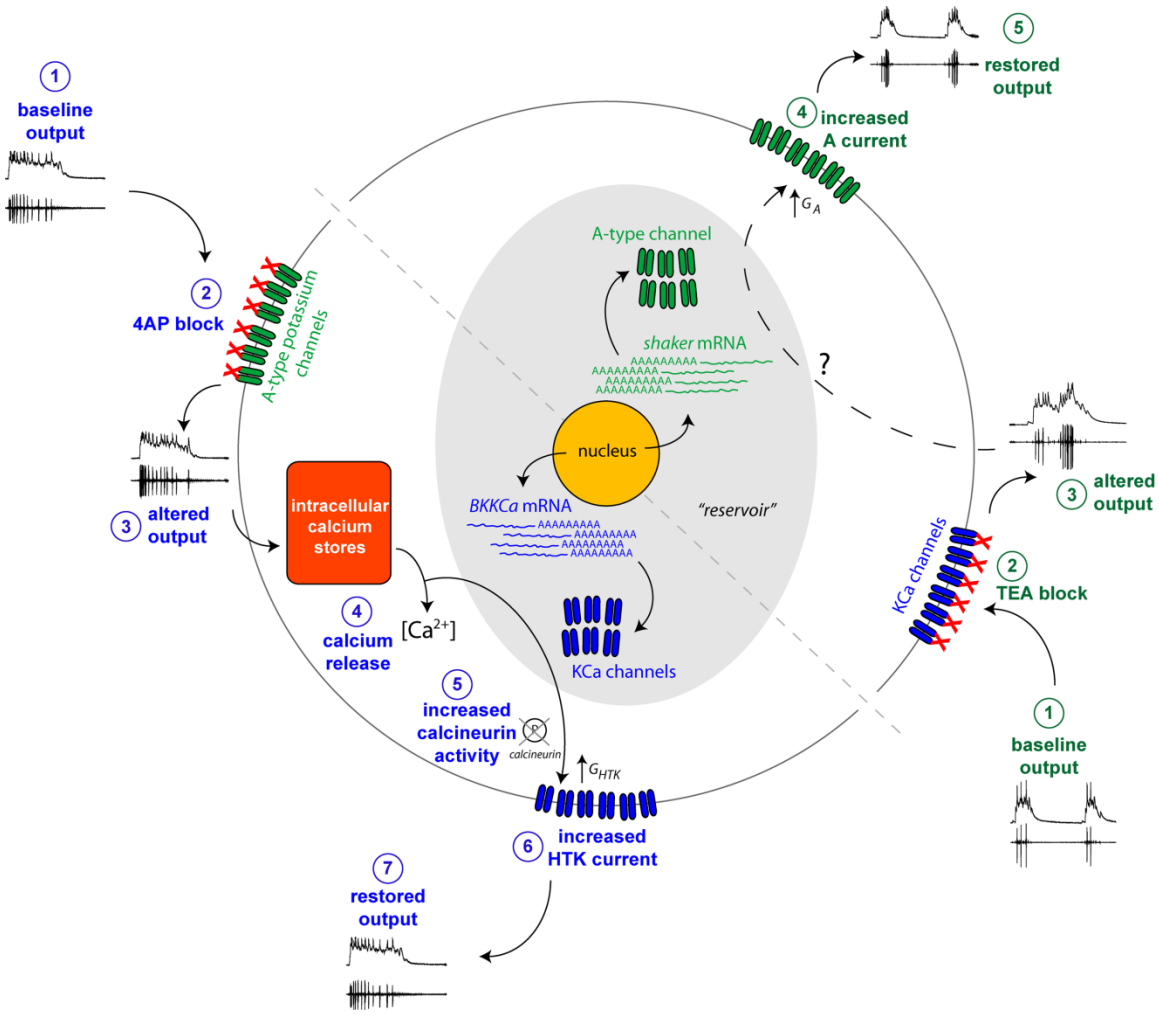
1
baseline output
2
4AP block
A-type potassium channels
3
altered output
intracellular calcium stores
4
calcium release
[Ca2+]
5
increased calcineurin activity
calcineurin
P
GHTK
6
increased HTK current
7
restored output
A-type channel
shaker mRNA
nucleus
BKKCa mRNA
"reservoir"
KCa channels
?
4
increased A current
GA
5
restored output
3
altered output
KCa channels
2
TEA block
1
baseline output

Figure 2.6 A working model for the induction of homeostatic plasticity of intrinsic excitability via rapid compensation between I_A and I_{KCa}. This model summarizes all of the data in the current study and provides a framework for interpretation and future experimentation. The two halves of the cell represent the distinct mechanisms induced by a block of I_A with 4AP (*left, blue pathway*) and a block of I_{KCa} with TEA (*right, green pathway). BLUE PATHWAY (4AP blockade):* The baseline activity (1) is disrupted by the block of A-type channels with 4AP (2), causing an alteration in the excitability of the cell and its output in the network, in this case rapid initial firing frequency (3). This change presumably results in the release of calcium from intracellular stores (4) that increases activity of the calcium-dependent phosphatase calcineurin (5). Calcineurin activity induces an increase in I_{KCa} (6), restoring the excitability of the cell and re-establishing motor neuron activity in the intact network (7). *GREEN PATHWAY (TEA blockade):* Baseline network activity (1) is disrupted via TEA blockade (2), causing substantial changes in the output properties of the motor neuron and the network (3). While the intracellular mechanisms remain unclear at this point, a subsequent increase in I_A that is independent of the pathway invoked by 4AP blockade compensates for loss of I_{KCa}, restoring output of the neurons and the network (5). This compensation is rapid (on the order of 1 hour), suggesting that there is an already existing "reservoir" or channel protein available that is maintained via positive co-regulation at the transcription/mRNA level of the channel genes responsible for I_{KCa} and I_A (*GRAY OVAL).*

CHAPTER THREE

Neurons within the same network independently achieve conserved output by differentially balancing variable conductance magnitudes

Biological and theoretical evidence suggest that individual neurons may achieve similar outputs by differentially balancing variable underlying ionic conductances. Despite the substantial amount of data consistent with this idea, a direct biological demonstration that cells with conserved output, particularly within the same network, achieve these outputs via different solutions has been difficult to achieve. Here we demonstrate definitively that neurons from native neural networks with highly similar output achieve this conserved output by differentially tuning underlying conductance magnitudes. Multiple motor neurons of the crab (*Cancer borealis*) cardiac ganglion have highly conserved output within a preparation, despite showing a 2-4 fold range of conductance magnitudes. By blocking subsets of these currents, we demonstrate that the remaining conductances become unbalanced, causing disparate output as a result. Therefore, as strategies to understand neuronal excitability become increasingly sophisticated, it is important that such variability in excitability of neurons, even among those within the same individual, is taken into account.

Neurons with similar and conserved output across individuals can exhibit 2-6 fold variability in their intrinsic conductances (Golowasch et al., 2002, Swensen and Bean, 2005b, Schulz et al., 2006, Goaillard et al., 2009a, Ransdell et al., 2012) as well as in ion channel mRNA levels (Schulz et al., 2006, Schulz et al., 2007b). This observation has motivated several computational studies that used populations of model cells with variable intrinsic properties and constrained output features to demonstrate that model neurons could achieve similar voltage output with disparate intrinsic parameters (Goldman et al., 2001b, Prinz et al., 2004b, Taylor et al., 2009, Ball et al., 2010b). This approach has complemented and extended accumulating biological evidence that is consistent with the idea that output features across identified cells may be conserved by both balance and compensation among key intrinsic conductances, rather than by tightly regulating the magnitude of individual conductances (MacLean et al., 2003, Swensen and Bean, 2005b, Grashow et al., 2010, Ransdell et al., 2012). However, most of these studies involve compensation that leads to conservation of output following perturbation of the cellular excitability (MacLean et al., 2003, Bergquist et al., 2010), often via gene knockout (Van Wart and Matthews, 2006, Nerbonne et al., 2008) or pharmacological manipulation (Swensen and Bean, 2005b, Ransdell et al., 2012). While these studies demonstrate that variability could arise as a result of such homeostatic plasticity, these studies do not address intrinsic variability found in these neurons with all conductances intact, or whether this variability represents differential tuning to conserved output *in vivo*.

We utilize the crustacean cardiac ganglion, which contains multiple large cell (LC) motor neurons that produce synchronous bursting output, to test whether individual neurons achieve conserved output by differentially balancing conductance magnitudes. We examine multiple motor neurons within the same ganglia, which are genetically identical and have similar output in the native network, and find that they have varying underlying conductances. Then by disrupting a select subset of conductances in these cells with pharmacological blockade, we demonstrate a corresponding disruption in conserved output. We believe this is the first direct demonstration that multiple neurons, particularly within the same neural network, naturally generate similar output by differentially balancing variable underlying conductances, independent of induced compensatory changes.

MATERIALS AND METHODS

Animals

Crabs (*Cancer borealis)* of either sex were purchased and shipped overnight from The Fresh Lobster Company (Gloucester, MA, USA). Crabs were kept at 12°C in artificial seawater. Dissections took place in chilled physiological saline: 440 mM NaCl, 26 mM MgCl2 13 mM CaCl2, 11 mM KCl, and 10 mM HEPES (pH = 7.4). Chemicals were obtained from Fisher Scientific (Pittsburgh, PA) unless otherwise noted.

Electrophysiology

All intracellular recordings were made from LC3, 4, and 5 somata. LC structure consists of a cell soma and proximal neurite that projects to a common spike initiation area located posterior to the anterior branch point (Hartline, 1967a, Tazaki and Cooke, 1983b, Cooke, 2002a, Ransdell et al., 2013) [see Fig 1A]. Somata were separated from action potential (AP) conductances (unless noted otherwise) by tightening a thread ligature past the anterior branch point on the nerve the LC was located in (see Fig. 1A, 2A, 2B). Isolated somata carry ionic conductances that generate driver potential output (Tazaki, 1972, Tazaki and Cooke, 1983b, Tazaki and Cooke, 1986, Cooke, 2002a), even with ligatures as close as 200 μm from the soma (Tazaki and Cooke, 1983b).

Experiments were performed in physiological saline at 12°C. Extracellular recordings were made with stainless steel pin electrodes in petroleum jelly wells placed on the nerve. Signals were amplified and filtered using a differential AC amplifier (A–M Systems, Sequim, WA). Intracellular recordings were made with glass electrodes containing 3 M KCl (8-17 MΩ) using an Axoclamp 2A amplifier (Axon Instruments, Union City CA)**.** Two-electrode voltage clamp (TEVC) and two-electrode current clamp (TECC) protocols were created, driven and recorded with Clampex 9.2 software (Axon Instruments). Recordings were analyzed with Clampfit 9.2 (Axon Instruments). R_{in} was measured in TECC with 10 negative current injection steps (t = 2 s, -1 to -10 nA).

TEVC measurements for I_A, I_{HTK}, I_{Ca}, and I_{NaP} were made using protocols described in detail in our previous work (Ransdell et al., 2012, Ransdell et al., 2013). Outward currents were measured at 0 mV, inward currents at peak conductance.

Stimulus Protocols

To generate current injection waveforms, we recorded voltage waveforms from LC somata during intact network activity. For Stimulus Protocol 1, this consisted of 20s recordings from LC3 that included four burst potentials with both pacemaker EPSPs and LC back-propagating APs (BPAPs). During this recording V_{rest} = -55 mV. For Stimulus Protocol 2, to remove LC BPAPs, we hyperpolarized the LC soma to -65 mV to eliminate spiking. This enabled us to record the voltage change caused by a single burst of pacemaker EPSPs. We then isolated LC3 with ligature and used the voltage waveforms recorded as the command voltage in TEVC. The average current injection over five sweeps necessary to generate each of the voltage waveforms was used for Stimulus Protocols 1 and 2.

Each stimulus protocol was applied at V_{rest} and four starting voltages (-60, -50, -40, -30 mV) controlled with DC current injection. Blockers (25 mM TEA or 1 mM 4AP) were applied to the preparation for 30 minutes, after which stimulus protocols were repeated at each starting voltage.

Statistics

Analyses utilized SigmaPlot 11.0 and Clampfit 9.2 software. R-values are results of Pearson correlation (Fig. 2) or cross-correlation function estimate (Fig. 3, 4) with a 10 ms lag; in cross-correlation analysis, the peak R-value across the lag period was used. Correlation analyses were conducted only between LCs of the same ganglion using the entire voltage trace from each stimulus protocol. After failing Shapiro-Wilk tests for normality, changes in R_{in}, V_{rest}, and differences between R-values before and after pharmacological blockade were analyzed with Mann-Whitney *U*-tests.

RESULTS

In the intact cardiac ganglion (Fig. 1A), bursts in LCs are initiated via excitatory input from pacemaker interneurons (Fig. 1B) that result in synchronous burst and AP generation in all five LC motor neurons (Fig. 1B). In addition, LC somata contain the intrinsic conductances that influence burst potentials (Fig. 1C). However, the magnitudes of these currents vary not only across animals (Fig. 1C), but even among cells of the same ganglion (Fig. 1D). If variability in current magnitude suggests that individual cells differentially balance their conductances to achieve a common output, then blocking a subset of conductances should reveal differential tuning of the remainder, as demonstrated by a shift away from conserved output. Our initial data were consistent with this hypothesis: when LCs were exposed to high-threshold K+ current (I_{HTK}) blocker (TEA – see Fig. 1D inset), their normally synchronous waveforms in spontaneously

active networks became desynchronized and variable (Fig. 1E). TEA application localized to LC somata is able to affect spiking output, causing changes in the spiking pattern as well as apparent desynchronization of spiking as revealed by a decrease in spike amplitude that we interpret as loss of summed, synchronous AP activity (Fig. 1F). This decrease in amplitude cannot be attributed to TEA block of APs, as the somata localization of the TEA in this experiment left axonal conductances intact. These data demonstrate that LC somatic conductances play a significant role in shaping waveform as well as spiking output in these cells.

Because cells in intact networks are subject to many factors that influence output, we employed an experimental strategy to test solely the influence of variable conductances on output in neurons isolated from their constituent network connections. To reliably demonstrate a shift away from conserved output at the single cell level following conductance block, we devised standardized, biologically relevant current injection protocols. We isolated the somata of the three anterior LCs from pacemaker synaptic input, electrical coupling, and BPAPs, effectively isolating their burst generating conductances (Fig. 2A, 2B). We then used current injection to characterize cell output before and after blocking conductances. In designing the protocol, which employs somatic current injections, we considered that somata naturally receive two kinds of current input: synaptic and BPAPs. We recorded these somatic input currents from cells in intact networks, and subsequently used these recordings as the basis for realistic current injections applied to isolated cell somata (Figs. 2A, 2B; see Methods). Stimulus Protocol 1 consists of both biologically realistic synaptic currents plus BPAPs (Fig. 2A).

Stimulus Protocol 2 consists solely of current injection of synaptic drive to the soma via pacemaker inputs (Fig. 2B). We first determined that our current injection protocols, when applied to isolated somata with all intrinsic conductances intact, produced virtually identical voltage responses across LCs as measured by cross-correlation analysis. Under control conditions, current injection elicited conserved membrane waveforms across LCs in the same network (Figs. 2 A1, B1 – controls). Thus the basis for our experiments is whether these conserved output responses are maintained subsequent to pharmacological blockade of conductances.

We considered four key points in testing the hypothesis of conserved output from variable underlying conductances. First, we ensured that individual conductance levels do indeed vary across isolated cells. We measured current levels carried by four ionic conductances in LC somata: I_{HTK} (high-threshold K^+ current, a combination of I_{Kd} and I_{KCa}), I_A (transient K^+), I_{Ca}, and I_{NaP} (persistent Na^+). Each current measured varied at least 2-4 fold across individual cells (Fig. 1C). Second, if output simply were constrained by electrical synapses between LCs, then isolated neurons should no longer produce conserved output from standardized current injection. This was not the case; isolated LCs with all conductances intact produced remarkably consistent output (Fig. 2, controls). Third, if conserved output is simply a result of isolated cells passively following current injection, then blocking conductances should not alter this output. This also was not the case; when I_{HTK} is blocked with TEA (Fig. 1D), cell output as a result of the standardized current injection was substantially altered (Fig. 2 A2, B2 – blue boxes). Finally, and perhaps most pertinent to the hypothesis, if cells are not differentially tuned

to produce similar output, then blocking a conductance might still be expected to alter output, but should produce uniform changes across cells. This was not the case; when TEA was applied to isolated LCs, and standardized current injection applied, the once similar outputs diverge between cells (Fig. 2) as revealed by significantly lower (and highly variable) R-values from cross-correlation analyses following TEA exposure (Fig. 3 A,B). To ensure that these differences were not due to changes in V_{rest} after TEA exposure, current injections were performed from native V_{rest}, as well as standardized baseline voltages ranging from -60 mV to -30 mV. TEA did not cause a significant change in V_{rest} (mean ± SD - control: -49 ± 7.03 mV, TEA: -46.3 ± 10 mV, $p = 0.23$, N=12). However, TEA did cause significant reduction in mean R-value between cells at V_{rest} , -50 mV, -40 mV, and -30 mV starting voltages, but not at -60 mV, in both Stimulus Protocols (Fig. 3A,B). At -60 mV, the depolarization in membrane potential due to current injection did not reach the activation voltages of most of the conductances (Ransdell et al., 2012, Ransdell et al., 2013). Therefore, the -60 mV data actually demonstrate what happens when these cells are simply passive followers of current injection, and support the result that at voltages where conductances are activated, there is a true loss of tuning when a subset of currents are blocked.

To ensure these results are not due to changes in input resistance (R_{in}) of cells in TEA, we analyzed relationships between R_{in} and activity. TEA did not significantly or predictably alter R_{in} (mean ± SD – control: 5.03 ± 2.4 MΩ, TEA: 5.25 ± 3.28 MΩ, $p = 0.795$, N=12). However, we predicted that if loss of conserved activity across LCs with blockade were a result of variable impact of the TEA on R_{in}, then the largest changes in

activity between cells should occur with the largest difference in R_{in} between those two cells. We found no such relationship between change in R_{in} of individual cells, or the difference in R_{in} between pairs of cells, with the change in R-value in the corresponding cross-correlation (Fig. 3C-F).

Finally, if this is a general phenomenon and not just specific to I_{HTK}, then blocking another conductance in this system also should result in loss of conserved output. We blocked a second K^+ current, I_A, using 4-aminopyridine (4-AP). 4-AP caused the same loss of conserved output in LCs (Fig. 4A) with both Stimulus Protocols, as well as an overall increase in variability of R-values (Fig. 4B).

DISCUSSION

Evidence for compensation of intrinsic excitability that stabilizes neuronal output has accumulated from nervous systems across phyla, ranging from the cardiac neurons used in this study (Ransdell et al., 2012) to mammalian systems (Desai et al., 1999, Nerbonne et al., 2008). This homeostatic plasticity of intrinsic excitability is likely a critical mechanism underlying neural network dynamics (Davis, 2006, Turrigiano, 2011a), and may be involved in disorders of neuronal excitability such as epilepsy (Echegoyen et al., 2007, Howard et al., 2007). These compensatory responses, and the changes and variability in ionic conductances they induce, are usually the result of pathology, injury, or experimental manipulations that substantially and drastically alter the parameter landscape of these neurons. Yet few of these model systems capture native

variability of neurons within unmanipulated networks. So the question remains, do neurons in native networks, that are genetically identical (i.e., cells within the same network), achieve similar output at least in part by differentially tuning the underlying intrinsic conductances via distinct mechanisms? It is this question, independent of compensation, that our study addresses.

We addressed several key components of this question in this study. First, we demonstrated that motor neurons of the cardiac ganglion have similar membrane potential waveforms within the same network, both during intact network activity (Fig. 1B) and as isolated neurons responding to biologically relevant current injection protocols (Fig. 2). This ability to record from unambiguously identified neurons both in intact networks and under experimentally controlled conditions, both of which are crucial to directly test the hypothesis in this paper, represents a key strength of this model system, and how it can contribute uniquely to this question. Second, we measured native current magnitudes of multiple ionic conductances, to ensure that these cells also showed variability in magnitudes of conductances as reported in other systems (Fig. 1C). Not only did these cells show 2-4 fold variability in their underlying conductances, but even cells within the same network showed substantial variability in current magnitudes (Fig. 1D). Third, we ruled out the possibility that the voltage waveforms of isolated cells were passively following external current injection (Fig. 2C, 2D). Finally, these preconditions allowed us to directly pose the experimental question: does natural variability in underlying current magnitudes result from differentially tuned conductances converging on similar output via distinct solutions? We tested this with a relatively straightforward

experimental design. Namely, if output is the result of finely balanced ratios of ionic conductances, then disrupting one conductance should cause each cell to experience a cell-specific de-tuning, resulting in loss of conserved output. Our results were entirely consistent with the hypothesis: blocking either I_{HTK} or I_A independently results in loss of similar output across three LC neurons within the same network (Figs. 2, 3A, 3B).

Similar manipulations in pacemaker neurons of the stomatogastric ganglion (STG) have yielded different results (Szucs and Selverston, 2006). In the STG, 4AP used to disrupt A-type current in paired pyloric dilator neurons, also reported to have variable conductance magnitudes (MacLean et al., 2005), showed little impact on synchronized activity between these cells (Szucs and Selverston, 2006). These data, while seemingly contradictory, are intriguing as Szucs et al. (2006) left chemical and electrical synaptic connectivity, as well as neuromodulatory inputs to these networks (Marder and Thirumalai, 2002), intact during 4AP application. We carefully selected cardiac LCs as a model where we have control over these higher order network properties, allowing us to focus solely on intrinsic excitability. Interpreted in the context of the Szucs and Selverston work (2006), convergent output as a result of differentially tuned conductances likely is only one layer of regulation in these systems ensuring synchronized output (see Prinz et al. 2004). Work is ongoing to determine whether and how higher order processes, such as electrical coupling and neuromodulation, ensure that cellular and network output are maintained in patterns necessary for robust function (Grashow et al., 2009, 2010, Marder, 2012).

The most parsimonious explanation for our results is that cells with variable underlying conductances are indeed individually tuned to produce conserved output. We believe these findings provide a clear and unambiguous demonstration of this phenomenon, helping unify a substantial amount of compelling and consistent evidence in multiple model systems, both biological and theoretical (Marder, 2011a, Marder and Taylor, 2011, Turrigiano, 2011a). It is striking that differential tuning is not simply found across different individuals, but is seen even among cells with in the same individual. One compelling question that arises from these findings is the nature of the developmental and post-developmental origin of this variability. Specifically, are individual neurons produced with common underlying conductance relationships that then diverge over time (via compensation), or is variability inherent to the initial development and tuning of a neuron, and maintained across the lifetime of the animal? Answers to these questions will rely on model systems that allow for identified neurons to be characterized effectively over both developmental and post-developmental time scales.

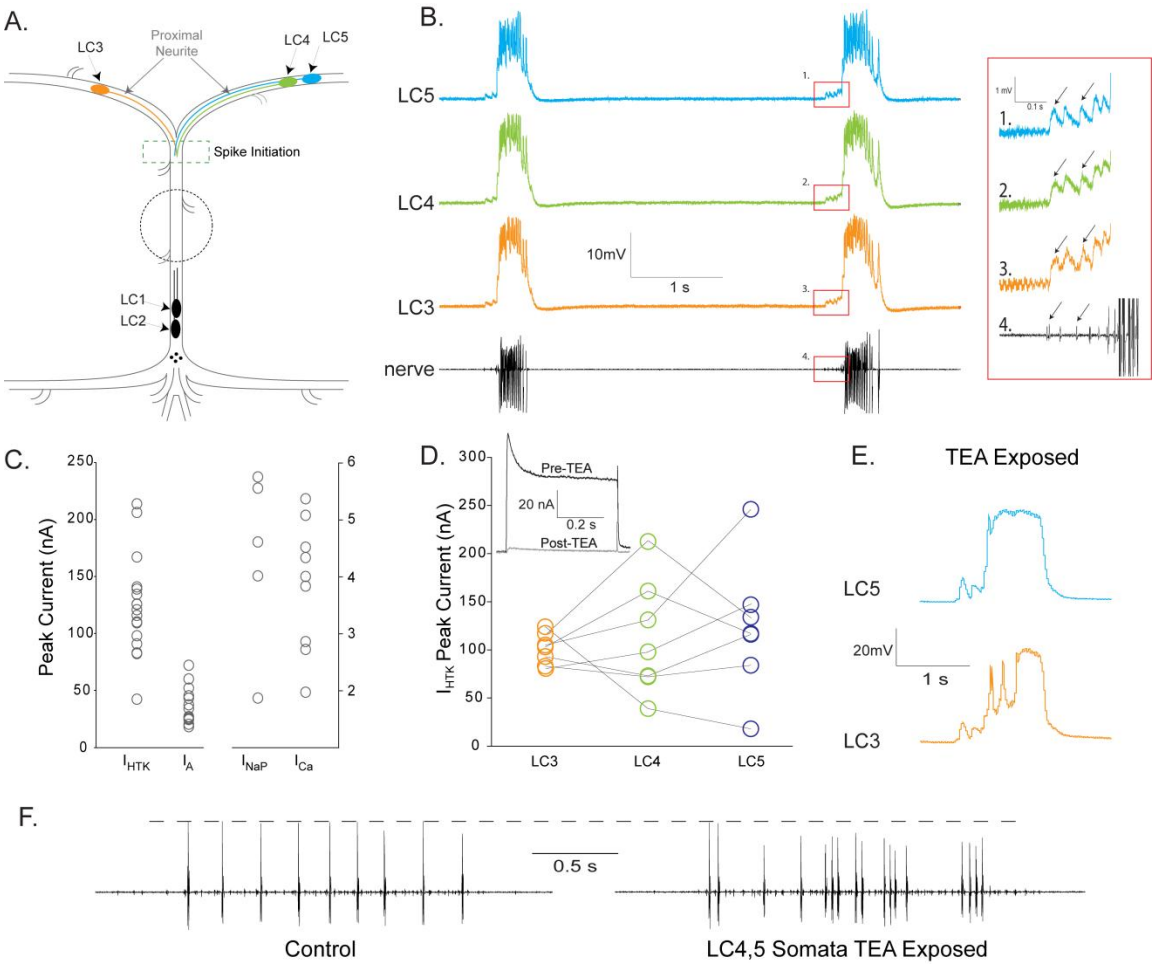
A.
LC3
Proximal Neurite
LC4
LC5
Spike Initiation
LC1
LC2
B.
LC5
LC4
LC3
nerve
10mV
1 s
1.
2.
3.
4.
1 mV
0.1 s
C.
Peak Current (nA)
250
200
150
100
50
0
6
5
4
3
2
I_HTK
I_A
I_NaP
I_Ca
D.
Pre-TEA
20 nA
0.2 s
Post-TEA
I_HTK Peak Current (nA)
300
250
200
150
100
50
0
LC3
LC4
LC5
E.
TEA Exposed
LC5
20mV
1 s
LC3
F.
0.5 s
Control
LC4,5 Somata TEA Exposed

Figure 3.1 A) Schematic of *C. borealis* cardiac ganglion showing location of LC somata (ovals) and pacemaker interneurons (small circles). Extracellular recordings are taken from the central nerve (dashed circle). All experiments were conducted on three anterior LCs 3-5 (colored ovals). These cells project a proximal neurite from their somata towards a common spike initiation zone region (green dashed box), and then axons continue posterior. **B)** Activity of LC neurons during spontaneous network activity. Extracellular recording (bottom trace) shows LC (tall spike) and pacemaker (short spike) APs. *Inset, red box*- enlarged recordings displaying that each pacemaker AP (small spike) results in an EPSP in all three anterior LCs. Two pacemaker APs and resulting EPSPs are labeled (arrows). **C)** Variability in LC inward and outward current magnitudes. **D)** I_{HTK} variability across LCs within the same network. Lines connect LCs from same individual. *Inset*: I_{HTK} is blocked by 25 mM TEA exposure (30 min). Current traces before (blue) and after (red) TEA were clamped at 0 mV step from -40 mV holding potential. **E)** TEA exposure in the intact network desynchronizes membrane potential waveforms of LCs during ongoing rhythmic activity. **F)** Spiking output (extracellular recordings) is affected by TEA applied to LC4 and LC5 somata. Dashed line for comparison of spike amplitudes. Traces were taken from the same recording well within 10 minutes of one another.

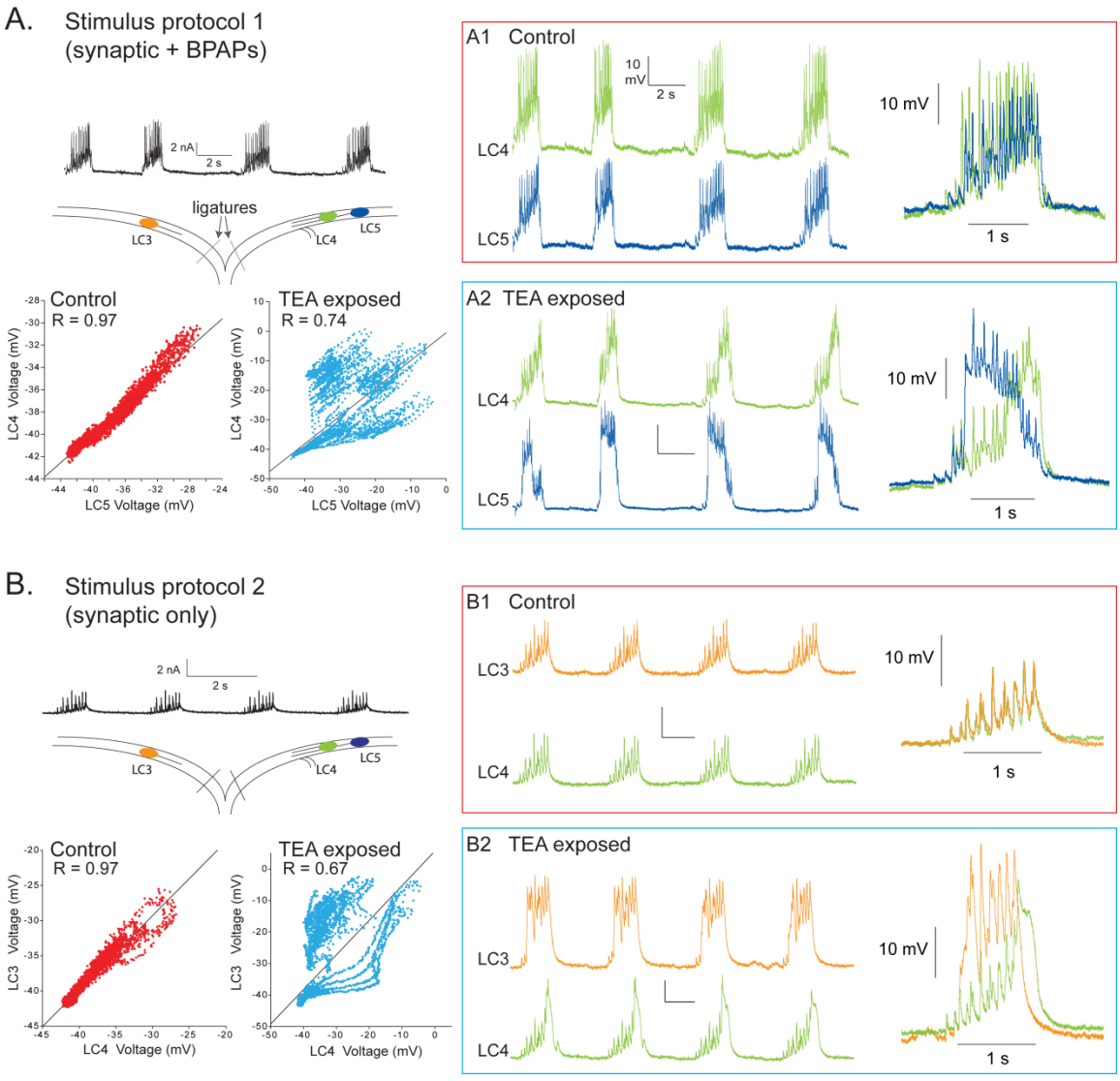
A.
Stimulus protocol 1
(synaptic + BPAPs)
2 nA
2 s
ligatures
LC3
LC4
LC5
Control
R = 0.97
TEA exposed
R = 0.74
LC4 Voltage (mV)
LC5 Voltage (mV)
A1 Control
10 mV
2 s
LC4
LC5
10 mV
1 s
A2 TEA exposed
LC4
LC5
10 mV
1 s
B.
Stimulus protocol 2
(synaptic only)
2 nA
2 s
LC3
LC4
LC5
Control
R = 0.97
TEA exposed
R = 0.67
LC3 Voltage (mV)
LC4 Voltage (mV)
B1 Control
LC3
LC4
10 mV
1 s
B2 TEA exposed
LC3
LC4
10 mV
1 s

Figure 3.2 Realistic current injection protocols used to test intrinsic excitability of isolated LCs. A. Stimulus protocol 1 reproduces both synaptic currents and back propagating APs (BPAPs). LCs 3, 4, and 5 are isolated from the network via thread ligatures (slash marks), and the stimulus protocol is applied before (A1 - control, red box) and after (A2 - TEA exposed, blue box) exposure to 25 mM TEA. Representative traces show the response to the entire stimulus protocol, and overlaid traces show the 4^{th} burst in the sequence. Scatterplots show pair-wise correlation of time matched voltages (sampled at 500Hz) of the waveforms shown in the representative traces. R-values are results of Pearson's correlation test for these two cells. Loss of conserved output is demonstrated by the lack of correlation in the scatterplot as well as the decrease in R-value. **B.** Stimulus protocol 2 reproduces synaptic currents LCs receive from pacemaker neurons. Experiments and analyses were performed as in Stimulus Protocol 1.

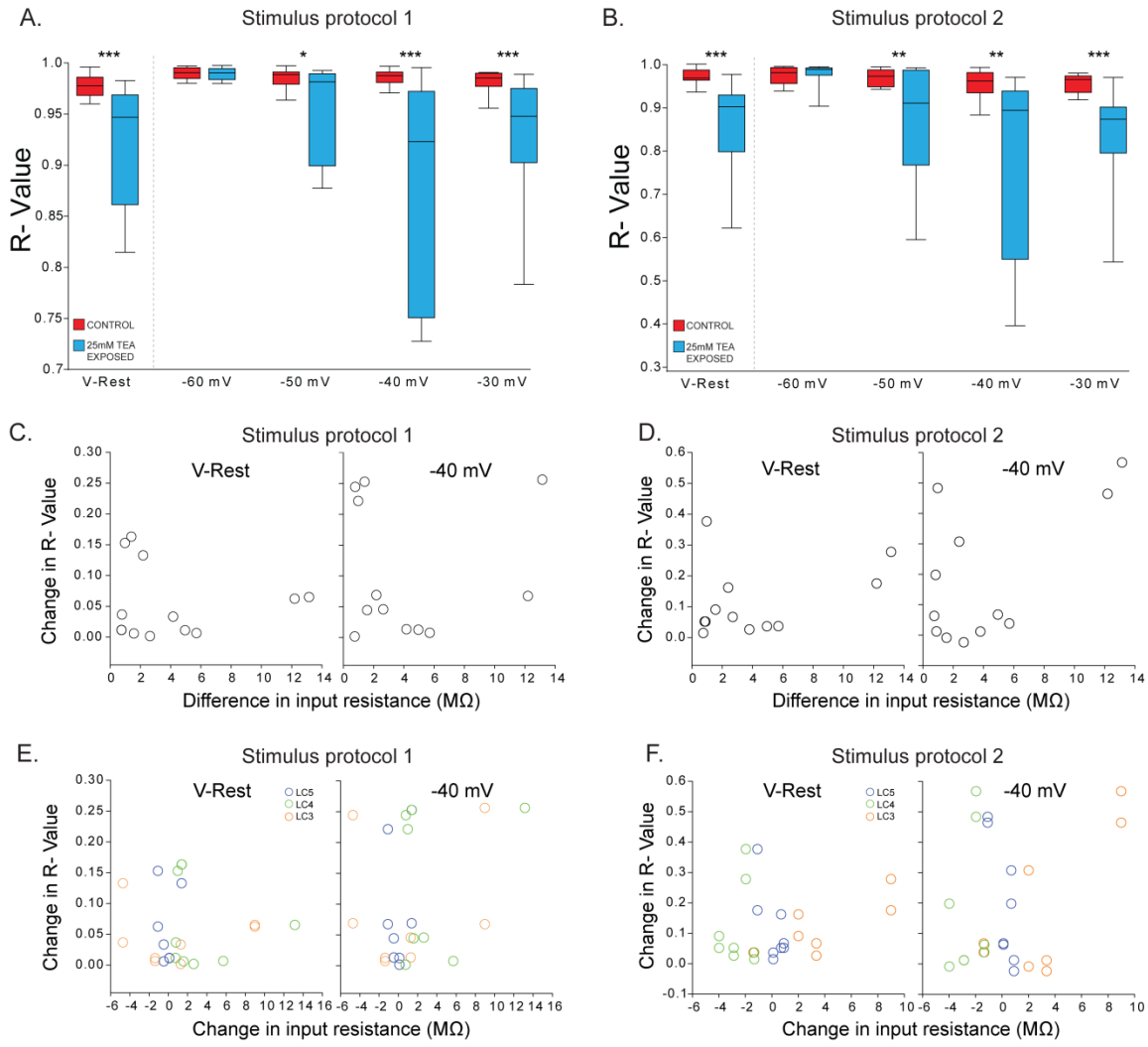
A.
Stimulus protocol 1
R- Value
CONTROL
25mM TEA EXPOSED
V-Rest
-60 mV
-50 mV
-40 mV
-30 mV
B.
Stimulus protocol 2
C.
Stimulus protocol 1
V-Rest
-40 mV
Change in R- Value
Difference in input resistance (MΩ)
D.
Stimulus protocol 2
E.
Stimulus protocol 1
LC5
LC4
LC3
Change in input resistance (MΩ)
F.
Stimulus protocol 2

Figure 3.3 Changes in output after TEA exposure. A-B. Box plots show distributions of R-values from cross-correlation analysis of LC voltage waveforms generated by Stimulus Protocol 1 (**A**) and Stimulus Protocol 2 (**B**) before (red boxes) and after (blue boxes) 25 mM TEA exposure. Lines within boxes mark the median, box boundaries represent 25^{th} and 75^{th} percentiles, whiskers represent maximum and minimum values. All comparisons were made between LCs of the same individual (N=12 comparisons across 6 individuals). Each stimulus was injected into an isolated LC at its natural V_{rest} and four starting voltages. Significant differences in median R-value were tested with Mann-Whitney *U*-tests, and are denoted by asterisks (*** - $p<0.005$, ** - $p<0.01$, * - $p<0.05$). **C-D.** Comparison of change in R-value with difference in R_{in} between LCs after TEA exposure for Stimulus Protocol 1 (**C**) and Stimulus Protocol 2 (**D**). **E-F.** Comparison of change in R-value with change in R_{in} after TEA exposure for Stimulus Protocol 1 (**E**) and Stimulus Protocol 2 (**F**).

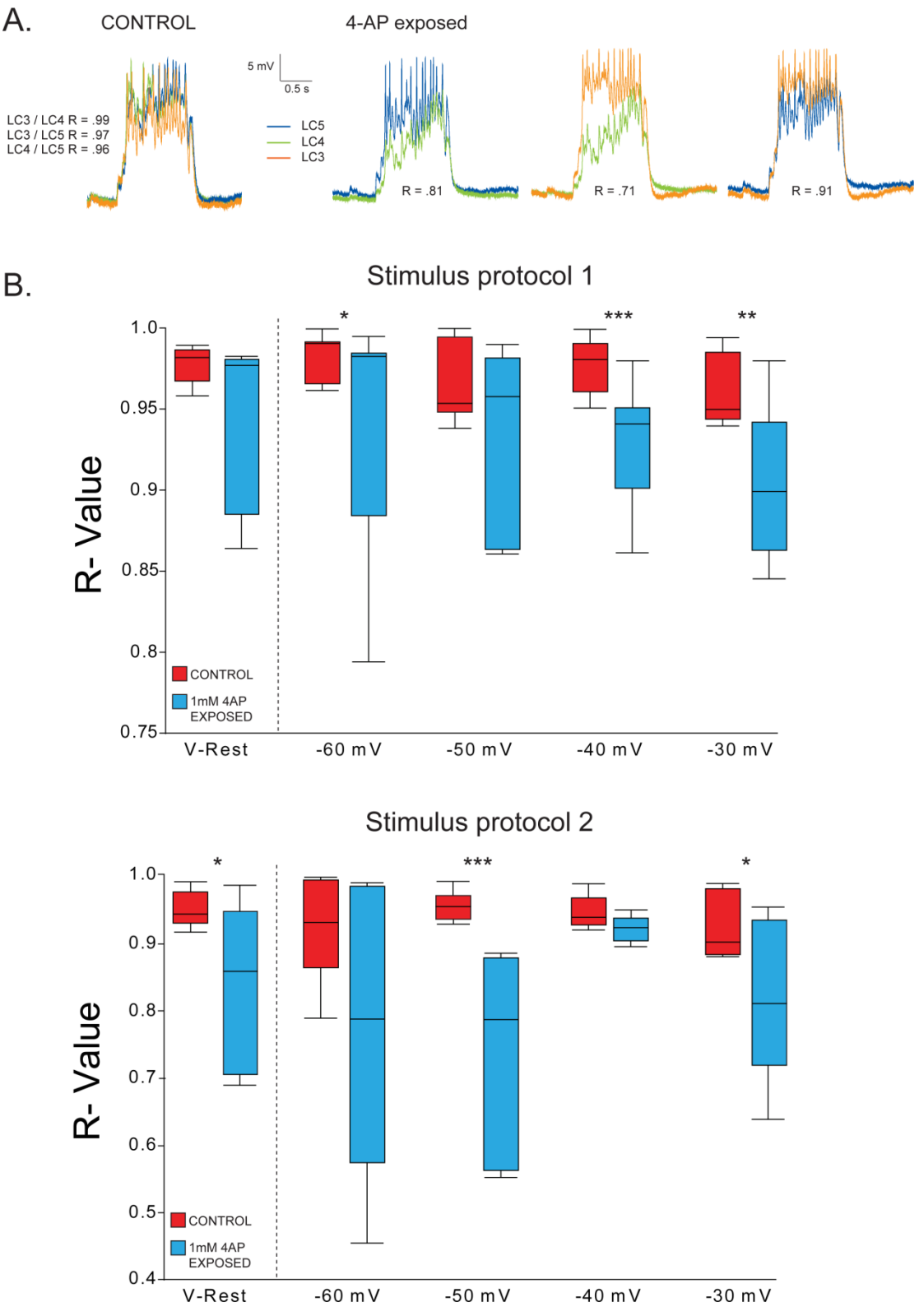
A.
CONTROL
4-AP exposed
5 mV
0.5 s
LC3 / LC4 R = .99
LC3 / LC5 R = .97
LC4 / LC5 R = .96
LC5
LC4
LC3
R = .81
R = .71
R = .91
B.
Stimulus protocol 1
R- Value
1.0
0.95
0.9
0.85
0.8
0.75
*
***
**
CONTROL
1mM 4AP EXPOSED
V-Rest
-60 mV
-50 mV
-40 mV
-30 mV
Stimulus protocol 2
R- Value
1.0
0.9
0.8
0.7
0.6
0.5
0.4
*
***
*
CONTROL
1mM 4AP EXPOSED
V-Rest
-60 mV
-50 mV
-40 mV
-30 mV

Figure 3.4 Effects of 4-AP on conserved output. A. Overlaid representative traces of LC responses to Stimulus Protocol 1 before and after 4-AP exposure. R-values from cross- correlation analyses as in Figure 3. **B.** Box plots show distributions of the R-values from cross-correlation analysis of isolated LCs voltage waveforms generated by Stimulus Protocols 1 and 2 before (red boxes) and after (blue boxes) 1 mM 4AP exposure. The line within the box marks the median, box boundaries represent the 25^{th} and 75^{th} percentiles, whiskers above and below represent the maximum and minimum values. All comparisons made between LCs of the same individual (N=7 and N=6 for Stimulus Protocols 1 and 2 respectively), as described in Figure 3. Differences in median R-value were tested with Mann-Whitney *U*-tests, and are denoted by asterisks (*** - $p<0.005$, ** - $p<0.01$, * - $p<0.05$).

CHAPTER FOUR

LC motor neurons co-regulate electrical coupling and intrinsic conductance properties to maintain synchronized burst output

Electrical synapses are often implicated in the synchronization of neurons within a circuit. The importance of gap junction communication is becoming increasingly appreciated in large scale neurological events such as brain rhythms (Marder et al., 2005) and epileptic seizures (Perez Velazquez and Carlen, 2000). Small, well defined and rhythmic networks, which utilize electrical coupling, are an ideal means to investigate how electrical coupling interact with other functional components of a rhythmic neural networks and can further our understanding of how groups of neurons achieve synchronous or asynchronous firing states. These model systems have recently shed light on the complexity of intrinsic excitability regulation and maintenance. Work in crustacean central pattern generators show that neurons with identical output, can have several fold variability in their intrinsic conductances (Golowasch and Marder, 1992, Schulz et al., 2006, Temporal et al., 2012); computational and biological evidence further suggest that conserved relationships between intrinsic conductances and network level properties act in maintaining similar output properties across cells with disparate intrinsic

organization (Prinz et al., 2004a, Ball et al., 2010a, Franklin et al., 2010, Ransdell et al., 2012). Here we ask if there are conserved relationships between electrical coupling strength and the disparate intrinsic organization of synchronized motor neurons, and if so are these relationships functional in maintaining synchrony. To do this we utilize the three anterior large cell (LC) motor neurons of the *Cancer borealis* cardiac ganglion. These cells have disparate intrinsic conductance organization, are electrically coupled and burst synchronously during network behavior.

We begin by exploring both the coupling strength and two intrinsic potassium currents across several animals; the purpose of this is to expose possible conserved relationships between these properties. We find that of the three anterior LCs, those which have more variability in the potassium current I_{HTK}, namely LC4 and LC5, also have greater amount of electrical coupling. Furthermore, the magnitude of I_{HTK} is positively correlated with the strength of electrical coupling between two LCs.

Next, we manipulate both electrical coupling and I_{HTK} to test if the correlations found between these properties are functional in maintaining LC synchrony. Using dynamic clamp to manipulate electrical coupling, and the pharmacological blocker TEA to inhibit I_{HTK}, we find when I_{HTK} is greater, LCs require a greater amount of electrical coupling to synchronize activity. This suggests that the correlation between I_{HTK} and coupling strength is functional in maintaining LC synchronization.

These results demonstrate that identified neurons maintain appropriate output, not only by maintaining relationships between intrinsic parameters, but also by co-regulation of intrinsic properties with network level properties such as electrical coupling.

Introduction

Computational and biological studies in the last decade have uncovered key principles in how neurons generate and maintain appropriate output. Using model systems in which neurons are identifiable from animal to animal we now understand that both network properties, such as electrical and chemical synaptic strength, and intrinsic properties, such as voltage gated currents and input resistance, can be variable across cells and networks, while maintaining identical outputs (Swensen and Bean, 2005a, Schulz et al., 2006, Schulz et al., 2007a, Goaillard et al., 2009b, Ball et al., 2010a, Ransdell et al., 2013). In short, there are multiple solutions to a given network / neuronal output. Studies also reveal that compensatory interactions among network and intrinsic properties result in conserved relationships which can be measured across animals (Ball et al., 2010a, Franklin et al., 2010, Ransdell et al., 2012); these relationships are thought to act in maintaining the signature output of the network or neuron. While these advances are significant, it is still unclear what part regulation of intrinsic properties, and what part regulation of network properties, play in maintaining functional output (for

review see Turrigiano, 2011B); furthermore, there are few biological studies which examine if there are co-regulatory mechanisms which bridge intrinsic properties with network level properties; that is, a conserved relationship between something intrinsic to a cell and a property of the network the cell functions in. These are questions this study aims to address by carrying out dual intrinsic (ionic currents) and network level (electrical coupling strength) measurements, and examining how relationships between these properties function in maintaining an important characteristic of network function like motor neuron synchronization.

The *C. borealis* cardiac ganglion is a central pattern generator (CPG) network of only nine neurons and two distinct cell types. Four SC interneurons drive five LC motor neurons to burst synchronously causing whole heart contraction. We know of three levels of regulation which contribute to the synchronous LC output. First, LCs receive the same excitatory input from the SC pacemaker neurons. Second, LC motor neurons within a network have disparate intrinsic conductances that are actively tuned to achieve similar levels of intrinsic excitability. Third, LCs are electrically coupled to one another, albeit with coupling conductances which are variable both within a network, and across networks. The following study is based on the hypothesis that because there is variability in these last two levels of regulation (intrinsic conductances, electrical coupling strength) there are likely conserved relationships between these two parameters, which are functional in maintaining synchronization.

We approach this experimentally in two steps. We first probe anterior LCs for relationships between electrical coupling and two voltage gated potassium currents ($I_{A,}$ I_{HTK}) known to affect LC bursts. We then test if these relationships are functional in LC synchronization by manipulating coupling strength via dynamic clamp, and intrinsic conductance via pharmacology, and examine how these manipulations affect burst synchronization across in anterior LC pairs.

Methods

Animals

Crabs (*Cancer borealis)* of either sex were purchased and shipped overnight from The Fresh Lobster Company (Gloucester, MA, USA). Crabs were kept at 12°C in artificial seawater. Dissections took place in chilled physiological saline: 440 mM NaCl, 26 mM MgCl2 13 mM CaCl2, 11 mM KCl, and 10 mM HEPES (pH = 7.4). Chemicals were obtained from Fisher Scientific (Pittsburgh, PA.

Electrophysiology

Dissection preparation and electrophysiology equipment were performed as in chapter three experimental methods.

Electrical coupling and R_{in} was measured in TECC with 15 negative current injection steps (t = 2 s, -1 to -15 nA). Coupling strength was always measured in both directions of an electrically coupled LC pair. Strength of electrical coupling was calculated as coupling coefficient (CC): $\mathbf{CC = \frac{\Delta V1}{\Delta V2}}$

Coupling strength was also measured as coupling conductance. Coupling conductance was calculated by taking the inverse of coupling resistance. To calculate coupling resistance (CR), independent of the two LCs input resistance, we used the following equation: $\mathbf{CR = \frac{(Rinput1 * Rinput2 - (R1 \rightarrow 2)^2)}{R1 \rightarrow 2}}$

Where R_{input1} is the input resistance of the cell 1, and $R_1 \rightarrow_2$ is the resistance from cell 1 to cell 2 due to electrical coupling. Coupling conductance is measured as the inverse of coupling resistance as in Haas et al. (2011).

Two-electrode voltage clamp (TEVC) and two-electrode current clamp (TECC) protocols were created, driven and recorded with Clampex 9.2 software (Axon Instruments). Recordings were analyzed with Clampfit 9.2 (Axon Instruments). TEVC measurements for I_A, I_{HTK} were made using protocols described in chapter 2 methods

section. Current clamp Stimulus Protocol 1, described in chapter 3 Methods section, was used to test LC excitability and synchronization.

Dynamic clamp experiments used Netclamp 1.0 software (Friedman Brain Institute, New York, NY) to insert artificial electrical coupling between two isolated LCs. To combine Netclamp driven artificial electrical coupling protocol with Clampex 9.2 driven Stimulus Protocol 1, both output signals were sent through a Brownlee model 410 instrumentation amplifier, where they were summed before being sent to the current injection electrodes. Using this setup, artificial electrical synapse was added between isolated LCs while Stimulus Protoocol 1 was simultaneously injected into the two cells. These protocols were administered after both cells were exposed to 25mM TEA for 10 minutes and never extended past 45 minutes TEA exposure. Cell pairings were always between LC3 and LC4 or LC3 and LC5. The following electrical coupling strengths were used for each cell pairing: 0 µS, .025 µS, .05 µS, .1 µS, .2 µS and .4 µS.

Statistics

Analyses utilized SigmaPlot 11.0 and Clampfit 9.2 software. R-values are results of Pearson correlation (Fig. 2) or cross-correlation function estimate (Fig. 3, 4) with a 10 ms lag; in cross-correlation analysis, the peak R-value across the lag period was used. Changes caused by TEA exposure were analyzed with a paired 2-tail T-test.

Results

Anterior LC to LC electrical coupling

The five LC motor neurons of the *C. borealis* cardiac ganglion are electrically coupled and fire synchronous bursts during normal network output. In this study we concentrate on the three anterior LCs as they can be easily isolated from network components via thread ligature placed just posterior to the anterior branch point (figure 1A). This reduced preparation offers three coupled motor neurons with disparate intrinsic properties that are able to fire synchronous burst potentials during normal network behavior (see Figure 3.1). All three anterior LCs (LC3 , LC4, LC5) are electrically coupled at the anterior branch point (Fig. 4.1A); there is additional local coupling between LC4 and LC5 somata (Fig. 4.1A). This additional local coupling likely causes LC4 and LC5 to have a greater total amount of electrical coupling to anterior LCs than LC3. Figure 4.1B shows mean coupling conductance on each of the anterior LCs (x-axis), from the additional two anterior LCs; 2 bars per cell, bar colors denote which LC the coupling conductance is impacting.

The clearest difference on the Figure 4.1B is total coupling conductance affecting LC3 is smaller than total coupling conductance affecting LC4 and LC5. We also find

that electrical coupling between LC4 and LC3 is significantly higher that coupling between LC5 and LC3 (two-tailed t-test, $p < .001$), this difference is likely because electrical coupling between LC3 and LC4 or LC5 takes place at the anterior branch point of the CG, and the somata (where measurements take place) of LC4 are closer to the anterior branch point than the somata of LC5.

Anterior LC I_{HTK} and I_A properties

Because LC3 (Fig. 4.1B orange bars) has a smaller amount of total electrical coupling to anterior LCs than LC4 (Fig. 4.1B green bars) and LC5 (Fig. 4.1B blue bars), we thought to examine if there is differential magnitude of the outward potassium currents I_A and I_{HTK} across the three anterior LCs. These currents were chosen because they can be measured without the use of pharmacological blockers, are known to be important to bursting output in these cells (See chapter 3) and can be quickly removed using the blockers TEA (I_{HTK}) or 4AP (I_A). In Figure 4.1C we show I_A (*upper*) and I_{HTK} (*lower*) magnitude at 0mV voltage step across multiple LC3, LC4 and LC5 neurons. We find that LC3, while having the least amount of total LC to LC coupling among the anterior cells, also has the smallest variability in I_{HTK} magnitude (quantified as coefficient of variation) across animals (Fig. 4.1D). I_A coefficient of variation did not coordinate with total coupling strength on LCs. Note: total electrical coupling present on each anterior LC was calculated by adding the mean coupling conductance a LC has with the two anterior LCs (mean values shown in Fig. 4.1B). We do not see a significant

difference in LC3, LC4 and LC5 magnitude of the two currents (Fig. 4.1C, $p > .05$ for all comparisons of current magnitude).

Because LC3 has the least amount of total electrical coupling, and also has the smallest coefficient of variation in I_{HTK} magnitude we hypothesize that LC3 may have a more constrained I_{HTK} parameter space because of a lack of LC to LC electrical coupling; or to be put another way, LC4 and LC5 I_{HTK} parameter space can be more variable because the two cells have stronger total electrical coupling to other anterior LCs, which may act in constraining output properties.

Does Variability in I_{HTK} affect LC burst output?

Before testing if the relationship between I_{HTK} variability and coupling strength are functionally important, we sought to test first, if the difference I_{HTK} parameter space can be measured as a function of, and is relevant to, the LCs intrinsic voltage response to depolarizing stimuli. To do this we apply Stimulus Protocol 1 (see Fig. 3.2) to anterior LCs before and after TEA exposure, just as in chapter 3. Only, instead of comparing LC voltage response across a single network of anterior LCs, we instead run cross correlations on LC3 with LC3 neurons in other animals (4 animals LC3 cells yield n=16 comparisons), and the same with LC4 and LC5. We hypothesize that if LC3 actually has a more constrained parameter space of I_{HTK}, then after TEA exposure (I_{HTK} removal), LC3 voltage response to Stimulus Protocol 1 will be less differential than LC4 and LC5

comparisons. Data support this hypothesis (see examples, Fig. 4.2B), with LC4-LC4 and LC5-LC5 correlations showing a significantly larger decrease in R-value (comparing voltage response to Stimulus Protocol 1) after exposure to TEA (Fig. 4.2C *Left*). This result is further demonstrated if we plot the change in R-value of LC3, LC4 and LC5 against the I_{HTK} coefficient of variability for LC3, LC4 and LC5 (Fig. 4.2C *Right*).

Relationships between current magnitude and coupling strength

Because LC4 and LC5 have a larger amount of variability, both in I_{HTK} magnitude and coupling strength, we thought this cell pairing is the most appropriate to probe for relationships between intrinsic current magnitude and coupling strength. We find that the combined magnitude of an LC4 / LC5 pairs I_{HTK} has a significant positive correlation with the cell pairs coupling conductance (data not shown, n=7, R-value = .87, p = 0.011). This relationship is significant if either LC4 or LC5's individual I_{HTK} magnitude is compared to the coupling conductance as well (Fig. 4.3A, LC4: $p<.05$; LC5: $p< 0.1$). This relationship is also present and significant ($p<.05$) if coupling coefficient is used rather than coupling conductance (Fig. 4.3B). There was no significant relationship found between LC4 / LC5 coupling conductance and LC4 I_A (n=5, p = .23) or LC5 I_A (n = 6, p = .284); though a larger sample size may be beneficial to ensure that no relationship exists.

Potential False relationship due to measurement error

We do not believe the I_{HTK} / coupling conductance relationship is an experimental artifact of voltage clamping in one cell, and recruiting additional membrane and I_{HTK} current in the cell which it is coupled to. During TEVC protocols to measure $I_{HTK,}$ the voltage in the coupled neuron is not typically depolarized enough to activate $I_{HTK.}$ Activation of I_{HTK} begins around -20mV (Fig. 2.3D); at 0mV voltage step- post-synaptic LCs peak voltage = -28.5 ± 8.3mV (n=7). Furthermore, in one experiment we carried out TEVC protocol to measure I_{HTK} magnitude of LC4 under regular conditions, and again with LC5 hyperpolarized via DC current injection. Under these two conditions we see less than 3% difference in current magnitude at 0mV (data not shown). This is in line with previous work which investigated the effect of electrical coupling on measured conductance magnitude in two PD neurons of the stomatogastric ganglion, results show that experimental errors are decreased (<10%) when measuring large outward potassium currents, and further reduced when measuring currents at more depolarized membrane potentials (Rabbah et al., 2005).

Does electrical coupling strength affect synchronization of LC output?

In chapter three we demonstrate that the anterior LCs have disparate intrinsic tuning, yet common levels of excitability, by applying realistic current injection protocols to isolated anterior LCs. These protocol are administered with all conductances intact, resulting in similar voltage responses across LCs, and again after uniformly removing a single potassium current, causing a disparate voltage response across anterior LCs. While these results demonstrate LCs tune similar excitability through differential intrinsic

properties, it does not take into account the electrical coupling across LCs, which likely also plays a part in maintaining a uniform and synchronous output. Now that we have found conserved relationships between coupling strength and I_{HTK}, an intrinsic property known to impact burst output in LCs, we begin to ask if these relationships are functional in producing synchronized bursts across network LCs.

To begin exploring how electrical coupling may maintain synchronous LC bursts, we carry out Stimulus Protocol 1 before and after I_{HTK} inhibition (TEA exposure); similar to what was done in chapter three. In this experiment however, there is one important difference; we leave electrical coupling between the LCs intact (no ligatures anterior of branch point), and administer the current injection protocols simultaneously to the two coupled LCs (see schematic, Fig. 4.4A). This simultaneous excitatory input is more realistic to what the coupled LCs undergo during normal network behavior, in which SCs provide very similar excitatory drive to coupled LCs (see Fig. 3.1). The goal of these experiments are to test if, like intrinsic properties, the network level property of LC-LC electrical coupling, also help in maintaining similar output across a network.

We find that when simultaneous current injections are administered to two electrically coupled LCs, those cells maintain very similar output, both before and after exposure to TEA. Correlation coefficient comparing the two coupled cells voltage response to stimulus protocol 1 was not significantly different after TEA exposure at cells

normal resting membrane potential (V-rest) (Fig. 4.4B, $p = 0.327$). When the two cells have a -40mV starting potential (achieved with DC current injection) the R-values are actually significantly increased after TEA exposure (Fig. 4.4C, $p = .01$). This contrasts with R-values obtained when stimulus protocols are injected into only one LC at a time, see Chapter 3 Results, in which R-values are significantly reduced after TEA exposure. These data suggest that electrical coupling, like tuning of intrinsic excitability, acts in constraining uniform voltage output between LCs.

A caveat to this experimental approach is that TEA exposure also causes a significant increase in coupling conductance between the two cells in which the stimulus protocol was administered (Fig. 4.4D); the mechanism(s) behind this increase are unclear, though this increase may be responsible for the significant increase in R-value at the –40mV starting potential (Fig.4.4C). This does not negate the result that electrical coupling helps maintain synchrony between LCs which are intrinsically "de-tuned" post-TEA exposure; however we cannot ensure that the strength of electrical coupling which is constraining output, is also physiologically relevant.

To affectively control coupling strength, and keep it within physiological range, while also using TEA to cause distinct intrinsic excitability between two LCs (as we do in chapter 3), we artificially insert electrical coupling between two isolated LCs using dynamic clamp. In these experiments we run Stimulus Protocol 1 on two isolated

anterior LCs (LC3 + LC4 or LC3 + LC5 pairings) within the same network, beginning after 10 minutes exposure to 25mM TEA. Stimulus protocol 1 is then run on the two cells with multiple, physiologically relevant coupling conductances, inserted via dynamic clamp (See Fig. 4.5A for experiment schematic) . We find, as is expected, that as coupling conductance increases the cross-correlation coefficient comparing the two LCs voltage response, also increases. In doing this across six animals we find that LC to LC synchronization is achieved within physiologically relevant levels of electrical coupling (Fig. 4.5B) after TEA exposure. Bar graph inset on Figure 4.5B shows that after TEA exposure, with only 0.1µS of electrical coupling added, R-values range from 0.93 – 0.99 across six animals. This suggests LC to LC electrical coupling allows synchronization of burst output after a "de-tuning" of intrinsic conductances via TEA exposure.

Are relationships between coupling strength and current magnitude involved in LC synchronization?

In Figure 4.5B we find that some LC pairs require more electrical coupling to achieve a high cross correlation coefficient, or synchronized response (see Fig.4.5B black line vs. blue line). To investigate if this is based on the LCs intrinsic conductance organization, we compare I_{HTK} of the two LCs in each pair with how synchronized the cells response to Stimulus protocol 1 is (R-value); we do this comparison at two artificially inserted coupling strengths: 0.05µS and 0.1µS.

Based on relationships between strength of coupling and I_{HTK} present in the native network (see fig. 4.1 and fig. 4.3) we have two hypotheses: First, we predict with increased variability in I_{HTK} magnitude, a LC pairing will require greater strength in electrical coupling to maintain output. This is based on the relationship between LC I_{HTK} coefficient of variation and total coupling strength on each anterior LC. As a reduced measure of I_{HTK} variability in a single cell pair, we use the difference in I_{HTK} magnitude between the two cells. This difference is correlated to the cross correlation coefficient achieved at 0.05µS and 0.1µS coupling strength (Fig. 4.5C, D). If the hypothesis is correct we predict that cells with a larger difference in I_{HTK} will have a lower R-value at designated coupling strengths, this would result in a negative correlation across experiments. We do not find this to be true, instead we see no statistically significant relationship between the difference in I_{HTK} magnitude and R-value at either .05µS or .1µS coupling strength.

The second hypothesis is based on the positive relationship between magnitude of I_{HTK} and strength of electrical coupling present across LC4 / LC5 pairs(Fig. 4.3). We hypothesize that if two neurons require more coupling to synchronize activity, because of higher levels of I_{HTK}, than after removing I_{HTK} those cells will have a lower R-value at a given coupling strength; thus we will see a negative correlation between I_{HTK} magnitude and R-value at the 0.05µS and 0.1µS coupling strengths. Experiments support this hypothesis, we find a negative correlation between combined I_{HTK} magnitude and the R-value generated with a .05µS and .1µS coupling conductance. These data indicate the

positive relationship we see between I_{HTK} magnitude and coupling conductance (Fig. 4.3) is functional in maintaining a synchronized output between LCs.

Discussion

In this chapter we find maintenance of a synchronized burst waveform across anterior LCs involves both tuning of intrinsic properties and electrical synaptic strength between anterior LCs. This is demonstrated in two relationships between the properties of the intrinsic conductance I_{HTK} and coupling conductance between anterior LCs. First we see that the three anterior LCs have different amounts of variability in the magnitude of I_{HTK}, with LC4 and LC5 I_{HTK} having a larger coefficient of variation than LC3 (Fig. 1B *lower*, 1D). LC4 and LC5 also have significantly more LC to LC electrical coupling than LC3 (Fig. 1C, 1D). Because LC to LC electrical coupling helps constrain and synchronize burst output (Fig.4B, C; Fig. 5B), we hypothesize that LC4 and LC5 are able to have a larger I_{HTK} parameter space than LC3, while maintaining synchronized output. To test if this hypothesis is functional, we examined how the difference in two LCs I_{HTK} magnitude correlates to the coupling conductance necessary to synchronize the two cells after TEA exposure. The reasoning in this experimental approach is if two cells have very different I_{HTK} magnitude, than this would represent a larger parameter space of I_{HTK}, and those cells would require a larger amount of coupling conductance to synchronize output, than a coupled pair with very similar I_{HTK} values. This was not the case. There

was no correlation with the difference in two cells original I_{HTK} magnitude with how much coupling was necessary to synchronize the two cells output (Fig. 5C,D).

This result, however does not displace the idea that variability in intrinsic properties may have a relationship with how much electrical coupling is necessary to synchronize output. It only demonstrates that a measure of I_{HTK} difference cannot be used to represent how disparate or similar two cell intrinsic conductance organization actually is. A better way to conduct this experiment would be to insert electrical coupling between LCs of the same number, as in LC3-LC3, LC4-LC4, and LC5-LC5. If LC3 does have a more constrained parameter space than LC4 and LC5, than we can expect that an LC3 neuron pair would not need as much electrical coupling to synchronize activity than LC4 pairs or LC5 pairs after disrupting intrinsic organization.

The second relationship we find is a positive correlation between I_{HTK} magnitude and coupling strength across the LC4 and LC5 coupled neurons. This positive correlation exists if only one LCs I_{HTK} magnitude is compared to coupling strength (data not shown), or the two cells combined I_{HTK} magnitude is compared to coupling strength (Fig. 3). Using dynamic clamp we go on to show that when two LCs original I_{HTK} values are high, after TEA exposure those two cells require more electrical coupling to synchronize output (Fig. 5E, F), thus suggesting the positive relationship between I_{HTK} and coupling strength has functional significance in regards to LC synchronization.

The next question that presents itself regarding the I_{HTK} / coupling strength correlation is what causes it. A problem in searching for co-regulated intrinsic and coupling strength properties is that intrinsic conductances, and even passive properties, can have a direct effect on coupling conductance(Saraga et al., 2006, Pereda et al., 2013). This has been demonstrated with I_{NaP} and low threshold potassium currents directly influencing coupling strength between neurons (Curti and Pereda, 2004, Haas and Landisman, 2011, Curti et al., 2012). We cannot treat coupling strength as a separate parameter from intrinsic conductances until it is demonstrated, perhaps with dynamic clamp, that the I_{HTK} measured is not directly affecting coupling conductance, and thus not also causing the relationship. However, we do not believe the positive correlation we see between coupling strength and I_{HTK} is the result of I_{HTK} current having a direct effect on coupling conductance. After TEA exposure, and removal of I_{HTK}, we actually see coupling conductance between LCs significantly increased; this result would argue that if I_{HTK} does affect coupling conductance, than its influence is to weaken, not strengthen, electrical coupling.

Still, we cannot conclude that I_{HTK}, or I_{HTK} alone, is co-regulated with coupling strength; a larger value of I_{HTK} may also be just a result, or symptom, of the intrinsic parameter(s) that are coregulated with coupling strength. In biological experiments we are limited by what properties we can measure at any given time, so we are unlikely to find a definite answer to this in biological experiments alone. This is an opportune time

for a LC conductance based modeling study, in which all intrinsic parameters may be examined in respect to LC to LC coupling strength and synchronization. A back and forth of modeling experiments / hypotheses, to biological testing of those hypotheses, would be an effective way to continue probing these relationships.

Ideas regarding the functional role of gap junctions in generating appropriate neural output has become more complex in recent years. While originally gap junctions were thought to be largely passive, bidirectional structures which allow the sharing of voltage changes between two neurons (Connors and Long, 2004); we now understand that gap junctions can be rectifying (Marder, 2009), plastic in strength (Haas et al., 2011) and can be shaped by the intrinsic conductances present in the two neurons (Curti and Pereda, 2004, Haas and Landisman, 2011, Curti et al., 2012). With a new appreciation of the dynamic properties gap junctions possess, it is important that we explore ways in which coupling strength between cells are regulated and how this impacts the functional output of the network. Using the anterior LCs of the *C. borealis* CG we have we have an appropriate model to explore possible mechanisms behind gap junction regulation, and if those mechanisms are functional in synchronization of motor output.

In this study we explore the possible co-regulation between intrinsic conductances of LC motor neurons with LC to LC coupling strength, we investigate these relationships in regards to functional output property of LC synchronization. The idea that this co-

regulation may be occurring, and important has already been investigated, but at the theoretical level with computational models (Manor et al., 1997, Perez Velazquez and Carlen, 2000, Soto-Trevino et al., 2001, Pfeuty et al., 2003). In this regard theoretical studies are used to reduce complicated model systems to study how gap junction properties, intrinsic membrane properties and network architecture interact, and are summed, to produce a given network phenotype such as burst and spike synchrony or asynchrony. Attempting to understand how so many parameters, and combinations of parameters, are likely regulated to control output is a difficult feat even from a theoretical perspective. A study by Soto-Trevino et al. (2001) demonstrate this when they investigate parameters which affect output of two coupled model stomatogastric neurons. In this study the investigators limit the parameters which are varied to coupling strength, compartmental structure and weather the coupled cells are distinct or similar in properties of excitability. They find that in varying these parameters they can generate a variety of network and neuron behaviors, with some being unintuitive. While this is an appropriate strategy, especially while dealing with large neural networks and / or multiple parameter states within the network, it is important to test ideas and principles derived from these theoretical studies in biological models. The *C. borealis* CG is ideally situated to do this; furthermore this model system has its own conductance based model which will allow an eventual back in forth between biological study results, and computational model predictions.

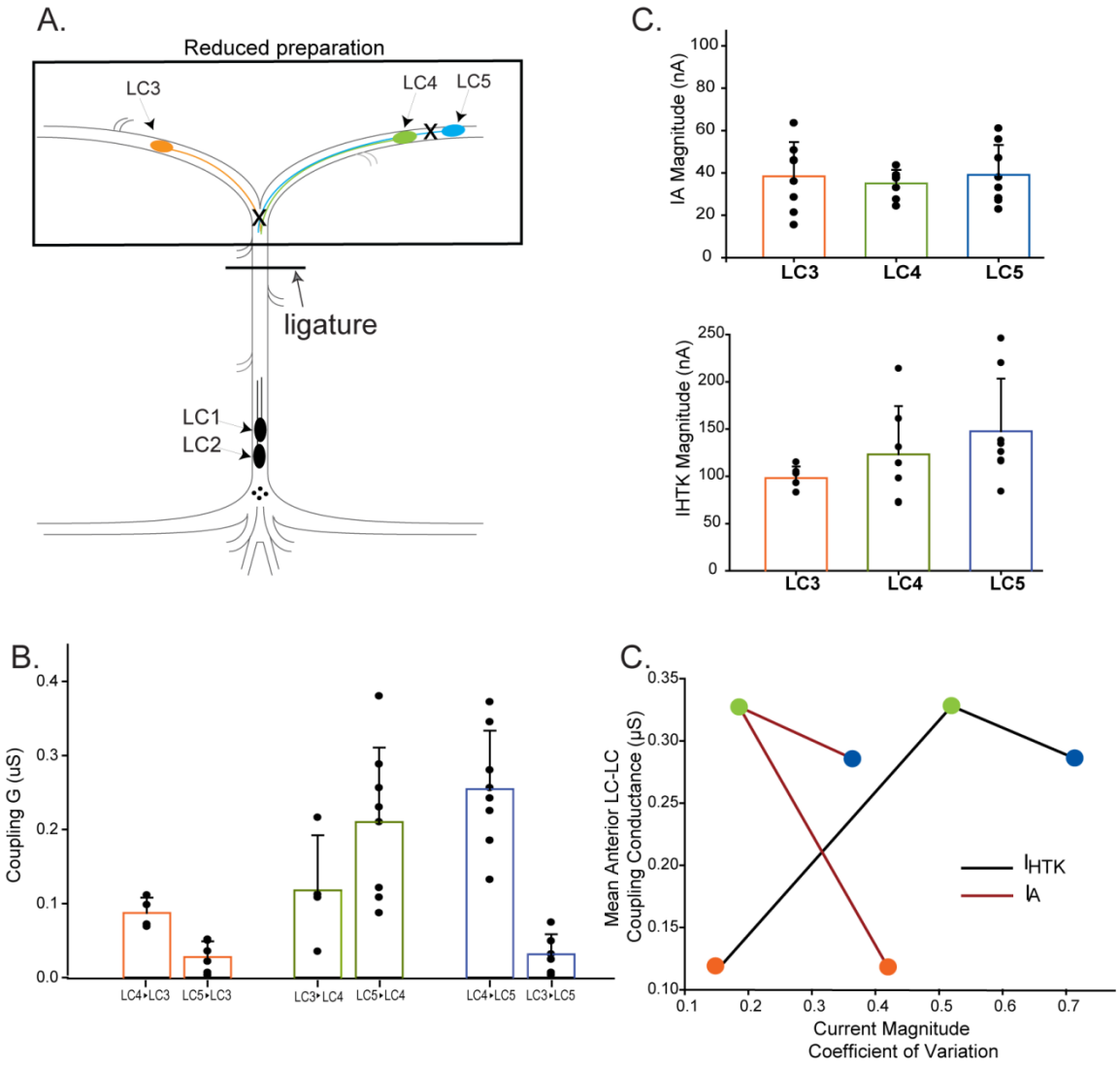
A.
Reduced preparation
LC3
LC4
LC5
ligature
LC1
LC2
C.
IA Magnitude (nA)
100
80
60
40
20
0
LC3
LC4
LC5
IHTK Magnitude (nA)
250
200
150
100
50
0
LC3
LC4
LC5
B.
Coupling G (uS)
0.4
0.3
0.2
0.1
0.0
LC4▸LC3
LC5▸LC3
LC3▸LC4
LC5▸LC4
LC4▸LC5
LC3▸LC5
C.
Mean Anterior LC-LC Coupling Conductance (µS)
0.35
0.30
0.25
0.20
0.15
0.10
0.1
0.2
0.3
0.4
0.5
0.6
0.7
Current Magnitude Coefficient of Variation
IHTK
IA

Figure 4.1 LC 3, LC4 & LC5 strength of coupling to other anterior LCs correlates with LC3, LC4 & LC5 variability in I_{HTK} magnitude. **A.** Schematic of reduced anterior LC preparation. "X" mark areas where electrical coupling is present between anterior LCs. Note: right branch "X" marks LC4 / LC5 local electrical coupling. Colors of LC3, LC4 and LC5 somata remain consistent throughout figures in Chapter 4. **B.** Mean ± Std. Dev. coupling conductance between anterior LCs. Circles overlaid on bar graph are individual LC coupling conductance values. Color of each bar indicate which LC the coupling conductance affects. **C.** Mean ± Std. Dev. of I_A (upper) and I_{HTK} (lower) in respect to LC3, LC4 and LC5. Individual LC current measurements overlaid on bars. **D.**) I_{HTK} (black line) and I_A (red line) coefficient of variation vs. mean total coupling conductance in respect to LC3, LC4 and LC5 (color coded). Note: total coupling conductance is calculated by adding together the mean coupling conductance of one LC with the two other anterior LCs. i.e. LC4 to LC3 conductance + LC5 to LC3 conductance = total LC3 coupling to anterior LCs.

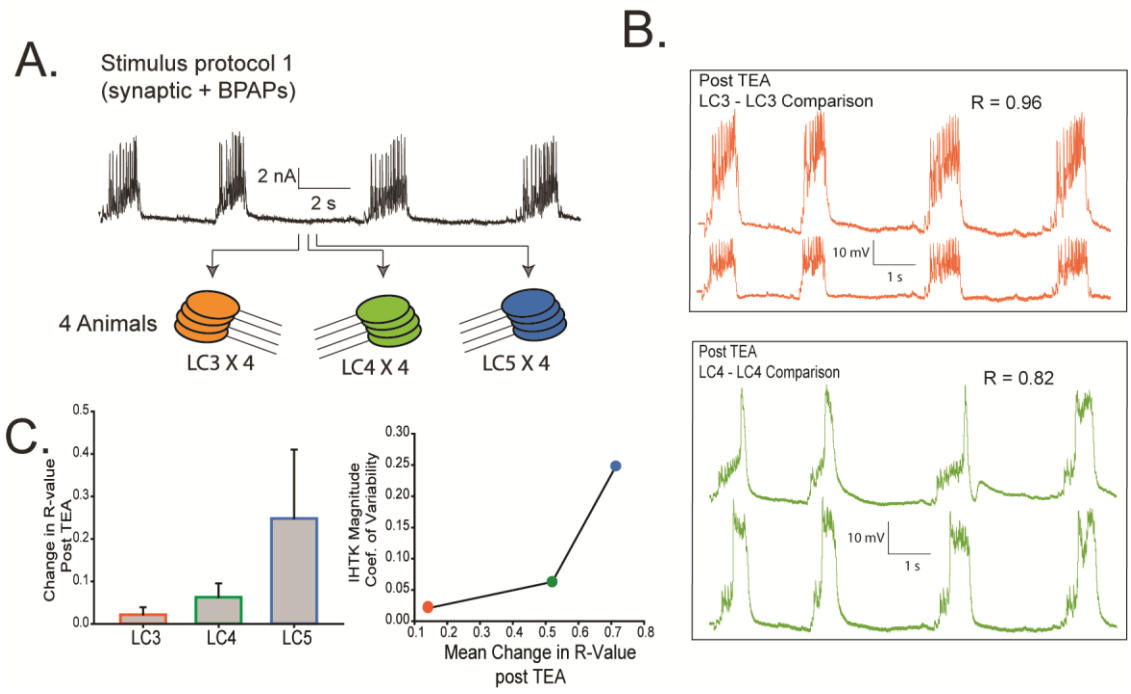

Figure 4.2 TEA exposure affects LC3, LC4 and LC5 differentially and in coordination with I_{HTK} coefficient of variation. A. Stimulus protocol one was injected in each anterior LC of four animals before and after TEA exposure. **B.** Example voltage response to Stimulus Protocol 1 comparisons. *Upper*- two LC3 neuron voltage response comparisons. *Lower*- two LC4 neuron comparisons. **C.** (*left*) Mean ± Std. Dev. change in R-value after TEA exposure. Voltage waveform in response to current injection was cross-correlated between LCs of a given type (LC3 was only compared to other LC3 cells). (*right*) Mean change in R-value after TEA exposure vs. I_{HTK} coefficient of variation in regards to each anterior LCs (color coded).

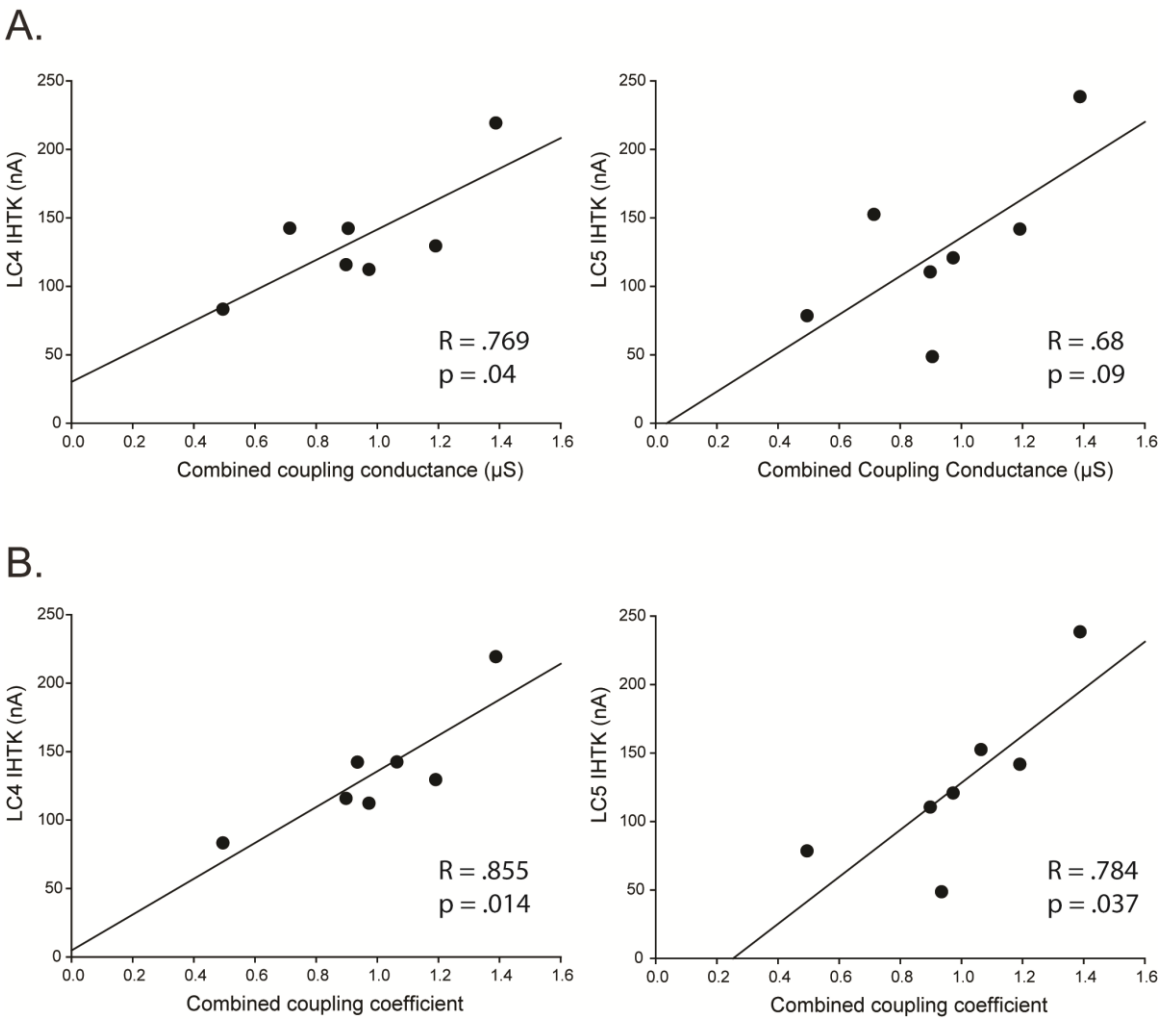

Figure 4.3 Coupling strength and I_{HTK} magnitude are positively correlated across LC4 / LC5 pairs. **A.** Coupling conductance vs. LC4 (*left*) and LC5 (*right*) I_{HTK} magnitude. **B.** Coupling coefficient vs. LC4 (*left*) and LC5 (*right*) I_{HTK} magnitude. I_{HTK} measured at 0mV voltage step.

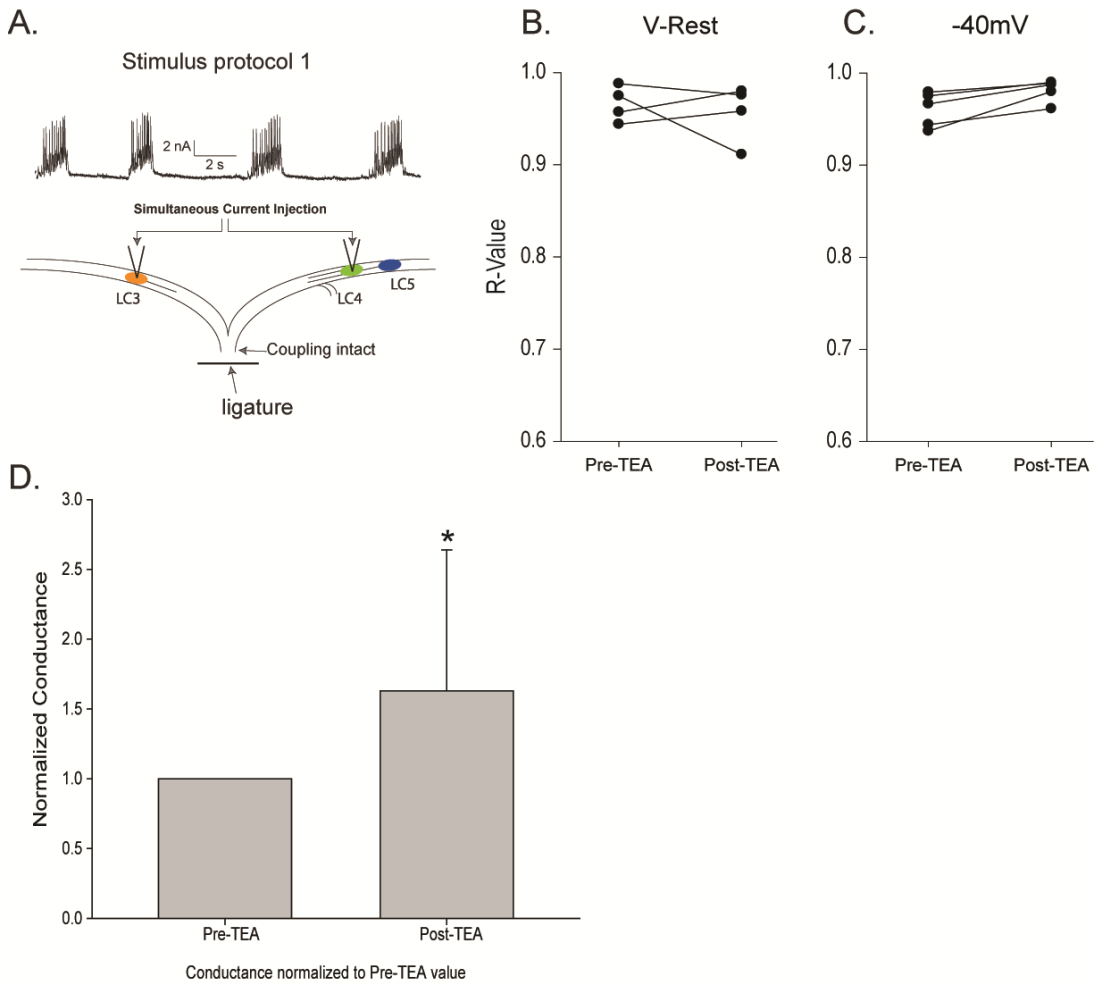

Figure 4.4 Synchronous voltage response to depolarizing stimuli is maintained by electrical coupling. A. Experimental diagram; Stimulus Protocol 1 is injected in two anterior LCs simultaneously before and after TEA exposure with electrical coupling intact. **B.** R-values are not significantly affected by TEA exposure when electrical coupling is left intact; current injection protocols are administered at LCs resting membrane potential. **C.** R-values are significantly increased by TEA exposure when electrical coupling is left intact; current injection protocols are administered at -40mV starting potential. DC current injection used bring starting potential to -40mV. **D.** Coupling conductance is significantly increased post-TEA exposure ($p = .04$). Coupling conductance normalized to pre-TEA conductance values.

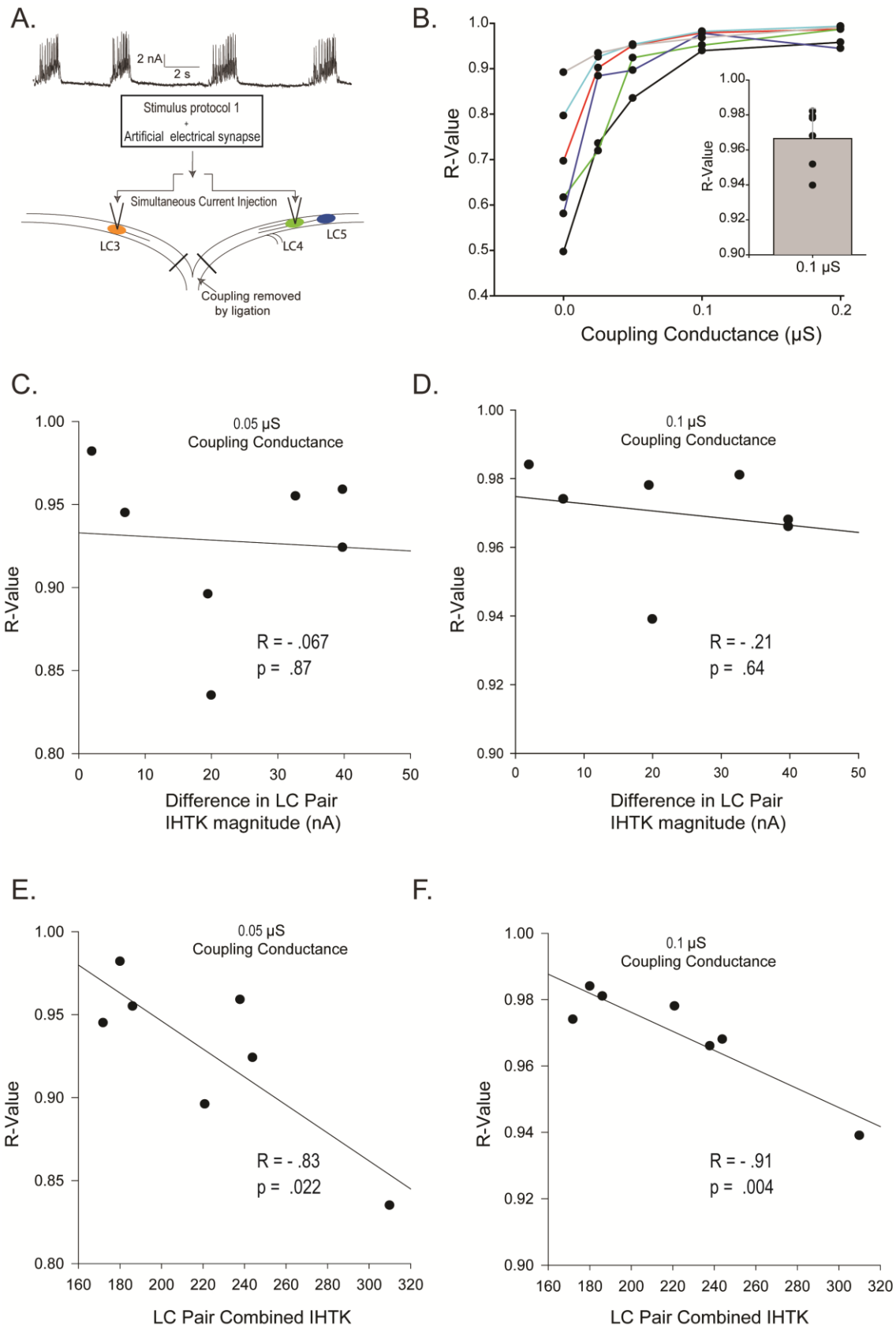
A.
2 nA
2 s
Stimulus protocol 1
+
Artificial electrical synapse
Simultaneous Current Injection
LC3
LC4
LC5
Coupling removed by ligation
B.
R-Value
Coupling Conductance (µS)
0.1 µS
C.
0.05 µS
Coupling Conductance
R = - .067
p = .87
Difference in LC Pair IHTK magnitude (nA)
D.
0.1 µS
Coupling Conductance
R = - .21
p = .64
Difference in LC Pair IHTK magnitude (nA)
E.
0.05 µS
Coupling Conductance
R = - .83
p = .022
LC Pair Combined IHTK
F.
0.1 µS
Coupling Conductance
R = - .91
p = .004
LC Pair Combined IHTK

Figure 4.5 Anterior LC electrical coupling and I_{HTK} magnitude are important in maintaining synchronous output. A. Experimental diagram- depolarizing stimuli and artificial electrical coupling are injected into two isolated anterior LCs simultaneously after TEA exposure. **B.** R-values comparing voltage response of two isolated LCs to depolarizing stimuli with different electrical coupling strength values (x-axis). Colored lines separate experimental preparations. *Bar graph inset*- Mean + std. dev. R-value measurements across six animals with 0.1 μS coupling conductance inserted between isolated LCs. **C-D.** Difference between I_{HTK} magnitude (x-axis) is not correlated to LC synchronization at .05 μS and .1μS coupling conductance values. **E-F.** I_{HTK} magnitude (x-axis) is significantly correlated to LC synchronization at .05 μS and .1μS coupling conductance values.

Conclusion

An important and fundamental problem in neuroscience is revealing how underlying parameters in neurons and neural networks, generate a particular electrical output. While the strategy to do this is a seemingly simple task of characterizing the underlying biophysical components behind neuronal excitability, recent experiments on model biological and theoretical systems, in which measurements can be taken from multiple cells with identical electrical output, have complicated the issue. Until recently it was thought that two neurons which generate the same output likely have identical underlying organization. Through computational and biological experiments this hypothesis has been fundamentally altered, arguing instead that multiple intrinsic solutions can be used to generate the same output (Golowasch et al., 2002, Prinz et al., 2004a, Taylor et al., 2009, Ball et al., 2010a). Biological studies have typically provided evidence for this hypothesis by characterizing variability, along with compensatory interactions, between two or more cellular properties underlying excitability. These interactions can take place between properties intrinsic to the cell (ionic channels / currents) (Guo et al., 2005, Haedo and Golowasch, 2006, Khorkova and Golowasch, 2007, Nerbonne et al., 2008, Ransdell et al., 2012, Temporal et al., 2012) and also among network level properties such as synaptic strength (Turrigiano, 2008, Turrigiano, 2011b, 2012).

Here we utilize the *C. borealis* CG LC motor neurons to continue investigating how small networks organize underlying properties to generate a stable and functional output. The crustacean CG is a unique model system in which different types of parameters underlying network output can be segregated and studied in isolation. I break these parameters into three general classes- intrinsic excitability properties of the cell, network level interactions and neuromodulation. In the above chapters we focus our investigations on LC intrinsic parameter regulation, along with how these intrinsic parameters appear to interact with network level properties.

Briefly summarizing, I make the following conclusions as a result of these studies:

1. LC motor neurons, within the same network, utilize differential tuning of intrinsic burst generating conductances, while maintaining similar levels of excitability.
2. Two of these intrinsic currents, I_A and I_{HTK}, maintain a negative relationship across LCs, and can rapidly compensate for one another via a post-transcriptional mechanism.
3. LC I_{HTK} also maintains a relationship with coupling strength between LCs, and this relationship is functional in synchronization of LC motor neuron output.

A general theme in these findings is that there are multiple levels of regulation which are active in maintaining appropriate output in LC motor neurons. Beyond sensory feedback from heart musculature, one level of regulation which is completely left out of these studies is neuromodulation. Previous work demonstrates that the *C. borealis* CG is responsive to neuromodulatory substances (Cruz-Bermudez & Marder, 2007). Building on what we currently know regarding maintenance of CG output, studies involving neuromodualtory effects on CG output can provide important information regarding homeostatic plasticity of networks under neuromodulation. For instance, we understand that internetwork LCs have disparate conductance organization tuned to similar levels of excitability. Because neuromodulation often causes changes in conductance organization (Marder, 2011, 2012), will a neuromodulatory substance applied to each of the CG LCs cause disparate levels of excitability across LCs within a network? A de-tuning of conserved excitability similar to what TEA accomplishes in Chapter 3? If so, does coupling across LCs protect against disparate excitability levels or LCs under neuromodulation, and maintain synchronous LC bursts? The potential of these type of experiments validate why the CG is an advantageous model, in that we are able to separate and study multiple types of parameters, along with how these types of parameters interact, to produce appropriate network output.

The studies described in the above chapters build a sound foundation for understanding how LC motor neurons utilize intrinsic currents along with network properties, to generate synchronous bursts. However, there is still much to do in this

regard. In collaboration with the lab of Satish Nair (University of Missouri- Columbia Department of Electrical Engineering) we have used biological measurements form *C. borealis* LCs to help generate a conductance based computational model of LC motor neurons, as well as the nine cell cardiac network. We believe that an evolving interaction between biological studies in the CG, and theoretical studies in this model, will be extremely beneficial to the generation and testing of hypotheses regarding how underlying properties are regulated and maintained to generate LC and CG network output.

While potential studies utilizing this model are endless, I will lay out two which I think can push the most recent CG research forward:

1. I mention in chapter 4 that it is difficult to ascertain if correlations between LC I_{HTK} and coupling strength is the direct result of active co-regulation, or if the I_{HTK} magnitude is instead a symptom of other LC conductance parameters which are co-regulated with electrical coupling strength. Using a computational model we could perform similar experiments, yet have access to the full complement of LC conductances, to investigate which may be co-regulated with electrical coupling strength. In this regard, we should also investigate and quantifiy single LC mRNA expression of genes involved in electrical coupling (*innexin*) and genes which contribute to I_{HTK} magnitude (*BKKCA, shab, shaw*).

2. One interesting feature of the CG is that five LCs are present in an individual network, which are synchronized in burst output, and do largely the same thing. Why do five redundant neurons exist? Especially with the reticular organization of the network (Garcia-Crescioni and Miller, 2011), why can there not be one LC motor neuron with an extensive neuritic projection? One hypothesis is that because the LC output is very important to the animal, having five electrically coupled cells will ensure that if one cell has incorrect level of excitability, the four coupled LCs would act to dampen or constrain the incorrect burst. Two example situations which may result in harmful disturbance to a LCs level of excitability: stochastic turnover of ion channel proteins, and other proteins affecting cell excitability, may momentarily disrupt the conserved excitability across network LCs throughout the lifetime of the animal. Also, neuromodulation, which is known to affect conductance organization, may cause disparate levels of excitability across the five LCs.

In both these examples electrical coupling across five redundant neurons may be necessary to constrain appropriate output. To test this idea we can isolate a single biological LC and, using dynamic clamp, connect the biological neuron to four model LCs via electrical synapse. We could then use TEA exposure to de-tune the excitability of the biological neuron, and study how coupling strength between the four model cells constrains the isolated LCs burst output. Alternatively, we could de-tune one, two, or three of the model cells and

investigate how coupling strength with the biological neuron acts in constraining burst output.

The two potential experimental discussed above are only the beginning of possible questions an interaction between the CG model and biology based experiments can be used to answer. The theme which will likely hold across future CG studies is that the investigator has control to selectively limit and study multiple levels of regulation which underlie both cellular and network output; that is, intrinsic organization of the single cell, synaptic network properties in the reticular CG network and neuromodulatory input. Here we have conducted studies characterizing the intrinsic biophysical properties of LC motor neurons, and homeostatic interactions which tune appropriate output via intrinsic conductance organization and electrical coupling. In doing this we have provided novel insights regarding underlying regulation of neuronal excitability, but perhaps more importantly, we provide a valuable electrophysiological characterization of a model system which has the potential to help answer important fundamental questions in neuroscience.

BIBLIOGRAPHY

Atkinson NS, Robertson GA, Ganetzky B (1991) A component of calcium-activated potassium channels encoded by the Drosophila slo locus. Science 253:551-555.

Bair W, Koch C, Newsome W, Britten K (1994) Power spectrum analysis of bursting cells in area MT in the behaving monkey. J Neurosci 14:2870-2892.

Ball JM, Franklin CC, Tobin AE, Schulz DJ, Nair SS (2010a) Coregulation of ion channel conductances preserves output in a computational model of a crustacean cardiac motor neuron. The Journal of neuroscience : the official journal of the Society for Neuroscience 30:8637-8649.

Ball JM, Franklin CC, Tobin AE, Schulz DJ, Nair SS (2010b) Coregulation of ion channel conductances preserves output in a computational model of a crustacean cardiac motor neuron. J Neurosci 30:8637-8649.

Bergquist S, Dickman DK, Davis GW (2010) A hierarchy of cell intrinsic and target-derived homeostatic signaling. Neuron 66:220-234.

Berlind A (1993) Heterogeneity of motoneuron driver potential properties along the anterior-posterior axis of the lobster cardiac ganglion. Brain Res 609:51-58.

Cattaneo A, Maffei L, Morrone C (1981) Two firing patterns in the discharge of complex cells encoding different attributes of the visual stimulus. Exp Brain Res 43:115-118.

Cens T, Rousset M, Kajava A, Charnet P (2007) Molecular determinant for specific Ca/Ba selectivity profiles of low and high threshold Ca2+ channels. J Gen Physiol 130:415-425.

Clapham DE (2007) Calcium signaling. Cell 131:1047-1058.

Cohen P, Holmes CF, Tsukitani Y (1990) Okadaic acid: a new probe for the study of cellular regulation. Trends in biochemical sciences 15:98-102.

Connors BW, Long MA (2004) Electrical synapses in the mammalian brain. Annual review of neuroscience 27:393-418.

Cooke IM (2002a) Reliable, responsive pacemaking and pattern generation with minimal cell numbers: the crustacean cardiac ganglion. Biol Bull 202:108-136.

Cooke IM (2002b) Reliable, responsive pacemaking and pattern generation with minimal cell numbers: the crustacean cardiac ganglion. The Biological bulletin 202:108-136.

Cruz-Bermudez ND, Marder E (2007a) Multiple modulators act on the cardiac ganglion of the crab, Cancer borealis. The Journal of experimental biology 210:2873-2884.

Cruz-Bermudez ND, Marder E (2007b) Multiple modulators act on the cardiac ganglion of the crab, Cancer borealis. J Exp Biol 210:2873-2884.

Cummings JA, Mulkey RM, Nicoll RA, Malenka RC (1996) Ca2+ signaling requirements for long-term depression in the hippocampus. Neuron 16:825-833.
Curti S, Hoge G, Nagy JI, Pereda AE (2012) Synergy between electrical coupling and membrane properties promotes strong synchronization of neurons of the mesencephalic trigeminal nucleus. The Journal of neuroscience : the official journal of the Society for Neuroscience 32:4341-4359.
Curti S, Pereda AE (2004) Voltage-dependent enhancement of electrical coupling by a subthreshold sodium current. The Journal of neuroscience : the official journal of the Society for Neuroscience 24:3999-4010.
Dai A, Temporal S, Schulz DJ (2010) Cell-specific patterns of alternative splicing of voltage-gated ion channels in single identified neurons. Neuroscience 168:118-129.
Davis GW (2006) Homeostatic control of neural activity: from phenomenology to molecular design. Annu Rev Neurosci 29:307-323.
Debanne D, Poo MM (2010) Spike-timing dependent plasticity beyond synapse - pre- and post-synaptic plasticity of intrinsic neuronal excitability. Frontiers in synaptic neuroscience 2:21.
Del Negro CA, Hayes JA (2008) A 'group pacemaker' mechanism for respiratory rhythm generation. J Physiol 586:2245-2246.
Del Negro CA, Koshiya N, Butera RJ, Jr., Smith JC (2002a) Persistent sodium current, membrane properties and bursting behavior of pre-botzinger complex inspiratory neurons in vitro. J Neurophysiol 88:2242-2250.
Del Negro CA, Morgado-Valle C, Feldman JL (2002b) Respiratory rhythm: an emergent network property? Neuron 34:821-830.
Desai NS, Rutherford LC, Turrigiano GG (1999) Plasticity in the intrinsic excitability of cortical pyramidal neurons. Nat Neurosci 2:515-520.
Echegoyen J, Neu A, Graber KD, Soltesz I (2007) Homeostatic plasticity studied using in vivo hippocampal activity-blockade: synaptic scaling, intrinsic plasticity and age-dependence. PLOS ONE 2:e700.
Elson RC, Selverston AI (1997) Evidence for a persistent Na+ conductance in neurons of the gastric mill rhythm generator of spiny lobsters. J Exp Biol 200:1795-1807.
Franklin CC, Ball JM, Schulz DJ, Nair SS (2010) Generation and preservation of the slow underlying membrane potential oscillation in model bursting neurons. Journal of neurophysiology 104:1589-1602.
French LB, Lanning CC, Harris-Warrick RM (2002) The localization of two voltage-gated calcium channels in the pyloric network of the lobster stomatogastric ganglion. Neuroscience 112:217-232.
Friel DD, Tsien RW (1992a) A caffeine- and ryanodine-sensitive Ca2+ store in bullfrog sympathetic neurones modulates effects of Ca2+ entry on [Ca2+]i. J Physiol 450:217-246.
Friel DD, Tsien RW (1992b) Phase-dependent contributions from Ca2+ entry and Ca2+ release to caffeine-induced [Ca2+]i oscillations in bullfrog sympathetic neurons. Neuron 8:1109-1125.

Garcia-Crescioni K, Fort TJ, Stern E, Brezina V, Miller MW (2010) Feedback from peripheral musculature to central pattern generator in the neurogenic heart of the crab Callinectes sapidus: role of mechanosensitive dendrites. Journal of neurophysiology 103:83-96.

Garcia-Crescioni K, Miller MW (2011) Revisiting the reticulum: feedforward and feedback contributions to motor program parameters in the crab cardiac ganglion microcircuit. Journal of neurophysiology 106:2065-2077.

George J, Baden DG, Gerwick WH, Murray TF (2012) Bidirectional influence of sodium channel activation on NMDA receptor-dependent cerebrocortical neuron structural plasticity. Proc Natl Acad Sci U S A 109:19840-19845.

Goaillard JM, Taylor AL, Schulz DJ, Marder E (2009a) Functional consequences of animal-to-animal variation in circuit parameters. Nature Neurosci 12:1424-1430.

Goaillard JM, Taylor AL, Schulz DJ, Marder E (2009b) Functional consequences of animal-to-animal variation in circuit parameters. Nature neuroscience 12:1424-1430.

Goldman MS, Golowasch J, Marder E, Abbott LF (2001a) Global structure, robustness, and modulation of neuronal models. The Journal of neuroscience : the official journal of the Society for Neuroscience 21:5229-5238.

Goldman MS, Golowasch J, Marder E, Abbott LF (2001b) Global structure, robustness, and modulation of neuronal models. J Neurosci 21:5229-5238.

Golowasch J, Abbott LF, Marder E (1999) Activity-dependent regulation of potassium currents in an identified neuron of the stomatogastric ganglion of the crab Cancer borealis. The Journal of neuroscience : the official journal of the Society for Neuroscience 19:RC33.

Golowasch J, Goldman MS, Abbott LF, Marder E (2002) Failure of averaging in the construction of a conductance-based neuron model. J Neurophysiol 87:1129-1131.

Golowasch J, Marder E (1992) Ionic currents of the lateral pyloric neuron of the stomatogastric ganglion of the crab. Journal of neurophysiology 67:318-331.

Grashow R, Brookings T, Marder E (2009) Reliable neuromodulation from circuits with variable underlying structure. Proc Natl Acad Sci U S A 106:11742-11746.

Grashow R, Brookings T, Marder E (2010) Compensation for variable intrinsic neuronal excitability by circuit-synaptic interactions. J Neurosci 30:9145-9156.

Graubard K, Raper JA, Hartline DK (1983) Graded synaptic transmission between identified spiking neurons. J Neurophysiol 50:508-521.

Guo W, Jung WE, Marionneau C, Aimond F, Xu H, Yamada KA, Schwarz TL, Demolombe S, Nerbonne JM (2005) Targeted deletion of Kv4.2 eliminates I(to,f) and results in electrical and molecular remodeling, with no evidence of ventricular hypertrophy or myocardial dysfunction. Circulation research 97:1342-1350.

Haas JS, Landisman CE (2011) State-dependent modulation of gap junction signaling by the persistent sodium current. Frontiers in cellular neuroscience 5:31.

Haas JS, Zavala B, Landisman CE (2011) Activity-dependent long-term depression of electrical synapses. Science 334:389-393.

Haedo RJ, Golowasch J (2006) Ionic mechanism underlying recovery of rhythmic activity in adult isolated neurons. Journal of neurophysiology 96:1860-1876.
Hage TA, Salkoff L (2012) Sodium-activated potassium channels are functionally coupled to persistent sodium currents. J Neurosci 32:2714-2721.
Harris-Warrick RM, Marder E, Selverston AI, Moulins M (1992) Dynamic biological networks the stomatogastric nervous system. In: Computational neuroscience, pp xvii, 328 p. Cambridge, Mass.: MIT Press.
Hartline DK (1967a) Impulse identification and axon mapping of the nine neurons in the cardiac ganglion of the lobster Homarus americanus. J Exp Biol 47:327-340.
Hartline DK (1967b) Impulse identification and axon mapping of the nine neurons in the cardiac ganglion of the lobster Homarus americanus. The Journal of experimental biology 47:327-340.
Hille B (2001) Ion channels of excitable membranes. Sunderland, Mass.: Sinauer.
Howard AL, Neu A, Morgan RJ, Echegoyen JC, Soltesz I (2007) Opposing modifications in intrinsic currents and synaptic inputs in post-traumatic mossy cells: evidence for single-cell homeostasis in a hyperexcitable network. J Neurophysiol 97:2394-2409.
Hurley LM, Graubard K (1998) Pharmacologically and functionally distinct calcium currents of stomatogastric neurons. J Neurophysiol 79:2070-2081.
Jeziorski MC, Greenberg RM, Anderson PA (2000) The molecular biology of invertebrate voltage-gated Ca(2+) channels. J Exp Biol 203:841-856.
Johnson BR, Kloppenburg P, Harris-Warrick RM (2003) Dopamine modulation of calcium currents in pyloric neurons of the lobster stomatogastric ganglion. J Neurophysiol 90:631-643.
Khorkova O, Golowasch J (2007) Neuromodulators, not activity, control coordinated expression of ionic currents. The Journal of neuroscience : the official journal of the Society for Neuroscience 27:8709-8718.
Kim M, Baro DJ, Lanning CC, Doshi M, Moskowitz HS, Farnham J, Harris-Warrick RM (1998) Expression of Panulirus shaker potassium channel splice variants. Receptors & channels 5:291-304.
Klee CB, Ren H, Wang X (1998) Regulation of the calmodulin-stimulated protein phosphatase, calcineurin. The Journal of biological chemistry 273:13367-13370.
Koulakov AA, Raghavachari S, Kepecs A, Lisman JE (2002) Model for a robust neural integrator. Nat Neurosci 5:775-782.
Lee A, Zhou H, Scheuer T, Catterall WA (2003) Molecular determinants of Ca(2+)/calmodulin-dependent regulation of Ca(v)2.1 channels. Proc Natl Acad Sci U S A 100:16059-16064.
LeMasson G, Marder E, Abbott LF (1993) Activity-dependent regulation of conductances in model neurons. Science 259:1915-1917.
Levi R, Samoilova M, Selverston AI (2003) Calcium signaling components of oscillating invertebrate neurons in vitro. Neuroscience 118:283-296.

Lin WH, Wright DE, Muraro NI, Baines RA (2009) Alternative splicing in the voltage-gated sodium channel DmNav regulates activation, inactivation, and persistent current. J Neurophysiol 102:1994-2006.
Lisman JE (1997) Bursts as a unit of neural information: making unreliable synapses reliable. Trends Neurosci 20:38-43.
Liu Z, Golowasch J, Marder E, Abbott LF (1998) A model neuron with activity-dependent conductances regulated by multiple calcium sensors. J Neurosci 18:2309-2320.
Liu Z, Song W, Dong K (2004) Persistent tetrodotoxin-sensitive sodium current resulting from U-to-C RNA editing of an insect sodium channel. Proc Natl Acad Sci U S A 101:11862-11867.
Loughney K, Kreber R, Ganetzky B (1989) Molecular analysis of the para locus, a sodium channel gene in Drosophila. Cell 58:1143-1154.
MacLean JN, Zhang Y, Goeritz ML, Casey R, Oliva R, Guckenheimer J, Harris-Warrick RM (2005) Activity-independent coregulation of IA and Ih in rhythmically active neurons. J Neurophysiol 94:3601-3617.
MacLean JN, Zhang Y, Johnson BR, Harris-Warrick RM (2003) Activity-independent homeostasis in rhythmically active neurons. Neuron 37:109-120.
Manor Y, Rinzel J, Segev I, Yarom Y (1997) Low-amplitude oscillations in the inferior olive: a model based on electrical coupling of neurons with heterogeneous channel densities. Journal of neurophysiology 77:2736-2752.
Marder E (2009) Electrical synapses: rectification demystified. Current biology : CB 19:R34-35.
Marder E (2011a) Variability, compensation, and modulation in neurons and circuits. Proc Natl Acad Sci U S A 108 Suppl 3:15542-15548.
Marder E (2011b) Variability, compensation, and modulation in neurons and circuits. Proceedings of the National Academy of Sciences of the United States of America 108 Suppl 3:15542-15548.
Marder E (2012) Neuromodulation of neuronal circuits: back to the future. Neuron 76:1-11.
Marder E, Bucher D (2001) Central pattern generators and the control of rhythmic movements. Current biology : CB 11:R986-996.
Marder E, Bucher D (2007) Understanding circuit dynamics using the stomatogastric nervous system of lobsters and crabs. Annu Rev Physiol 69:291-316.
Marder E, Bucher D, Schulz DJ, Taylor AL (2005) Invertebrate central pattern generation moves along. Current biology : CB 15:R685-699.
Marder E, Taylor AL (2011) Multiple models to capture the variability in biological neurons and networks. Nat Neurosci 14:133-138.
Marder E, Thirumalai V (2002) Cellular, synaptic and network effects of neuromodulation. Neural Netw 15:479-493.
Mironov SL, Usachev JM (1991) Caffeine affects Ca uptake and Ca release from intracellular stores: fura-2 measurements in isolated snail neurones. Neurosci Lett 123:200-202.

Misonou H (2010) Homeostatic regulation of neuronal excitability by K(+) channels in normal and diseased brains. The Neuroscientist : a review journal bringing neurobiology, neurology and psychiatry 16:51-64.
Morgado-Valle C, Beltran-Parrazal L, DiFranco M, Vergara JL, Feldman JL (2008) Somatic Ca2+ transients do not contribute to inspiratory drive in preBotzinger Complex neurons. J Physiol 586:4531-4540.
Mulkey RM, Zucker RS (1993) Calcium released by photolysis of DM-nitrophen triggers transmitter release at the crayfish neuromuscular junction. J Physiol 462:243-260.
Nerbonne JM, Gerber BR, Norris A, Burkhalter A (2008) Electrical remodelling maintains firing properties in cortical pyramidal neurons lacking KCND2-encoded A-type K+ currents. The Journal of physiology 586:1565-1579.
Olson RO, Liu Z, Nomura Y, Song W, Dong K (2008) Molecular and functional characterization of voltage-gated sodium channel variants from Drosophila melanogaster. Insect Biochem Mol Biol 38:604-610.
Overton PG, Clark D (1997) Burst firing in midbrain dopaminergic neurons. Brain research Brain research reviews 25:312-334.
Partridge LD, Swandulla D (1988) Calcium-activated non-specific cation channels. Trends Neurosci 11:69-72.
Pena F, Parkis MA, Tryba AK, Ramirez JM (2004) Differential contribution of pacemaker properties to the generation of respiratory rhythms during normoxia and hypoxia. Neuron 43:105-117.
Pereda AE, Curti S, Hoge G, Cachope R, Flores CE, Rash JE (2013) Gap junction-mediated electrical transmission: regulatory mechanisms and plasticity. Biochimica et biophysica acta 1828:134-146.
Perez Velazquez JL, Carlen PL (2000) Gap junctions, synchrony and seizures. Trends in neurosciences 23:68-74.
Pfeuty B, Mato G, Golomb D, Hansel D (2003) Electrical synapses and synchrony: the role of intrinsic currents. The Journal of neuroscience : the official journal of the Society for Neuroscience 23:6280-6294.
Prinz AA, Billimoria CP, Marder E (2003) Alternative to hand-tuning conductance-based models: construction and analysis of databases of model neurons. J Neurophysiol 90:3998-4015.
Prinz AA, Bucher D, Marder E (2004a) Similar network activity from disparate circuit parameters. Nat Neuro 7:1345-1352.
Prinz AA, Bucher D, Marder E (2004b) Similar network activity from disparate circuit parameters. Nat Neurosci 7:1345-1352.
Rabbah P, Golowasch J, Nadim F (2005) Effect of electrical coupling on ionic current and synaptic potential measurements. Journal of neurophysiology 94:519-530.
Ransdell JL, Faust TB, Schulz DJ (2010) Correlated Levels of mRNA and Soma Size in Single Identified Neurons: Evidence for Compartment-specific Regulation of Gene Expression. Front Mol Neurosci 3:116.

Ransdell JL, Nair SS, Schulz DJ (2012) Rapid homeostatic plasticity of intrinsic excitability in a central pattern generator network stabilizes functional neural network output. J Neurosci 32:9649-9658.
Ransdell JL, Temporal S, West NL, Leyrer ML, Schulz DJ (2013) Characterization of inward currents and channels underlying burst activity in motor neurons of the crab cardiac ganglion. Journal of neurophysiology.
Rose CR (2002) Na+ signals at central synapses. Neuroscientist 8:532-539.
Rubin JE, Hayes JA, Mendenhall JL, Del Negro CA (2009) Calcium-activated nonspecific cation current and synaptic depression promote network-dependent burst oscillations. Proc Natl Acad Sci U S A 106:2939-2944.
Ruegg UT, Burgess GM (1989) Staurosporine, K-252 and UCN-01: potent but nonspecific inhibitors of protein kinases. Trends in pharmacological sciences 10:218-220.
Rutecki PA (1992) Neuronal excitability: voltage-dependent currents and synaptic transmission. Journal of clinical neurophysiology : official publication of the American Electroencephalographic Society 9:195-211.
Sah P (1995) Different calcium channels are coupled to potassium channels with distinct physiological roles in vagal neurons. Proc Biol Sci 260:105-111.
Sakurai A, Wilkens JL (2003) Tension sensitivity of the heart pacemaker neurons in the isopod crustacean Ligia pallasii. The Journal of experimental biology 206:105-115.
Saraga F, Ng L, Skinner FK (2006) Distal gap junctions and active dendrites can tune network dynamics. Journal of neurophysiology 95:1669-1682.
Schulz DJ, Goaillard JM, Marder E (2006) Variable channel expression in identified single and electrically coupled neurons in different animals. Nat Neurosci 9:356-362.
Schulz DJ, Goaillard JM, Marder EE (2007a) Quantitative expression profiling of identified neurons reveals cell-specific constraints on highly variable levels of gene expression. Proceedings of the National Academy of Sciences of the United States of America 104:13187-13191.
Schulz DJ, Goaillard JM, Marder EE (2007b) Quantitative expression profiling of identified neurons reveals cell-specific constraints on highly variable levels of gene expression. Proc Natl Acad Sci U S A 104:13187-13191.
Selverston AI (2010) Invertebrate central pattern generator circuits. Philosophical transactions of the Royal Society of London Series B, Biological sciences 365:2329-2345.
Senatore A, Spafford JD (2010) Transient and big are key features of an invertebrate T-type channel (LCav3) from the central nervous system of Lymnaea stagnalis. J Biol Chem 285:7447-7458.
Soto-Trevino C, Thoroughman KA, Marder E, Abbott LF (2001) Activity-dependent modification of inhibitory synapses in models of rhythmic neural networks. Nature neuroscience 4:297-303.
Spafford JD, Chen L, Feng ZP, Smit AB, Zamponi GW (2003) Expression and modulation of an invertebrate presynaptic calcium channel alpha1 subunit homolog. J Biol Chem 278:21178-21187.

Spafford JD, Dunn T, Smit AB, Syed NI, Zamponi GW (2006) In vitro characterization of L-type calcium channels and their contribution to firing behavior in invertebrate respiratory neurons. J Neurophysiol 95:42-52.
Spafford JD, Zamponi GW (2003) Functional interactions between presynaptic calcium channels and the neurotransmitter release machinery. Curr Opin Neurobiol 13:308-314.
Swandulla D, Lux HD (1985) Activation of a nonspecific cation conductance by intracellular Ca2+ elevation in bursting pacemaker neurons of Helix pomatia. J Neurophysiol 54:1430-1443.
Swensen AM, Bean BP (2005a) Robustness of burst firing in dissociated purkinje neurons with acute or long-term reductions in sodium conductance. Journal of Neuroscience 25:3509-3520.
Swensen AM, Bean BP (2005b) Robustness of burst firing in dissociated purkinje neurons with acute or long-term reductions in sodium conductance. J Neurosci 25:3509-3520.
Szucs A, Selverston AI (2006) Consistent dynamics suggests tight regulation of biophysical parameters in a small network of bursting neurons. J Neurobiol 66:1584-1601.
Taddese A, Bean BP (2002) Subthreshold sodium current from rapidly inactivating sodium channels drives spontaneous firing of tuberomammillary neurons. Neuron 33:587-600.
Tang S, Mikala G, Bahinski A, Yatani A, Varadi G, Schwartz A (1993) Molecular localization of ion selectivity sites within the pore of a human L-type cardiac calcium channel. J Biol Chem 268:13026-13029.
Taylor AL, Goaillard JM, Marder E (2009) How multiple conductances determine electrophysiological properties in a multicompartment model. J Neurosci 29:5573-5586.
Tazaki K (1972) The burst activity of different cell regions and intercellular co-ordination in the cardiac ganglion of the crab, Eriocheir japonicus. J Exp Biol 57:713-726.
Tazaki K, Cooke IM (1979) Ionic bases of slow, depolarizing responses of cardiac ganglion neurons in the crab, Portunus sanguinolentus. Journal of neurophysiology 42:1022-1047.
Tazaki K, Cooke IM (1983a) Neuronal mechanisms underlying rhythmic bursts in crustacean cardiac ganglia. Symposia of the Society for Experimental Biology 37:129-157.
Tazaki K, Cooke IM (1983b) Separation of neuronal sites of driver potential and impulse generation by ligaturing in the cardiac ganglion of the lobster, *Homarus americanus*. J Comp Physiol A 151:329-346.
Tazaki K, Cooke IM (1986) Currents under voltage clamp of burst-forming neurons of the cardiac ganglion of the lobster (Homarus americanus). J Neurophysiol 56:1739-1762.
Tazaki K, Cooke IM (1990) Characterization of Ca current underlying burst formation in lobster cardiac ganglion motorneurons. J Neurophysiol 63:370-384.

Temporal S, Desai M, Khorkova O, Varghese G, Dai A, Schulz DJ, Golowasch J (2012) Neuromodulation independently determines correlated channel expression and conductance levels in motor neurons of the stomatogastric ganglion. Journal of neurophysiology 107:718-727.
Thoby-Brisson M, Simmers J (1998) Neuromodulatory inputs maintain expression of a lobster motor pattern-generating network in a modulation-dependent state: evidence from long-term decentralization in vitro. The Journal of neuroscience : the official journal of the Society for Neuroscience 18:2212-2225.
Thoby-Brisson M, Simmers J (2002) Long-term neuromodulatory regulation of a motor pattern-generating network: maintenance of synaptic efficacy and oscillatory properties. Journal of neurophysiology 88:2942-2953.
Tobin AE, Cruz-Bermudez ND, Marder E, Schulz DJ (2009) Correlations in ion channel mRNA in rhythmically active neurons. PloS one 4:e6742.
Tseng HA, Nadim F (2010) The membrane potential waveform of bursting pacemaker neurons is a predictor of their preferred frequency and the network cycle frequency. J Neurosci 30:10809-10819.
Tsien RW, Lipscombe D, Madison DV, Bley KR, Fox AP (1988) Multiple types of neuronal calcium channels and their selective modulation. Trends Neurosci 11:431-438.
Tsunoda S, Salkoff L (1995) The major delayed rectifier in both Drosophila neurons and muscle is encoded by Shab. The Journal of neuroscience : the official journal of the Society for Neuroscience 15:5209-5221.
Turrigiano G (2011a) Too many cooks? Intrinsic and synaptic homeostatic mechanisms in cortical circuit refinement. Annu Rev Neurosci 34:89-103.
Turrigiano G (2011b) Too many cooks? Intrinsic and synaptic homeostatic mechanisms in cortical circuit refinement. Annual review of neuroscience 34:89-103.
Turrigiano G (2012) Homeostatic synaptic plasticity: local and global mechanisms for stabilizing neuronal function. Cold Spring Harbor perspectives in biology 4:a005736.
Turrigiano G, Abbott LF, Marder E (1994) Activity-dependent changes in the intrinsic properties of cultured neurons. Science 264:974-977.
Turrigiano G, LeMasson G, Marder E (1995) Selective regulation of current densities underlies spontaneous changes in the activity of cultured neurons. The Journal of neuroscience : the official journal of the Society for Neuroscience 15:3640-3652.
Turrigiano GG (2008) The self-tuning neuron: synaptic scaling of excitatory synapses. Cell 135:422-435.
Van Petegem F, Chatelain FC, Minor DL, Jr. (2005) Insights into voltage-gated calcium channel regulation from the structure of the CaV1.2 IQ domain-Ca2+/calmodulin complex. Nat Struct Mol Biol 12:1108-1115.
Van Wart A, Matthews G (2006) Impaired firing and cell-specific compensation in neurons lacking nav1.6 sodium channels. J Neurosci 26:7172-7180.
Wilson GF, Magoski NS, Kaczmarek LK (1998) Modulation of a calcium-sensitive nonspecific cation channel by closely associated protein kinase and phosphatase activities. Proc Natl Acad Sci U S A 95:10938-10943.

Wisgirda ME, Dryer SE (1994) Functional dependence of Ca(2+)-activated K+ current on L- and N-type Ca2+ channels: differences between chicken sympathetic and parasympathetic neurons suggest different regulatory mechanisms. Proc Natl Acad Sci U S A 91:2858-2862.

Yamoah EN, Kuzirian AM, Sanchez-Andres JV (1994) Calcium current and inactivation in identified neurons in Hermissenda crassicornis. J Neurophysiol 72:2196-2208.

Yang J, Ellinor PT, Sather WA, Zhang JF, Tsien RW (1993) Molecular determinants of Ca2+ selectivity and ion permeation in L-type Ca2+ channels. Nature 366:158-161.

Yoshimura H (2005) The potential of caffeine for functional modification from cortical synapses to neuron networks in the brain. Curr Neuropharmacol 3:309-316.

Zhang B, Harris-Warrick RM (1995) Calcium-dependent plateau potentials in a crab stomatogastric ganglion motor neuron. I. Calcium current and its modulation by serotonin. J Neurophysiol 74:1929-1937.

Zhang B, Wootton JF, Harris-Warrick RM (1995) Calcium-dependent plateau potentials in a crab stomatogastric ganglion motor neuron. II. Calcium-activated slow inward current. J Neurophysiol 74:1938-1946.

Zuhlke RD, Pitt GS, Tsien RW, Reuter H (2000) Ca2+-sensitive inactivation and facilitation of L-type Ca2+ channels both depend on specific amino acid residues in a consensus calmodulin-binding motif in the(alpha)1C subunit. J Biol Chem 275:21121-21129.

VITA

I was born in Columbia, Missouri to parents Beverly and John Ransdell who are originally from Hannibal, Missouri. I grew up in Columbia with two older brothers and one older sister and attended David H. Hickman High School. In high school I was able to take several advanced placement courses during my Junior and Senior Years. One of these courses was AP Psychology; the instructor, Mrs. Fick, taught in a compelling way and pointed out that the physical basis behind many psychiatric disorders are currently unknown. This compelled me to explore possible career paths in neuroscience research.

I attended the University of Minnesota- Twin Cities and majored in Neuroscience. During my time as an undergraduate I worked in several laboratories which involved multiple areas of neuroscience research. These included molecular neuroscience (Dr. Robert Elde), behavioral neuroscience (Dr. Marilyn Carroll) and systems / cellular neuroscience (Dr. Karen Mesce). In Dr. Mesce's lab I was astonished at how researchers were able to take simple, yet important behaviors, in this case leech locomotion, and dissect the neural circuit mechanisms responsible. This physical characterization of circuit function, and connection to important behavioral output, triggered in me an immediate fascination.

After graduating with a B.S. in Neuroscience I was accepted into the University of Missouri- Columbia Biological Sciences Ph.D. program. During the application process I met with Dr. David Schulz and discussed his unique approach to understanding circuit mechanisms using a combination of electrophysiology and molecular biology techniques. His ideas and biological questions convinced me to join his lab which I worked in for the next five years. Since finishing my undergraduate I married my wife Chi, had a son Joseph and gained a new and better perspective on scientific reasoning. I accepted a postdoctoral position in Dr. Jeanne Nerbonne's laboratory at Washington University in St. Louis. In Dr. Nerbonne's laboratory I will continue to study mechanisms behind regulation of excitability, only in mammalian cortical neurons and human myocytes. I plan to remain active in neuroscience research throughout my career.